POLITECNICO
MILANO 1863

SCUOLA DI INGEGNERIA INDUSTRIALE
E DELL'INFORMAZIONE

Design and prototyping of a medical device for needle-less injections

Tesi di Laurea Magistrale in
Advanced Mechanical Design

Author: **Luca Bondioli**

Student ID: 10631734
Advisor: Prof. Mario Guagliano

Academic Year: 2021-22

Ringraziamenti

Vorrei ringraziare la mia famiglia, mio papà Lorenzo e mia mamma Marina per avermi sostenuto e aiutato nel mio percorso universitario e per avermi trasmesso il valore della cultura e dello studio come strumento per avere successo nella vita. Grazie anche a tutti gli altri membri della mia famiglia per l'affetto.

Un grazie ad Alessandro Dondi e Sacha Ceretti di Dondi Ingegneria S.r.l.
per avermi affidato il progetto dello sviluppo della siringa per le iniezioni senz'ago, e per la professionalità dimostrata durante il lavoro.

Luca Bondioli
Milano, marzo 2022

Abstract

In the last years, needle-free injection systems were created to solve problems related to the presence of a steel needle for inject a medical fluid. A needle-free syringe has, first of all, the advantage of generating painless injections due to the high speed of the thin fluidic needle produced by its orifice at the tip. The easiest way to provide the required thrust for inject is by means of a compression spring, but in the state of the art technology some drawbacks and room for improvements has been found: integrating the loading system inside a single device, have a pressure control on the patient skin to ensure a complete medical fluid injection without any leakage and a integrated lock system preventing any undesired injection without the user control. The ease of use had to be a main feature for this new device and least but not last, it had to be reasonably small and aesthetically pleasant. During the very first design step, problem solving techniques based on the Theory of Inventive Problem Solving (TRIZ) were applied to explore possible solutions and overcome technical problems. Patent search was performed to acquire inspiration from the state-of-the-art solutions and avoid any future patent infringement. During the nest design steps for the first prototype, Autodesk Inventor Professional wand used for the mechanical design and subsequently Design for X (DfX) techniques were used for simplify and drive the final assembly toward a manufacturable and workable product. Structural validations of the critical components were performed with a preliminary analytical approach, where possible, and with Finite Elements simulations using Abaqus CAE. The FEM validation was focused on maximum stress static assessment with convergence analysis, calculation of safety factor and fatigue assessment. After creating the components, the mechanical and electrical parts were assembled in the laboratory of Dondi Ingegneria S.r.l.; and finally the first prototype was tested. These tests showed that required effort for load the system was moderated and the device had the capability of exert the necessary thrust to create a fluidic needle and inject the fluid.

Keywords: needle-less syringe, fluidic needle, medical device, patent search, TRIZ, mechanical design, Design for X, Finite Element Method, prototyping.

Sommario

Negli ultimi anni, i sistemi d'iniezione senz'ago sono stati creati per risolvere problemi legati alla presenza di un ago d'acciaio per iniettare un fluido medico. Una siringa senz'ago ha, prima di tutto, il vantaggio di generare iniezioni indolori grazie all'alta velocità del sottile ago fluidico prodotto dal suo orifizio in punta. Il modo più semplice per fornire la spinta necessaria per iniettare è per mezzo di una molla di compressione, ma nello stato dell'arte della tecnologia sono stati trovati alcuni inconvenienti e spazio per miglioramenti: integrare il sistema di caricamento all'interno di un unico dispositivo, avere un controllo della pressione sulla pelle del paziente per garantire un'iniezione completa di fluido medico senza alcuna perdita e un sistema di blocco integrato che impedisca qualsiasi iniezione indesiderata senza il controllo dell'utente. La facilità d'uso doveva essere una caratteristica principale per questo nuovo dispositivo e, ultimo ma non meno importante, doveva essere ragionevolmente piccolo ed esteticamente piacevole. Durante la primissima fase di progettazione, sono state applicate tecniche di problem solving basate sulla Teoria della Soluzione dei Problemi Inventivi (TRIZ) per esplorare possibili soluzioni e superare i problemi tecnici. La ricerca dei brevetti è stata eseguita per acquisire ispirazione dalle soluzioni allo stato dell'arte ed evitare qualsiasi futura violazione brevettuale. Durante le fasi di progettazione del primo prototipo, Autodesk Inventor Professional è stato utilizzato per la progettazione meccanica e successivamente sono state utilizzate tecniche di Design for X (DfX) per semplificare e guidare l'assemblaggio finale verso un prodotto fabbricabile e funzionante. Le validazioni strutturali dei componenti critici sono state eseguite con un approccio analitico preliminare, dove possibile, e con simulazioni agli elementi finiti utilizzando Abaqus CAE. La validazione FEM si è concentrata sulla valutazione statica dello sforzo massimo con analisi di convergenza, calcolo del fattore di sicurezza e valutazione della fatica. Dopo aver creato i componenti, le parti meccaniche ed elettriche sono state assemblate nel laboratorio della Dondi Ingegneria S.r.l.; ed infine il primo prototipo è stato testato. Questi test hanno mostrato che lo sforzo richiesto per caricare il sistema era moderato e il dispositivo aveva la capacità di esercitare la spinta necessaria per creare un ago fluidico e iniettare il fluido.

Parole chiave: siringa senz'ago, ago fluidico, dispositivo medico, ricerca brevetti, TRIZ, progettazione meccanica, Design for X, Finite Element Method, prototipazione.

Contents

List of Figures

List of Tables

List of Symbols

Variable	Description	Unit of measure
η	safety factor coefficient	adimensional
μ_s	static friction coefficient	adimensional
ϵ	strain value	$\mu m/m$
σ_y	yield stress	MPa
UTS	ultimate tensile strength	MPa
K_i	geometrical factor	adimensional
K_t	stress intensity factor	adimensional
K_f	fatigue notch factor	adimensional
q	notch sensitivity factor	adimensional
$\lvert\ \rvert$	length modulus	mm

Introduction

The present thesis work is based on the project of an innovative device for medical needle-free injections, whose purpose was to improve important points in state of the art technology and produce an easy to use, safe and compact system suitable for medical environment. Needle-free injection devices are not new on the market; since the 18 December 1866 the first jet injector to administer medicine under enough pressure to penetrate the skin without the use of a needle appeared from the invention of Dr. Jean Sales-Girons at l'Académie Impériale de Médecine, in Paris [1]. A jet injector is a type of medical injecting syringe device used for drug delivery, in which a narrow, high-velocity stream of liquid penetrates the outermost layer of skin to deliver medication targeting underlying tissues of the epidermis or dermis, fat, or muscle. The jet stream is generated by the ampoule having a thin orifice on its tip (Figure 1), by its piston compression in an enclosed liquid-filled chamber. The hammer compressing the ampoule's piston is usually pushed after by release of a compressed metal spring which can be compressed by operator muscle power, hydraulic fluid, built-in battery-operated motors, compressed air or gas, and other means. Since the jet injector breaks the barrier of the skin, there is a risk of blood and biological material being transferred from one user to the next, but this problem was solved by using a mono-use syringe. Another problem was related to the "splash-back" phenomenon related to the jet stream striking the outer skin at a high velocity causing the jet stream to ricochet backwards [2]. In order to solve this problem a minimum pressure of the ampoule over the patient's body is needed, but in many state of the art devices of this kind no pressure sensor is present for control the pressure and this function is devoted to the users common sense. In August 14, 2014 the U.S. Food and Drug Administration (FDA) approved the use of PharmaJet Stratis 0.5 ml needle-free jet injector for delivery of a flu vaccine (AFLURIA by bioCSL Inc.) in people between eighteen through sixty-four years of age [3].

Figure 1: Needle-free syringe.

1 | The initial concept

1.1. The technical and aesthetic need

The very first idea of a medical device integrating a loading system for store mechanical energy to perform needle-free injections and an electrical system for guide the injection pressure and prevent out of control injections has been conceived by the CEO of Dondi Ingegneria S.r.l. Alessandro Dondi. The first aesthetic concept model, with only external plastics design has been developed by the industrial designer Federico Villa in the 2018. The challenge of the present project, explained in this master thesis work, was to create a mechanical device with the following characteristics:

- Compatible with standard needle-free ampoule, as shown in Figure 1.
- Moderate in overall size and handy for the user.
- Spring loading system integrated inside the same tool.
- Keep the overall "boomerang" shape chosen by the industrial designer.
- Use a main spring for storing mechanical energy, easy to be loaded.
- Having a frontal ring able to detect system pressure on patient's body.
- Integrated electrical system for injections control able to unlock when pressure has reached a certain threshold limit.
- Electrical components powered by an internal rechargeable battery.

The mechanical spring was the key element to exert the needed thrust to compress the needle-less ampoule hammer and ensure the full fluid injection. This element was taken from a previous patented injection system called The Injex® Needle Free Injector [4]; the system was disassembled and analysed, and the spring maximum force when compressed was measured 200 N. Another important aspect of the project was to reduce the force needed for compress the spring by the user while keeping the overall system's weight low. The needle-less ampoule had a metric fillet M5 on its base which could be screwed firmly

to the injector's body; this because it must withstand the impact force exerted by the spring when released. The electrical part integrated in the device had to play the role of controlling the right pressure on patient's body just before the injection; this was an important point since if the pressure wasn't enough the fluid could be plashed elsewhere without perform a full injection. And likewise the lock system was a safety point since it could block any undesired injection, as for example caused by the user hitting accidentally the device and splashing out the medical fluid. This control on pressure has been conceived to be performed by three pressure sensors or on-off switches connected to a ring support coming in contact with the patient's body and able to detect the right pressure for injection and to inform when system was ready to inject. For the aesthetic and ergonomic part of the invention a study on shapes and innovative styling elements was performed by a professional industrial designer, as mentioned before, with the purpose of communicating the qualities of the possible new brand and create a comfortable and handy to use medical device, the first conceptual design can be seen from the rendering in Figure 1.1.

Figure 1.1: Needle-free device first conceptual design.

1.2. State of the art research

Before proposing ideas and tackle a specific technical problem, it is advisable to perform a patent search to find already available solutions that solve the same or similar problem. This is not the only reason why it is a good practise to patent search before any attempt of technical inventive problem solving: the aim of prior art patent research is to find out if an invention is new, sufficiently different from the existing technology and, at the end, if it is patentable. Other collateral information one can retrieve browsing patent database are in which directions main actors of a certain field/market are addressing the problem, in which directions target problems appear to be not undertaken, in which directions you are positioning your solutions with respect to the existing ones and which technology trends can be recognized. For patent search there are many patent databases and some of them are free to use as Espacenet, Patent Scope and Patent Inspiration. Before start exploring with databases search engine it is useful to know that instead browsing inside the international patent portals by insert keywords one can start searching by using the "scheme" of alphanumeric classification describing different groups of patents [5]. In Espacenet "catchwords" are recurrent words for which a specific classification code is assigned, and these codes can be used to include or exclude groups and types of patent classes relevant or not to the research. In Patent Scope after writing the key-words of the research field it is possible to display the results by International Patent Classification (IPC) code and see which are the most relevant patent class in that field. In case of needle-free injection devices the only relevant IPC code was "A61M" where A stands for "HUMAN NECESSITIES", "61" include the "MEDICAL OR VETERINARY SCIENCE; HYGIENE" and "M" includes "DEVICES FOR INTRODUCING MEDIA INTO, OR ONTO, THE BODY". By setting the browser to search only patents with this IPC code, irrelevant patents could be excluded. For further focusing on really relevant invention it was important to remember that just typing key words in the search engine could miss the point, because the typed words could be contained only in the title and abstract but most of the relevant information could be written in the description or, even more important, in the patent claims. In a patent the claims are the most important part, they are the "legal core" of the intellectual property, i.e. they define the features of the invention to be protected. There are independent and dependent claims: an independent claim is a broader description of the invention, it fixes the main elements and feature of the novelty and helps prevent patent circumventions; the dependent claims are more specific description of the invention and can include how it is produced and the implementation of it, tailored to fit exactly to potential infringing products. For these reasons, in patent search, including words that could be contained in the patent claims is of outmost importance. For our scope the

patent application date could be set within the last 10 years and the related technologies using gas or electric field to exert the thrust force could be excluded focusing only in the inventions using a spring to inject the medical fluid contained in the ampoule. At the end the first string used in Patent Scope database for a proper patent search was:

```
EN_ALL:(IC:("A61M") AND AD:([01.01.2012 TO 01.02.2022]) AND
EN_DE:(("needle" AND ("less" OR "free") AND ("medical" OR "hospital" )
AND "inject*"))) AND EN_CL:("SPRING" AND ("AMPOULE" OR "SYRINGE")
NOT("GAS" OR "ELECTRIC*" OR "MAGNETIC"))
```

With the use of these patent search techniques the most relevant ideas regarding needle-free injection technology were retrieved using Espacenet and Patent Scope. The most relevant inventions found in this field were US9408972B2 [6], US9700675B2 [7] and EP0930905B1 [8]. This last patent application was related to Injex®, a needle free injector that delivers a fine stream of medication subcutaneously by means of a mechanical spring; the main tool without loading system can be seen in Figure 1.2.

Figure 1.2: INJEX 30 needle-free model.

When the relevant patents were retrieved it was necessary to understand them by analysing the document and see what was the room of improvement left by their claims. The standard rules for patent breaking are:

1. Identify the components of the invention and their alternative denominations (using the description).
2. Classify the components, identify the hierarchy (using the description).
3. Identify functional interactions, perform a functional analysis (from independent claims).

4. Complete the functional diagram with relevant attributes and annotations (from independent claims).
5. Investigate the possibility to trim (radically modify) at least one component of the functional model (inventive part).

The new invention must be not obvious with respect to the prior art, meaning that it must be a technical improvement of existing system using known technical features or principles or a transfer of technology from one technical field to another. One way of determining whether a difference from an existing invention to a new one is "insubstantial" or not, is the so called "Triple-identity Test" [9]. Under the triple-identity test, the differences between the feature in the accused device and the limitation literally recited in the patent claim may be found to be "insubstantial" if the feature in the accused device:

1. Performs substantially the same function (addresses the same problem).
2. In substantially the same way.
3. To yield substantially the same result.

The bottom line of patent breaking is that the procedure most not include obvious changes to avoid one of the three inventive parts stated before, but an invention must be substantially modified with the purpose to change the structure of the invention. As exposed in point 3 and 4 of patent breaking steps, one way to analyse critically invention claims is to build a Functional Model of the independent and relevant dependent claims. The Functional Model is a tool in which the elements and relations described in the claims are displayed in one diagram; it is useful to clarify and display the functioning of a target technical system, identify possible conflicts in it, and support the proposal of actions to improve the previous system. The Functional Model was performed on patent EP0930905B1 [8], one of the closest invention to our idea to be developed in the project and, as can be seen in Figure 1.3, it was composed by a injector device composed of a cylindrical housing holding internally a spring and a hammer releasing the impact pressure on the ampule. Other relevant elements of the invention were the trigger, the coupling mean linking the ampule to the cylindrical housing and the safety interlock assembly which holds the trigger in place preventing release of stored energy unless the ampule is coupled to the injector. From the analysis of dependent claims the loading base for the injector was composed by a rectangular base with a movable cover and a cocking mean moving jointly with the cover that compress the spring inside the injector. The elements in purple represented the ones mentioned in the dependent claims while the yellow and green elements were the ones described in the independent claim; the green element was not part of the inventive

step claimed in the patent. From the present analysis, it was observed that the loading base was separated form the injection body and that no pressure control was present on the systems; all these were areas of improvement in which it was possible to build up technical novelties.

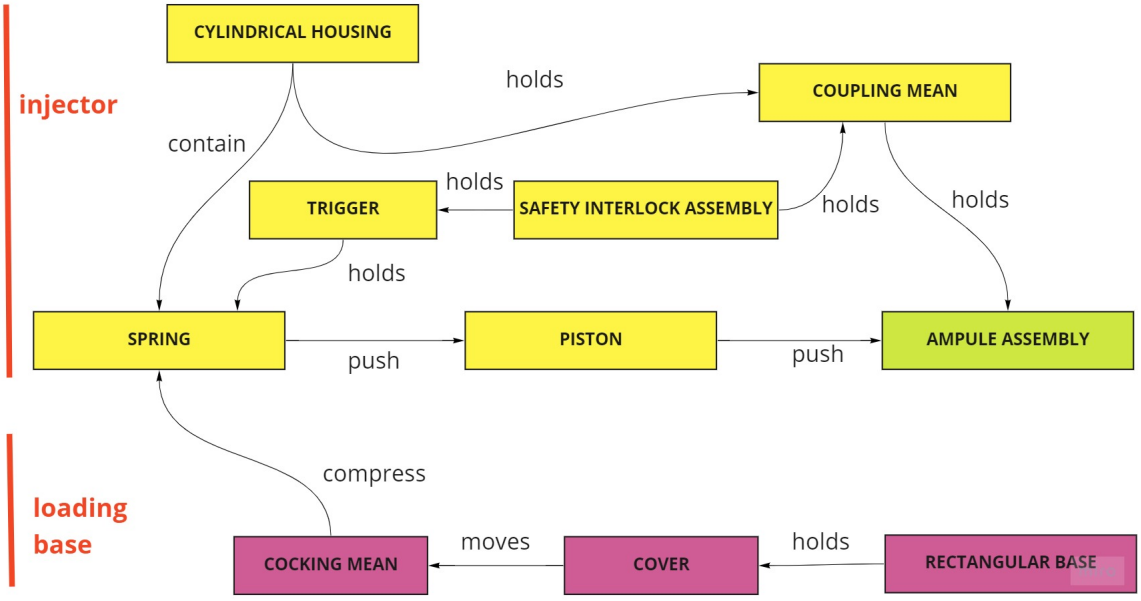

Figure 1.3: Functional Model of EP0930905B1.

1.3. First concept development

1.3.1. Functional model definition

TRIZ is a systematic approach for understanding and solving any problem and a catalyst for innovation and new inventions. Beginning in 1946, TRIZ was developed by the Soviet inventor Genrich Altshuller; TRIZ in Russian means "Teoriya Resheniya Izobretatelskikh Zadatch" or in English, "The Theory of Inventive Problem Solving". Years of Russian research into patents uncovered that there are only 100 known solutions to fundamental problems [10], and through a systematic approach TRIZ helps finding ideal solutions to real technical problems.

In the functional model created on patent EP0930905B1 claims, the loading cycle has been devoted to a loading base external to the injector main body, and this left place to apply rule: "The law of transition to a super-system" [10] from TRIZ Theory, which states that when a system exhausts the possibilities of further significant improvement, it is included in a super-system as one of its parts. In this case the base had only the function to load the spring and this function could be transferred inside the injector body

itself removing the need of a loading base; the lever for the force application had to be transferred in the injector's body as well, and it could become the device handle. Since a critical point was having a spring system "easy to be loaded" and "handy for the user" here the first technical "contradiction" was found, because if the device handle was long it could exert a higher force with less effort to compress the spring (longer lever) but it could result in a less handy and less aesthetically pleasing device, reversely a short handle would result into a more user-friendly device but with a harder handle to be activated by user's hand to load the spring (shorter lever). Moreover, with the idea of integrated system, removing the external loading system, no more base placed on a steady surface was present but the user had to load the system while holding it in his/her hands; also this point could be a drawback for the easy of use, resulting in a trickier device instead of a better one. The first part of the problem concerning the system handle had a technical contradiction concerning its length. A contradiction in TRIZ theory [11] is a conflicting requirement, an improvement in one part at the expense of something else getting worse, or when the same requirement is needed in opposite states but at different times or places. It occurs when two different measurable parameters of the system conflict each other, leading to a stop in the inventive process, but if properly handled giving the opportunity to generate breakthrough inventions. In the case of this system the control parameter was the "handle/lever length" and it has been schematized as in Figure 1.4.

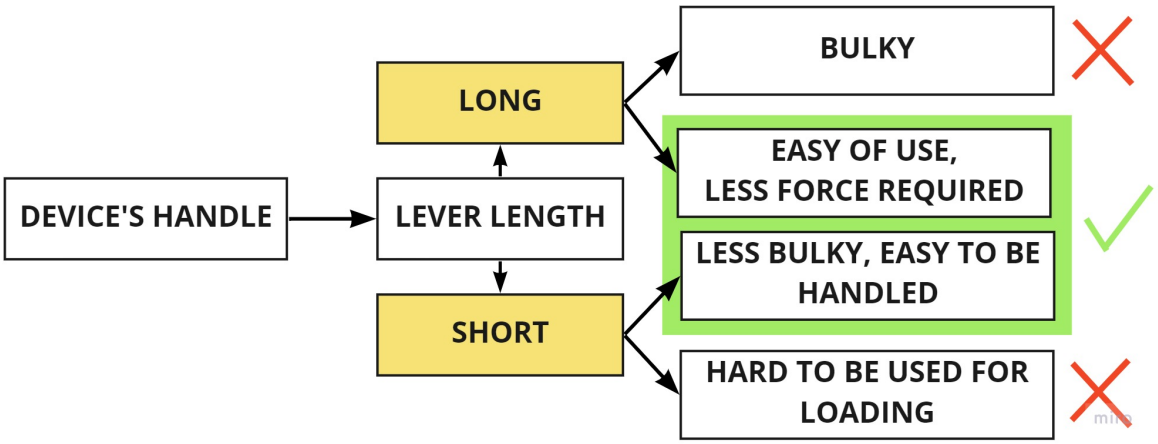

Figure 1.4: TRIZ model of contradiction.

One way to overcome a contradiction is operate a "separation on condition" meaning finding a solution to achieve both positive desired results answering to the question:

> `Do we really want the control parameter to assume the value ''long'' under any operating condition and do we really want the control parameter assume the value ''short'' under any operating condition?`

The answer to this question was negative so the "separation upon condition" was a candidate direction toward solution. Practically speaking, the conceived answer was a system having a short lever length when the user had no need to apply forces to compress the spring, as when he/she holds the device against the patient's arm, and a longer lever arm when the user had to apply the force at the lever for get the spring compressed, i.e. during loading. A new idea for an extensible and retractable handle arm was born, having both the desired characteristics when needed, at the right time.
Another problem in the spring loading step could arise from the spring stiffness and the limited force available by the user, meaning have a system too hard to be loaded by a human arm especially after many loading cycles in one day. In TRIZ when a function between two elements of a technical system is insufficiently satisfactory is called "insufficient useful function" meaning it has to be further handled to become ideal. For improve an insufficient useful function, before opt for a change in technology or working principle, it is always better first thinking if it can be fixed keeping the same working principles already present in the system; this for reduce the number of modifications and time consumption in generating ideas and search for applicable working principles. The questions to seek solutions for enhance an insufficient useful function are:

- Check if tool (source of function) or the object (effect of function) can be modified to enhance the interaction.
- Check if environment can be modified to allows a better interaction between tool and the object.
- Check if time or timing of function delivering can be modified to improve the interaction; matching/unmatching frequencies is included.
- Check if another field can be placed in parallel with the existing function, having a series of interactions with the same final purpose.

For allow an easier interaction between the user arm, pushing the lever handle, and compressing the spring, an adjustment in timing seemed to offer a way to reduce the effort required. The idea was to have a multiple strikes loading system instead of a single strike loading system as in torque multipliers; with this solution a trigger would have had the task to keep the compressive energy stored at each strike, attached to a toothed bar, attached to the spring, with teeth equal to the number of strikes required to full load the spring. This idea was developed from sketches to real 3D models and physical produced elements, as shown in the following chapters.
Unlike an "insufficient useful function", an "harmful function" in TRIZ is a completely undesired function to be removed from the system. After creating the system scheme of

elements and functions, it was found that an harmful function was present between the force transmission kinematic and the spring at the time the operator had the device fully loaded and had to perform the injection, that is when the spring's stored energy had to be released, by snapping the hammer attached to the spring and compressing the ampoule. Specifically the harmful function was that the kinematic system absorbed energy or even could block the spring-hammer system during the spring release, preventing the proper injection, as can be seen in Figure 1.5.

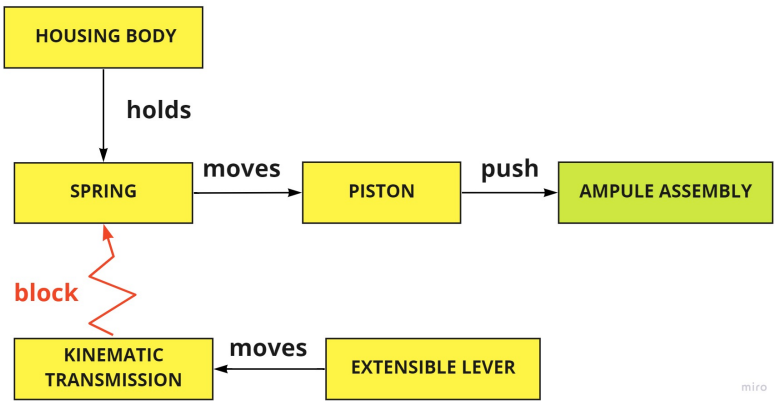

Figure 1.5: Functional analysis of harmful function.

The inventive problem solving approach was applied, before seeking a technology substitution and changing completely the working principle, and in case of an harmful function the questions to check are:

- Check if the harmful function can be eliminated by removing the tool (source of function) or the object (effect of function), transferring the useful functions to another element if necessary.
- Check if tool and object can be separated, erasing the undesired interaction.
- Check if a barrier can be added *between* tool and object, adding another element.
- Check if the harm can be attracted on another already existing element or another element that can be added in the system.
- Check if it is possible counteract the harmful action, adding another function in opposition to it.

The solution chosen was to separate the kinematic transmission (tool) and the spring (object) with a system that was able to connect these two elements and lever during only the loading, and separate them in space during the shooting (injection) phase. In this way,

during the release of spring's accumulated energy (injection), the spring-hammer system was able to move freely without obstacles. To put this idea into practice and generate new elements to be placed inside the functional scheme, a rack and pinion (cogwheel) system attached to the hammer was designed with a mechanical tooth, that was called "thrust hook", attached to the lever bar able to come in contact with the pinion (cogwheel) and rotate it when the system was dedicated to load the spring, and able to detach from it when there was no loading need. Applying these principles for inventive problem solving, a new functional model for the invention was developed, for analyse the system altogether and having a starting base for further improvements and subsequent patent claims; it is shown in Figure 1.6.

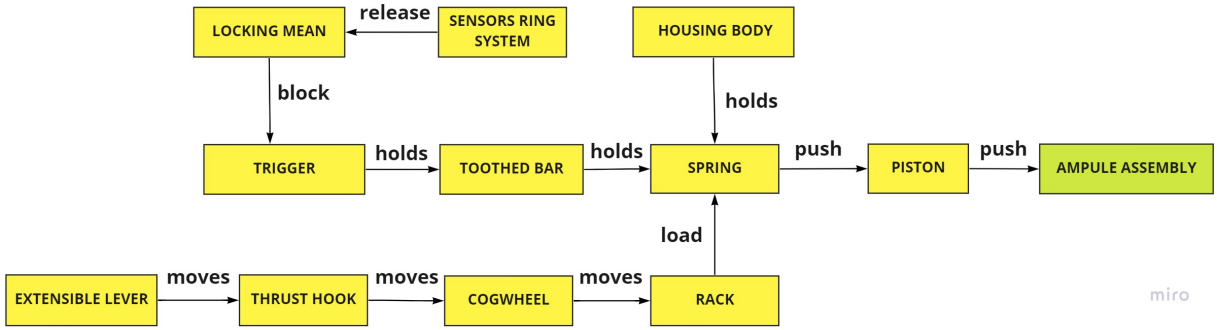

Figure 1.6: Functional Model of the new needle-less injector.

1.3.2. Working principles research and application

To find the effective physical components able to perform a required function, a list of effects related to working principles was of primary importance. Such online database exist and it is called TRIZ Effects Database, it provides answers to queries in the form of a list of effects to find the real application to perform a specific task, and in case of "transforming kinetic energy" into "mechanical energy" a solution found and accepted was "rack and pinion" coupling. In our specific case, for better exploit the separation between the thrust hook (tooth attached to the lever bar) and cogwheel (pinion), as mentioned in Section 1.3.1, the cogwheel was modified to have smaller teeth in the inner part coming in contact with thrust hook during the loading, and standard teeth outside always in contact with the rack's teeth. In Figure 1.7 the first sketches of the loading system and the cogwheel can be seen, in the internal cogwheel side there were shark-tooth-shaped teeth, being pushed forward when the thrust hook came in contact with them, while when the lever arm was retracted in its original position the thrust hook could slide over the cogwheel inner teeth. This idea took inspiration from the bike free-wheel technology

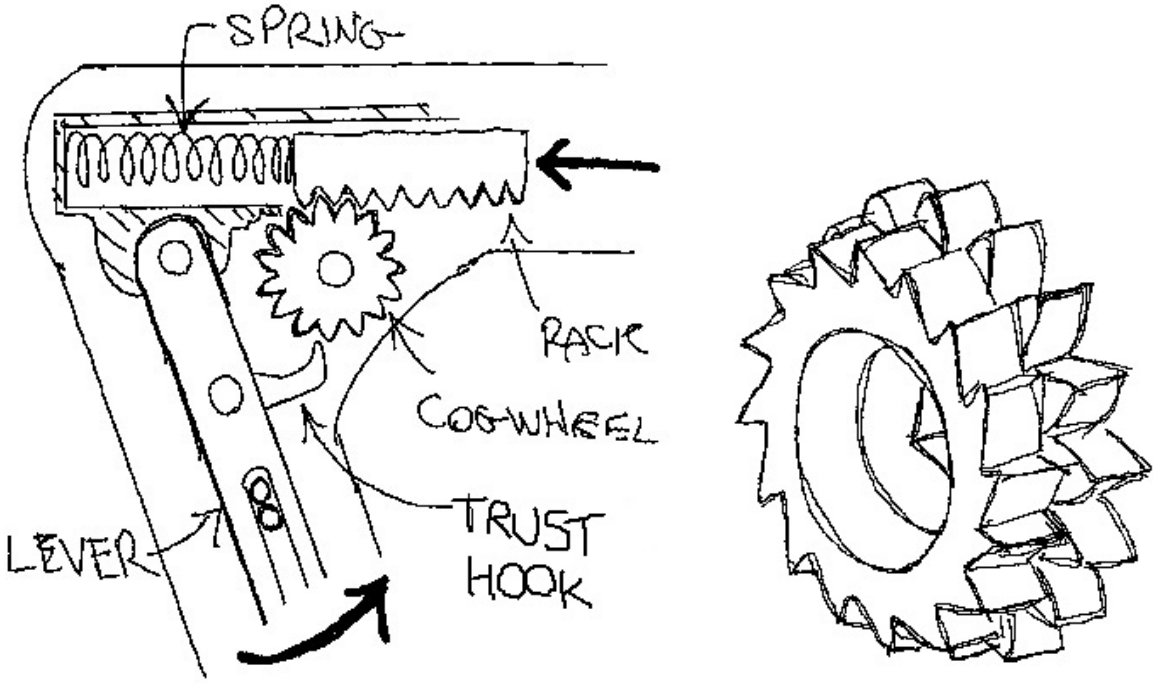

(a) Loading system first sketch.

(b) Cogwheel first sketch.

Figure 1.7: First sketches on loading system.

where the mechanical system have a similar shape and functioning, since in one direction of rotation torque is transmitted through mechanical teeth coupling, while in the opposite rotational direction, there is a sliding contact between them. The external cogwheel's standard teeth are in contact to the rack attached to the hammer during both forward and backward rotation.

Inside the syringe's handle containing the extensible lever, the working principle chosen was a system composed by two bars hinged and moving specularly with respect to the main housing body and with an internal bar sliding inside them. This solution gave the advantage to insert a resistant fulcrum between the external bars and the inner bar, as shown in Figure 1.8. It was important in this area to have parts with enough mechanical strength for a proper functioning over time. In this way the lever arm could be extended when a longer lever arm was necessary for load the spring, and when was not it could be retracted. The sliding motion between bars could be simplified having plastic washers with low friction coefficient: they were chosen of circular shape inserted inside the two bolts creating the sliding fulcrum and coming in contact among each sliding surface.

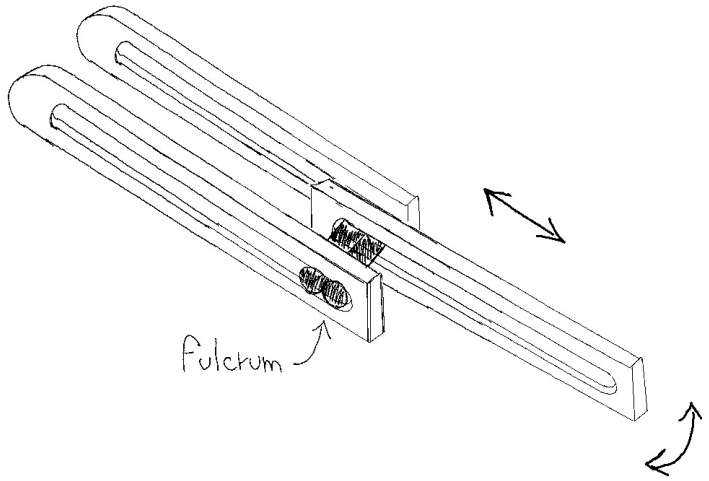

Figure 1.8: Sketch of extensible.

When the forward lever movement brought the thrust hook in contact with the cogwheel, rotating it, the rack attached to the hammer was moved backward, compressing the spring. At each different strike loading movement, the spring system was kept in place by a trigger, allowing energy to be stored; as can be seen in sketch of Figure 1.9. As stated before the loading step was not a single strike loading but a multiple strikes loading action, and at each strike the potential energy stored in the compressed spring was locked by a trigger that blocked the system in position. The trigger could work to keep the spring system compressed by means of a toothed bar fixed to the hammer, and the strikes designed to load completely the spring were four; for this purpose the toothed bar had four teeth as well. Only when the trigger was released by the "start button" the toothed bar, hammer and spring were left free to snap forward and release the mechanical energy for the injection.

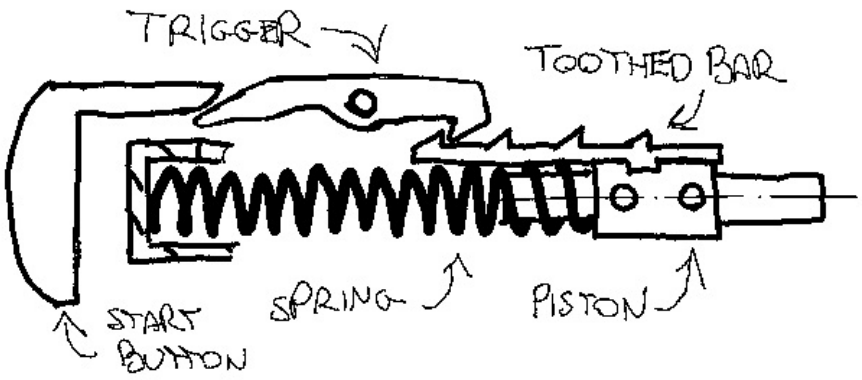

Figure 1.9: Sketch of spring lock system.

Another element that had to be developed in its working principles was the sensor ring system. As first idea it was composed by a solid ring with three circular supports sliding on the syringe main body, where three stiff plungers inserted in its three supports were pressed against three on-off switches inside the injector's body. These three stiff plungers had three preloaded springs with gauged stiffness; they had to be fully compressed only when the pressure on the patient's body reached the right threshold for a safe injection, without any medical fluid loss. The task of these on-off switches was to electrically notify when the three spring were fully compressed, namely the device pressure on patient's skin had reached the right value and the safety system could be unlock. Considering that the system had to work in a medical environment, subjected to sanitizations, frequent cleanings, etcetera, it was important to keep any sensor inside the device body in a protected environment. The preliminary sketch of the ring sensor system can be seen in Figure 1.10, where three on-off switches were designed on two separated printed circuit boards (PCB) connected through cables to the main hardware board and battery.
Regarding the positioning of the ampoule containing the medical liquid, a base with a threaded hole in the middle were designed. To simplify the user in screw the ampoule on this base a back and forth sliding system was design: it could be pulled out when more space for screwing was necessary while retracted inside after that, moreover two movable buttons were attached to the base and could be moved by the user's fingers back and forth. The problem was having a lock/brake system for the syringe sliding base able to activate and block it while the hammer pushed the ampoule, avoiding any forward undesired sliding action. The working principle selected for this type of mechanical constrain was a double snap-fit joints system composed by an inner snap-fit placed over the syringe sliding base, and a larger outer one fixed on syringe's main housing body.

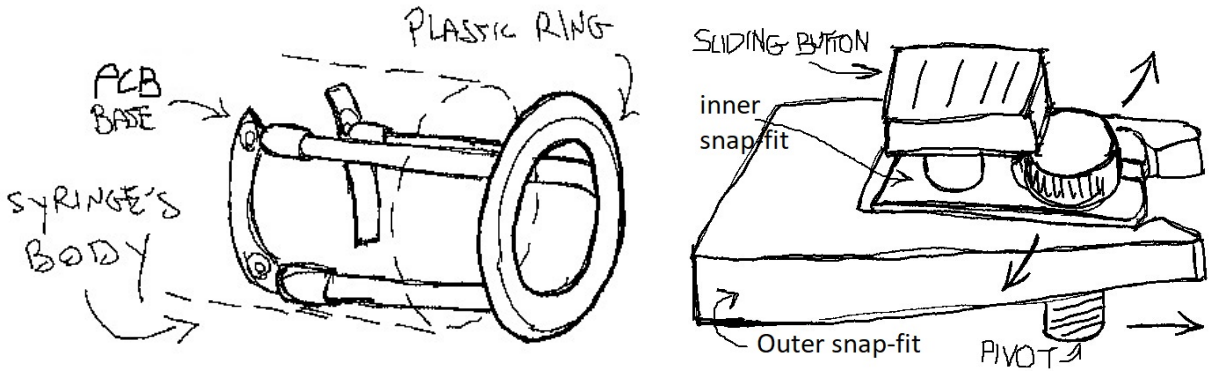

(a) Ring sensor system.

(b) Double snap-fits lock-brake system.

Figure 1.10: First sketches.

The inner smaller snap-fit was joined with the sliding base by means of a pivot; this pivot was screwed to the sliding base but not to the smaller snap-fit, it was just just constraining the vertical direction of it and allowing some millimeters in the horizontal displacement direction. When the pressure was applied on the ampule, it would tend to move the sliding base with the pivot screwed over, the pivot would have to push the inner snap-fit arms tending to open them, and this movement would have to open the outer snap-fit arms activating the brake system in such a way to absorb energy and block any forward sliding. The inner and outer snap-fits arms opening would increase the planar footprint area and coming in interference with the main syringe housing body generating friction and force absorption with it. This snap-fit energy brake system was considered to be able to absorb energy and avoid any uncontrolled forward sliding movement of the base. Instead when the user had to pull the syringe sliding base outside to remove or replace the ampoule, he/she could have pulled the sliding button fixed to the inner snap-fit, and in this case the pivot would not be in contact with the inner snap-fit arms, but with the back part of it. In this way the inner snap-fit arms were not opened by the pivot, and consequently they would not open the outer snap-fit and the mechanical break could not be activated, letting the inner snap-fit to slide outside the the outer one and the sliding base moving forward. The first sketch of the idea is shown in Figure 1.10.

2 | Preliminary design

2.1. Model development and first system analysis

A mechanical system is defined by the Dictionary of Mechanical Engineering [12] as "an organized and coordinated ensemble, formed by one or more complementary machines or plants, designed and realized to give to the user a safe, reliable, effective, economic service". In this chapter the 3D models were created, starting from the ideas generated in the previous chapter by inventive problem solving techniques, using Autodesk Inventor Professional. The geometries, shapes and mechanical interactions created in this chapter were preliminary, generated using principles of standard mechanical engineering practise. They will be improved, as described in the next chapter, using methods and tools for advanced mechanical design.

2.1.1. Dynamic coupling: lever system

For the purpose of finding out the maximum force on user's hand moving the loading lever, the first kinematics diagram was created using 3D models in Autodesk Inventor environment. A useful graphical method for analyse and calculate forces in a mechanical system in equilibrium is the "Graphical Method of Forces in Equilibrium Condition" [13]. The graphical method is used for display the state of equilibrium driven by forces exchange, and it is based on the fact that forces are applied vectors that can be drawn on the mechanism itself with the right magnitude, orientation and direction. Then the force vectors are translated keeping the same direction and length (magnitude) to form a closed polygon (if the system is in equilibrium) and at each force is applied a scale factor in mm/N, allowing to obtain the unknown force magnitude by measuring the graphical length. For understand which force vectors and in which direction are applied it is necessary to apply the principle of action and reaction, third Newton's law. The syringe device equilibrium condition was analysed when the force required by the user's hand was maximum, that is when the spring was fully compressed and exerted a force equal to 200 N. The cogwheel radius was assumed equal to R = 10 mm and the angle between the

spring axis and lever was 70°, this value was taken from the initial concept design idea for the new product, the "boomerang shape" tilt angle. In Figure 2.1, the force vector balance can be seen, where F1 was the force due to the compressed spring, Fa was the force applied by the thrust hook to the system and the last force in green was the one generated in the hinge between the lever and the housing body. The angle "a" between force Fa and F1 was 148° while the angle "b" was 14°; these values were taken from assembly measurement tool in Autodesk Inventor environment. Knowing the magnitude of force vector F1 and assigning at it a known arbitrary length, the value of force Fa could be calculated with the ratio between two vectors length:

$$Fa = \frac{|\ Fa\ |}{|\ F1\ |} \cdot F1 = 0.78 \cdot 200 = 156N; \tag{2.1}$$

.

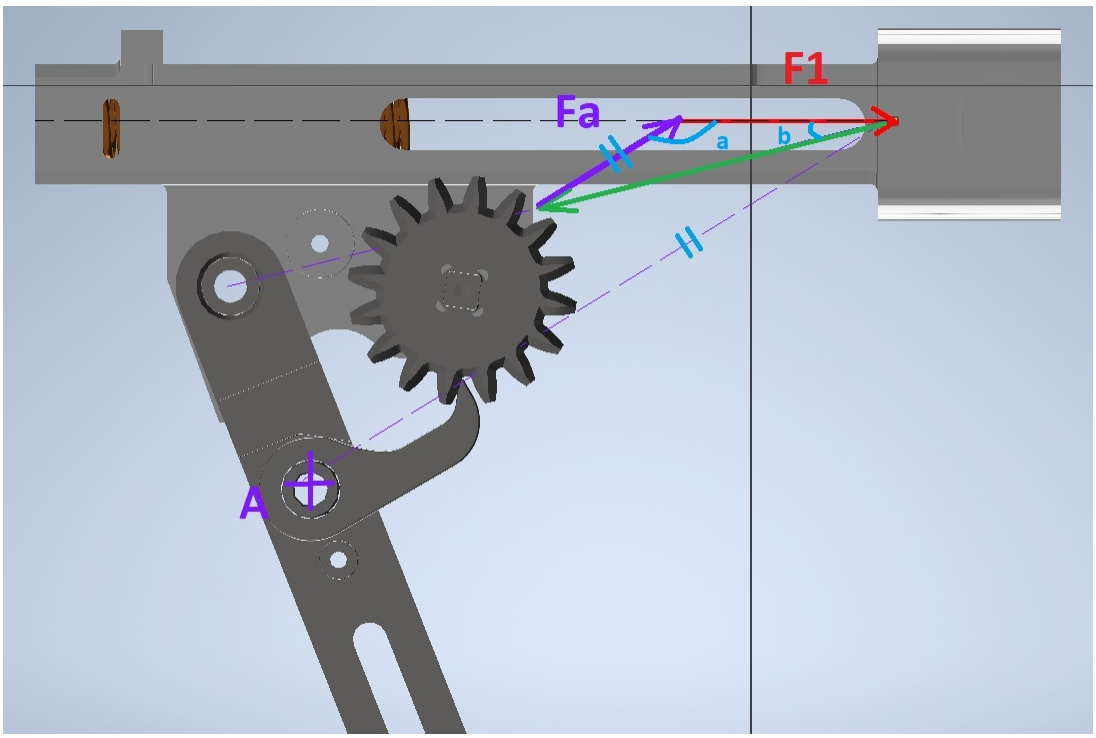

Figure 2.1: Graphical method of forces in equilibrium condition.

The length of the extended lever was L = 200 mm and the distance between the thrust hook's hinge (point A) and the lever's hinge was AF = 25 mm. From the balance of momentum around the lever hinge, the value of force applied to the extended lever's extreme edge, where the user's hand would be placed, resulted:

$$F = \frac{Fa\ \cdot AF}{L} = \frac{156 \cdot 25}{200} = 19.5\ N; \tag{2.2}$$

This force value would be acceptable considering that, in average, user's muscular force tolerance limit is set to 25 N for a repetitive fingers/hand motion, to avoid injuries or physical problems due to the excessive force (value taken from Design for Assembly literature [14]). In addition, the force of 19.5 N was reached only at full spring compression, while in the previous strikes it was much lower.

2.1.2. Dynamic coupling: trigger system

Another important mechanism to be developed was the trigger attached to the toothed bar. Once again the graphical method of forces in equilibrium condition could be used to evaluate the force vector acting on the trigger. In Figure 2.2, the force due to full compressed spring was F1 while Fs was the force applied to the trigger by an hypothetical vertical spring placed at point A, to keep the trigger in grip downward. The value obtained for Fs with the given distances was:

$$Fs = \frac{|\,Fs\,|}{|\,F1\,|} \cdot F1 = 0.32 \cdot 200 = 64\ N; \tag{2.3}$$

where the modulus of Fs and F1 were measured lengths of force vectors Fs and F1 respectively. The value Fs = 64 N was too high for being assigned to a small spring placed in position of point A, because a too large spring occupying too much space was needed to exert a such vertical force. Moreover in that area only few millimeters of space were available and only a small spring could be fitted in, for this reason this solution could not be actuated.

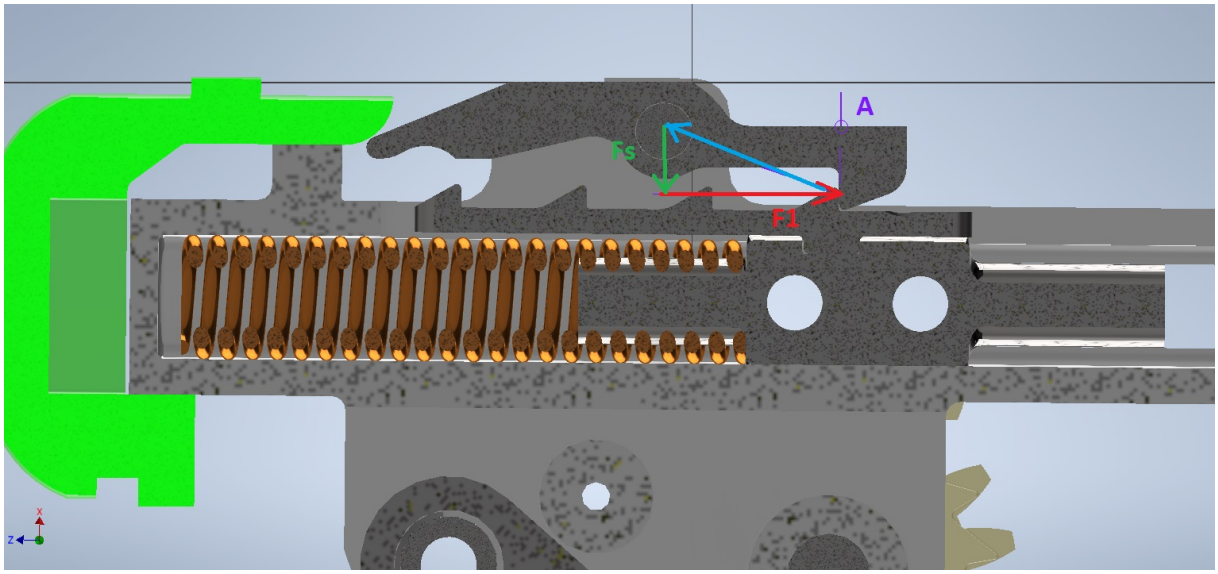

Figure 2.2: Graphical method of forces in equilibrium condition.

To reduce the magnitude (i.e. the length) of force vector Fs, the force vector F1 had to be tilted upwards of a certain angle. In case of a tilted trigger's tip in contact with a tilted tooth of the toothed bar, the forces interchange direction could be changed and tilted upwards in such a way that their vectorial direction passed by trigger hinge center. With this solution the force vector Fs could be reduced up to 0, with all the force needed to keep the trigger in place devoted to the trigger pivot instead of a vertical small spring. With this solution the small spring placed on the trigger point A could be placed anyway to just ensure the trigger would be always placed downward, ready to block the toothed bar while in contact with it. The new design for the trigger-lock mechanism can be seen in Figure 2.3. In this case the calculated force Fs was:

$$Fs = \frac{|\,Fs\,|}{|\,F1\,|} \cdot F1 = 0.11 \cdot F1 = 22\ N; \tag{2.4}$$

As first attempt the angle of tilt was kept as explained, since in the model no friction force was considered, but the result culd be further improved by increasing the angle of tilt, directing the F1 force upwards consequently reducing the value of Fs.

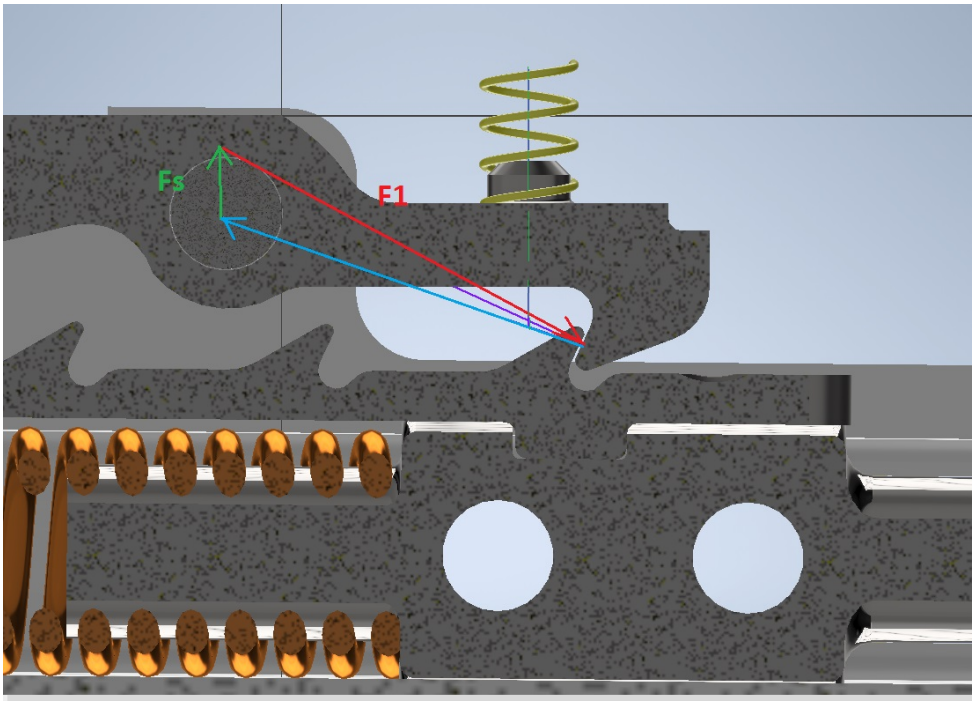

Figure 2.3: Graphical method of forces in equilibrium condition.

2.1.3. Dynamic coupling: snap-fit brake system

Once spring loading step was completed, the next stage for the user was to pull out the syringe sliding base and screw the ampule, full of fluid, on it. The mechanism holding the sliding base in place during the impact, as explained in Section 1.3.2, was the double snap-fit brake mechanism. This mechanism can be seen modelled in 3D in Figure 2.4, where "Snap-fit 1" was the inner snap-fit joint, "Snap-fit 2" was the outer snap-fit joint and "Opening crew" was the metallic pivot screwed upon the sliding base able to open the inner and the outer snap-fit arms when the spring force would be exerted to the ampoule attached to the sliding base. When both the inner and the outer snap-fits were opened by the pivot, the system would absorbed energy and act as a mechanical brake on the housing body. The sliding buttons were pulled by the user when the sliding base had to be moved forward; in this case the inner snap-fit did not not open its arms but, since the pivot did not push against its surfaces, it could pass over it coming out from the outer snap-fit joint, moving the sliding base forward.

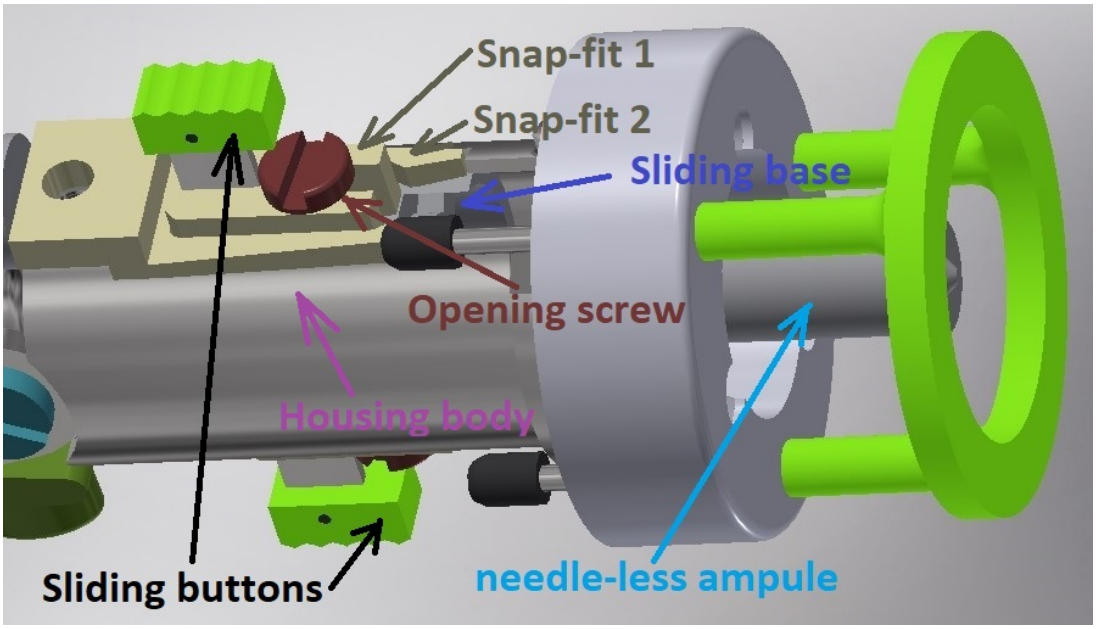

Figure 2.4: Braking mechanism with double snap-fit joint.

2.2. Functional optimization between components

Optimization is defined by the Oxford Dictionary of Mechanical Engineering [15] as "A mathematical method which seeks to maximize a performance function or minimize a function representing unsatisfactory performance by updating the set of inputs to the system or process. The term is also applied more generally to the process of improving a design, process, etc". In this section a system optimization toward a more workable, improved and user-friendly machine was performed. At this stage it was not achieved the definitive optimization process, but the focus was on modify the single components for improve the mechanical and functional interaction between them. Here, the basis for further improvements using predictive simulation software were set. In fact at this phase of design process, designers take on the development of the model and critically analyse the functioning of the mechanism with a point of view to solve and improve the overall design and geometries of single parts. The assessment of needed components and right selection of geometries has been the key point to accomplish the preliminary design.

2.2.1. System force transmission optimization

A key element that could be improved in the assembly was the one laying over the hammer and gripped with the trigger after loading: the toothed bar. The first improvement applied to this element was to add a shoulder on the bottom side of it, matching with a corresponding shoulder on the hammer upper part. This technical solution allowed to remove the high shear force on screw fixing the toothed bar to the hammer, when the spring pressure was applied to it. Another improvement on this element was focused on teeth outline: this was the place where the interchange of forces with trigger took place, and enough surface area was required to reduce high local stress and undesired slips in the gripping between these two elements. Grooves at the teeth base, as shown in Figure 2.5, were able to increase the contact surface and improve the force transmission as well mechanism stability.

The hammer was designed to move backward and forward during each loading and hitting cycle, and the element that was considered to be attached to the hammer, as described in Section 1.3.2, was the rack. For the purpose of improve the ease of force transmission between elements, the system was designed with two racks instead of one, and two cog-wheels instead of just one, with racks fixed on the hammer by means of two screws. These elements were design mirrored to each other to enhance the system stability, making two groups of elements working in parallel, as can be seen in Figure 2.6, Figure 2.7 and Figure 2.8.

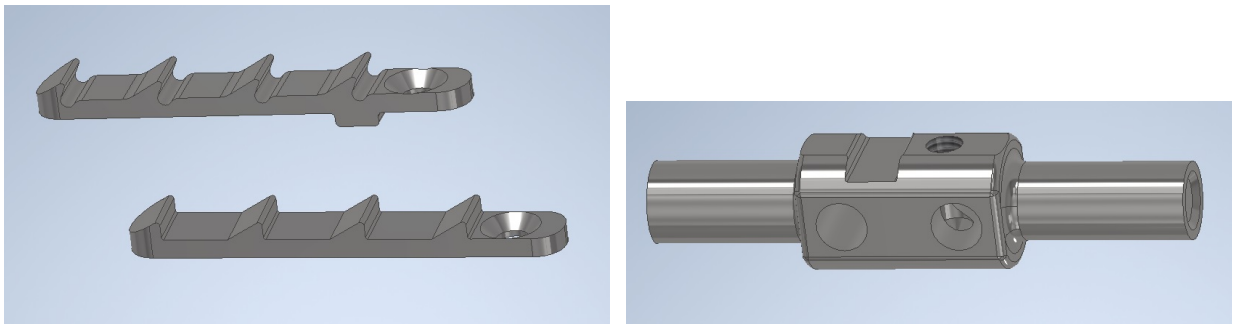

(a) Toothed bar (b) Piston/hammer.

Figure 2.5: Toothed bar design improvement.

The coupling between racks and cogwheels were designed to move symmetrically while moving the hammer backwards and loading the spring: during the shooting phase they were still connected with the hammer so they could move in the opposite direction while the hammer snapped forward by the spring. Each rack was designed to have a couple of crew holes, and a protruding part laying on the housing body and sliding over it to constrain the racks in vertical direction, moreover stabilize the mechanism to avoid unwanted torques generated during the loading, see Figure 2.6.

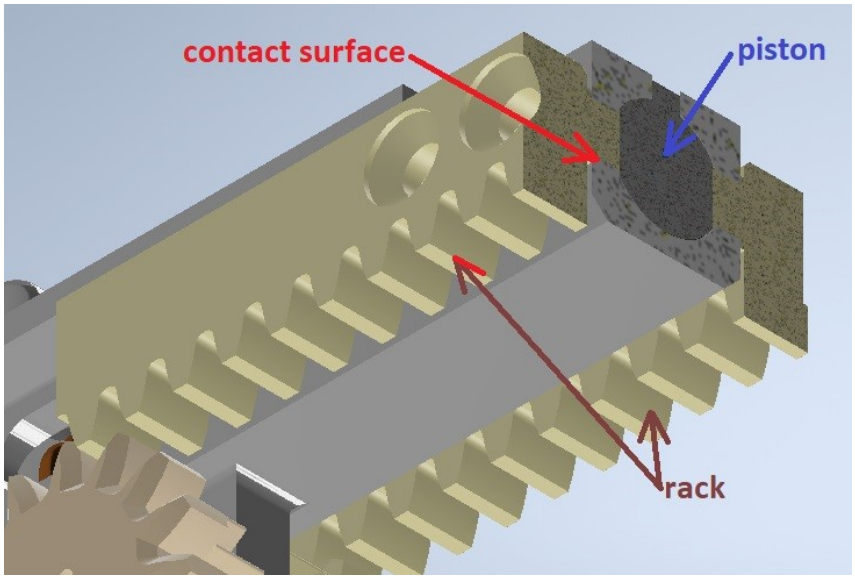

Figure 2.6: Double rack design.

The two symmetrical cogwheels were supported by a shaft, which was placed in a circular support of the housing body. For increase the system efficiency in this coupling, it was needed that the contact surface between each cogwheel and the housing body was as small as possible. As can be seen in Figure 2.7, the internal part of the cogwheels was designed

with a large hole containing part of the housing body and fitted with it in such a way to have no lateral contact; just a small portion of area was in contact between them and this was the horizontal movement constraint. It was necessary for the housing body to have a contact length with the shaft (H in green color in Figure 2.7) of at least 1.5 its diameter; this is a general rule applicable in sliding contact between mechanical elements [13]. Given that in medical environment no liquid lubricants are permitted a self-lubricating system had to be consider or compatible materials for a low dynamic friction coefficient had to be selected.

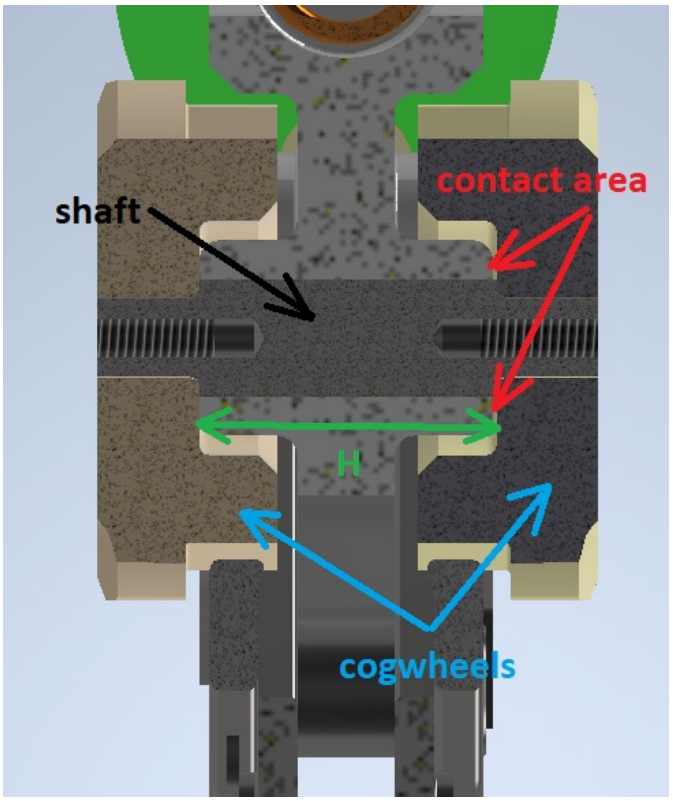

Figure 2.7: Cogwheels contact area.

During the cogwheels rotation it was necessary to ensure a synchronous force transmission with racks, in other words they had to rotate synchronously, and for ensure this condition the two shaft extremities in grip with cogwheels were designed to have squared heads. This design solution ensured both the symmetrical transmission of motion and enough contact area in the coupling for an appropriate exchange of forces. In cogwheels, after a squared cut in the middle was performed, holes of 1.5 mm were added to the cut square edges, and this solution allowed the maximization of the contact area with shaft coupling, since the fillet radius at the shaft edges could be kept very low (R = 0.2 mm), as can be see in Figure 2.8. In the mechanism, two cogwheels were moved by the thrust hook coming in contact with the internal shark-tooth-shaped teeth, as shown in Figure 2.8,

and pushing them to rotate until the end stroke. To ensure constant contact during the motion, the thrust hook had to be controlled in its position, otherwise, due to the high pressure on this component, the response would be having it slip away and loosing the grip. In this movement, to have a perfect alignment and position control of the thrust hook at the very beginning of contact and at stroke end, two constraints were place on the top and bottom of it. These constraints were two shaped extrusions on the lateral lever bars, designed accordingly with the thrust hook lateral shape, as can be seen in Figure 2.9.

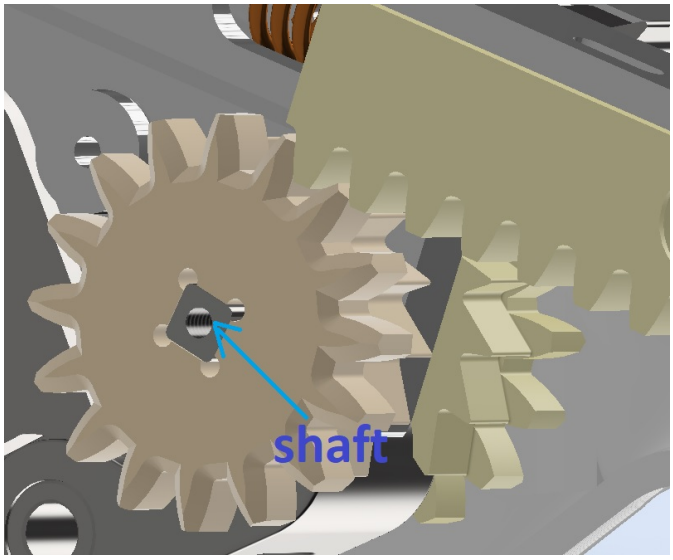

Figure 2.8: Shaft-cogwheel coupling.

As described also in Section 1.3.1 (before the loading step) the thrust hook was, as first, not in contact with cogwheels which were left free to move. During contact (loading step), for ensure the right and continuous contact, the thrust hook was pushed upwards against the bar's upper constraint by a torsional spring element placed between the lateral lever bars, around the thrust hook pin. During the loading motion the thrust hook moved progressively downward to the lower constraint until the stroke end, then the lever was pulled backward to its original position and the thrust hook slid over the shark-tooth-shaped teeth. The back and forth movement is thus repeated four times in total. The torsional spring had only the function to keep this element pushed upward to ensure the proper initial contact position. During the loading step the thrust hook force vector was designed to be perpendicular to the cogwheels radius for a better dynamic efficiency in transferring the force to compress the spring.

2.2.2. Design toward a more user-friendly system

The first part coming in contact with the user's hand was the plastic handle, containing the extensible bar. The external plastics had to have a maximum diameter of 36 mm and a length of at least 60 mm for fit into a average human's hand; these were ergonomic considerations important to be implemented for reach the goal of a device with "moderate overall size and handy for the user". During loading, the user grasped with both hands the system: one hand was placed on handle and the other one over the external plastics of housing body. The housing body external plastics diameter chosen for keep the size low and host all the mechanical components was 38 mm, and for these plastics a minimum overall thickness of 2 mm had to be ensured to avoid any breakage caused by hands grasp pressure. For reduce the mechanism's overall lateral footprint on racks side, two indentations (circular countersinks to the right rack) were created for hosting inside the two screws used to fix the racks with hammer; this solution was adopted to reduce the lateral space. For the same purpose the cogwheels teeth were chamfered externally, this could reduce the overall footprint of these elements and the overall lateral size as well. Keeping low plastics diameters was also a fact of aesthetic appearance and a trial to follow the original syringe external design, Figure 2.10.

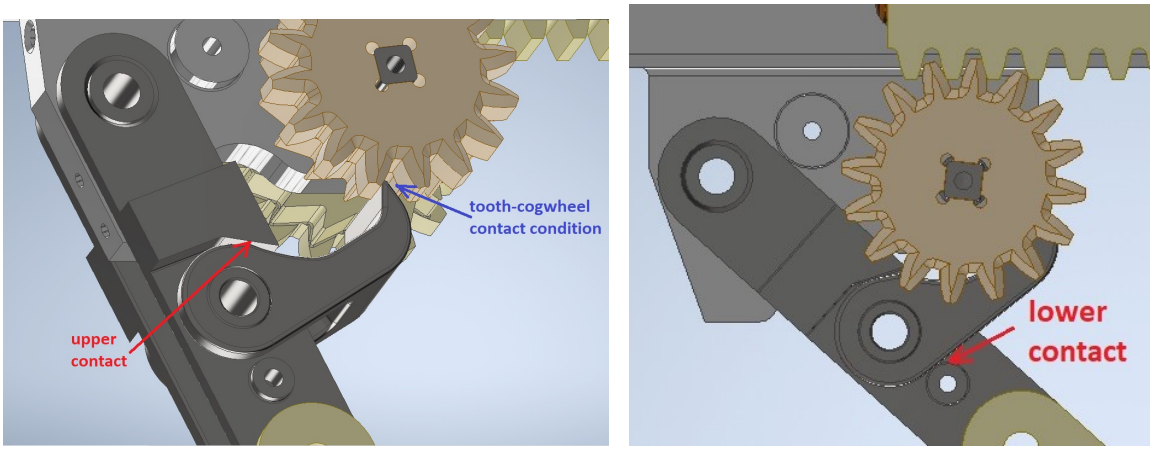

(a) Thrust hook upper constrain. (b) Thrust hook lower constrain.

Figure 2.9: Thrust hook upper and lower motion constrains.

Figure 2.10: First device rendering.

To keep the handle plastic in position when it was set back to its original position, against the main body plastics (after loading) two lateral snap-fit joints were created, as can be seen in Figure 2.11.

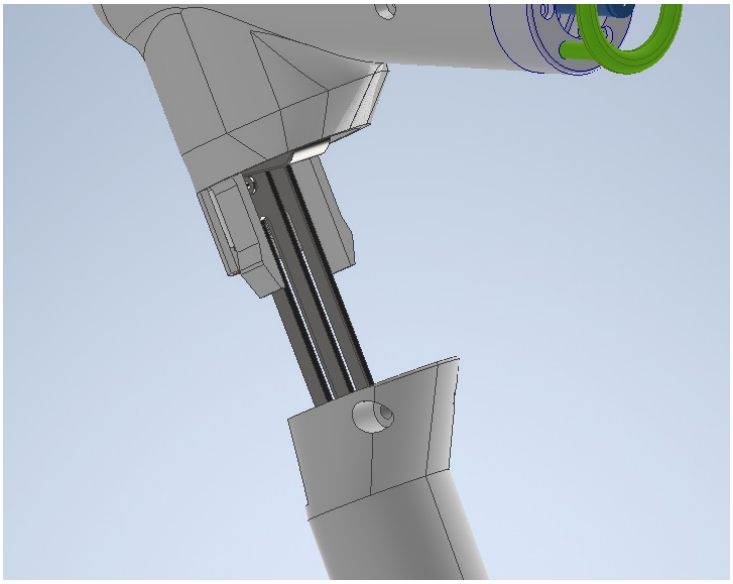

Figure 2.11: Lateral snap-fit joints.

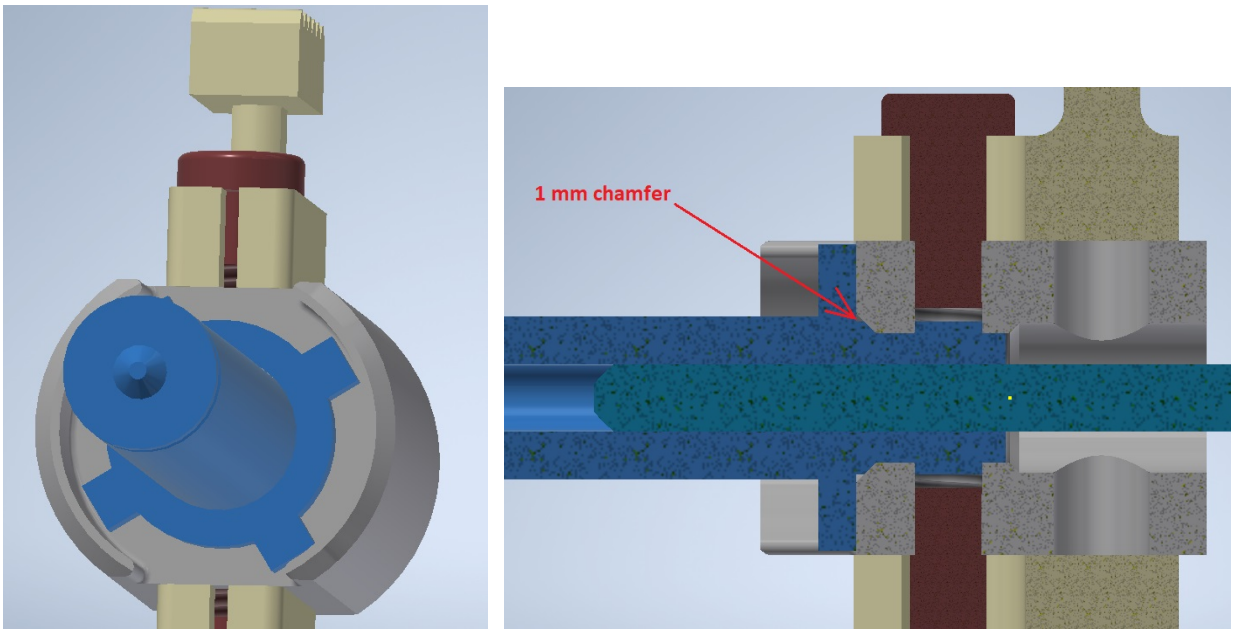

(a) Sliding base's edges (b) Sliding base's chamfer

Figure 2.12: Sliding base system.

These snap-fit joints had to be designed in such a way that no excessive force was needed to insert the handle but with enough stiffness to keep the handle firmly in place; the calculations relatively to the material and geometry selection for them are displayed in Chapter 4.

After the loading cycle was completed the user slid the ampule base forward and screwed the ampule on it. The base was designed with the point of view to avoid any mistake made by the user in screwing phase, as undesired misalignment between ampoule and syringe base. As can be seen in Figure 2.12, the base sides were extruded out to have a higher edge fitting exactly with the ampule external perimeter, in this way if the ampule axis was not perfectly aligned it could not be screwed creating a mechanical interference with these edges. In addition to that a chamfer of 1 mm was added around threaded hole's perimeter, just before the thread: this solution helped the ampoule to be guided inside the hole, aligning it, and avoiding any mistake during screwing. Another important coupling considered to simplify the interaction machine-user was the start button that opened the trigger, letting the system to inject. This button had an extended flap sliding on the trigger and during this motion the trigger tip, on the other side, was lifted making it loosing contact with the toothed bar, allowing the mechanism to snap. The angle of attach button-trigger had to be designed in order to have a progressive force application during sliding and at the same time a short button stroke (of few millimeters). The start button was designed with two springs, one upward and the other downward, to send back

the button to its initial position after it was pushed. In the contact between these two elements low friction coefficient was necessary to reduce the force at user's finger to push the button forward, Figure 2.13. To achieve this condition materials with low friction coefficients and with low roughness in the contact area, or materials treated to reduced the friction coefficient in the area of interest, had to be taken into account.

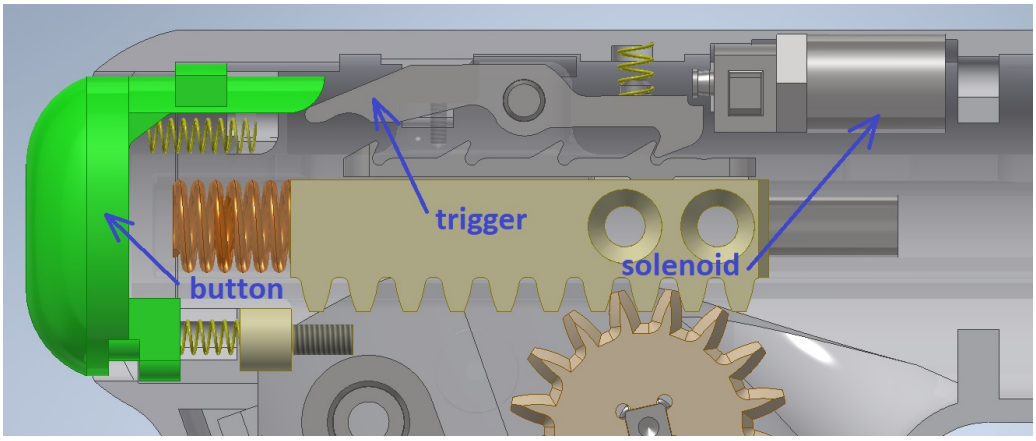

Figure 2.13: Trigger-button sliding system.

Another important system to be implemented into the assembly was the lock system for trigger, designed to avoid any undesired injection without the user control. To block the trigger a linear pull solenoid was considered, placed in longitudinal direction, as can be seen in Figure 2.13. In its unexcited position, its plunge was not retracted but left open to block the trigger movement; this was the position when no loading nor shooting was necessary for the system; this block on position allowed to operate in a safe way for the user avoiding accidental openings. When the solenoid was electrically exited its plunge was retracted inside and the trigger was left free to open if pushed: this condition would happen when the user had to load the spring system, this because the toothed bar had to be left free to slide and open the trigger coming in grip with it. At the end, when the user was ready to inject, the sensor ring was placed against the patient's body and this element was designed with plastic and smooth shapes to improve the tactile perception with patient's skin.

3 | Detailed design

In this chapter the project of needle-less syringe will be faced using techniques from advanced mechanical design practise, which means the assembly obtained so far will be analysed as a whole and improved using the Design for X techniques [16]. Under the label Design for X or Design for Excellence, a wide set of specific design guidelines are summarized. Each design guideline addresses a given issue that is caused by, or affects the traits of the product. The design guidelines usually propose an approach and corresponding methodologies that may help to generate and apply technical knowledge to control, improve, or even invent particular traits of a product. In the next Chapter all the critical components will be validated first analytically, where possible, and then with Finite Element Method (FEM) simulations, then the final shapes and materials will be chosen for each component, for an economical and durable design. At the end components technical drawings with relative tolerances and specifications will be displayed.

3.1. Design for X

The common points to all different DfX techniques (this makes the approach quite different from the traditional "good design practice") are the following [16]:

1. Talking about DfX, no matter what is the X (the design aspect), the design approach is finalized to improve some aspect of the project (manufacturability, assemblability, eco-sustainability, etcetera); the DfX techniques assume a quantitative (economic) performance evaluation of the proposed design solution.

2. The DfX techniques are applied horizontally, involving both the design engineers and the production ones (concurrent engineering).

3. By applying the DfX techniques it is possible to early address the design solutions and decisions and it is possible to choose those better satisfying the different requirements and present the best production cost. During the design stage possible changes have a lower impact in the total development effort.

3.1.1. Design for Manufacturing

The success of a product depends on the profit it generates and this latter is a function of the selling price and costs. The number of sold items and the sale price are mainly determined by the overall quality and complexity of the product. Design for Manufacturing (DfM) techniques aim to minimizing the manufacturing costs while maintaining a suitable product quality. The unit manufacturing cost of a product consists of costs in three categories [17]:

1. Component costs: The components of a product may include standard parts purchased from supplier. Other components are custom parts, made according to the manufacturers design from raw materials. Some custom components are made in the manufactures own plant, while others may be produced by suppliers according to design specifications.

2. Assembly costs: Discrete goods are generally assembled from parts. The process of assembling almost always incurs labor costs and may also incur costs from equipment and tooling.

3. Overhead costs: Overhead is the category used to encompass all of the other costs. The type of costs directly related to DfM are the support costs, which are costs associated with material handling, quality assurance, purchasing, shipping, receiving, facilities and equipment/tooling maintenance. These are the support systems required to manufacture the product, and these costs do greatly depend upon the product design.

In our assembly it could be observed that the extensible lever arm for loading was composed by two external different bars and an internal one sliding up and down, while extending and retracting it. The two lateral bars, instead of being two different mirrored pieces, could be manufactured as a single piece. This solution remove a redundant upper constraint (lateral extrusion) for the thrust hook but would reduce the manufacturing costs since the computer numerical control (CNC) mill machine could produce two identical pieces in series instead of two different ones, reducing the machine set-up time. The material selected for these lateral bars and the central sliding bar was an aluminium alloy such Aluminium 6068-T6; this choice in Design for Manufacturing was justified since aluminium is easier to be worked and cut compared to steel because it is soft and it chips easily. This aluminium alloy was less expensive than inox steel, and required less power to be machine and leading to a lower CNC tools wear, for this reasons having parts in aluminium it was a choice in accordance with DfM techniques. In Figure 3.1 it is shown how the same bar element was used in two different positions.

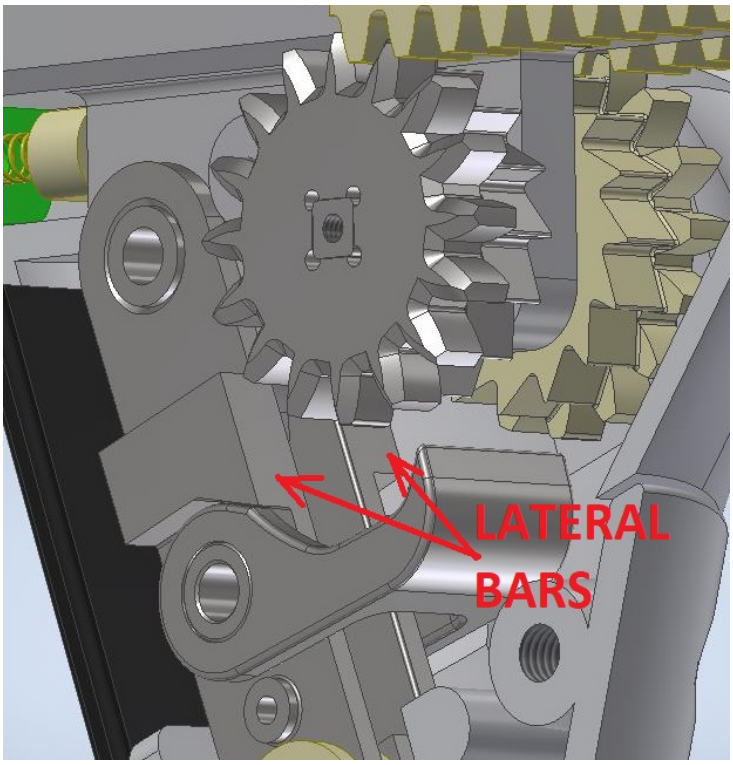

Figure 3.1: DfM: double lateral bar.

For the same reasons explained before for aluminium parts in DfM application, the housing body containing the main spring was designed to be manufactured in Aluminium 6082-T651 too. In addition to components manufacturability, the choice of aluminium was compliant with the system weight reduction, in fact the aluminium has a density of 2.7 g/cm^3, which for a piece volume of 22071.112 mm^3 resulted in a weight of 60 g; if the same piece would be made of steel with a density of 7.850 g/cm^3 the weight was 173 g, almost three times the weight with aluminium alloy. In general for custom parts, where it is technically feasible and no specific characteristics are required, aluminium alloy instead of steel is a DfM selection. These choices will be compared with other DfX techniques in the dedicated sections, and in Chapter 4 the geometries and materials will be validated through Finite Element Analysis before the final design decisions. Another application of DfM in assembly components was to keep each fillet and internal radius above 0.7 mm, where to manufacture them a small tool tip was required. This because many mechanic shops do not use milling machine tips with diameter lower than 1.5 mm, and very small tips can be broken easily, increasing the manufacturing costs. This solution did not include the external radius or tool machining radius (in many machine tool it is equal to 0.2 mm) since they do not require small tool tips but are part of machining processing. One last rule to apply in DfM was to avoid complex geometries for all the

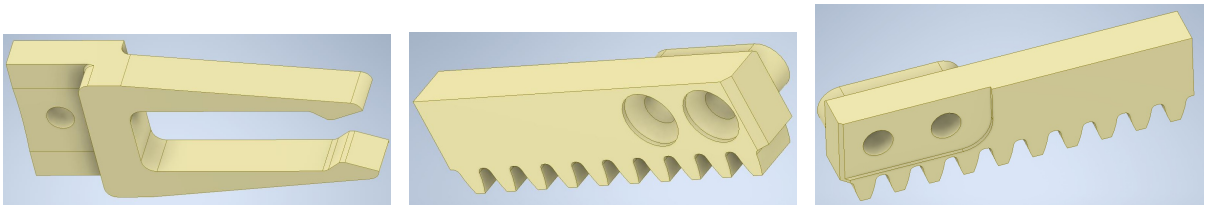

(a) Outer snap-fit joint. (b) Right plastic rack. (c) Left plastic rack.

Figure 3.2: Parts modelled for a future injection moulding application.

parts made with CNC machines, this decreased manufacturing time and costs. More complex geometries were left for 3D printing technology, allowing a smaller impact on manufacturing time than CNC machined parts even with complex geometries. For parts assigned to 3D printing technology particular attention was payed on their shape and geometry for a future injection moulding production, as can be seen in Figure 3.2.
Injection moulding production technique [18] is suitable for large scale production, and the parts produced with this technique must be properly designed to reduce production costs. One first factor that impacts on costs is the mould complexity: a mould with a high number of cavities influence the machining time for produce it and has a higher clamp force required to keep it closed during the injection. A general guideline for design a part for injection moulding is that the main wall should have uniform thicknesses and tapered sides, thus making easier extraction from mould and to avoid possible distortion due to not uniform cooling. Another important rule is to use ribs and avoid relevant thickness changes, as well as not using too tight tolerances, even because the general ones are usually fine. In the components walls adequate angles to extract the part from mould must be prescribed. It is very important to minimize the parts thickness, even using more expansive materials and/or ribs, since the production cost is proportional to the square of cooling time (t^2), but anyway the ribs thickness should be no more than 60% of the wall thickness, to avoid possible voids and defects. Another important rule is to use adequate fillet radii to avoid strong notch effects and to make easier the polymer flow in the mould. For the syringe external plastics a general wall thickness of 2 mm was selected, only in few zones a larger thickness was chosen to strengthen the area locally, but with a maximum of 3 mm thickness. All the plastic bosses for screw, as well as the other extruded details, were designed with tilted side walls, as can be seen in Figure 3.3. No sharp edges or thick connections were used for the plastics to obtain the first prototype design close to the plastics design for future injection moulding productions.

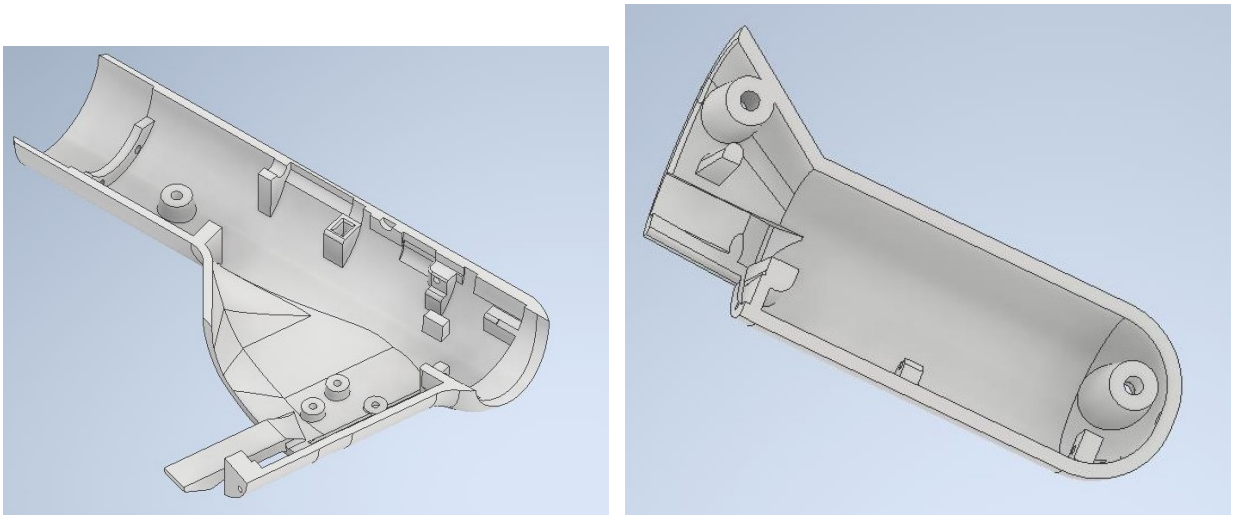

(a) Central body's plastic. (b) Handle's plastic.

Figure 3.3: External plastics designed for injection moulding application.

3.1.2. Design for Assembly

The right use of Design for Assembly (DfA) techniques is the application of a series of structured guidelines leading engineers toward the definition of a product able to cut the costs and to reduce the manufacturing issues [19]. Fewer parts in a product means less time to assemble them and DfA is a design process and concepts application for generate a product assembly containing as little parts as possible, easy to be handled and assembled together. The basic concept is that with a minimal number of parts, it is easier to assemble a product but it is also time-saving, which in return saves costs. DfA can lead to improvements in the reliability and quality of the product because a smaller assembly with fewer components have also less probability to fail than a component with a large number of components, thus with DfA the product can be produced to last for a longer period. The key principles of Design for Assembly are:

1. Reduce the total number of parts.
2. Develop a modular project.
3. Use standard components.
4. Design multi-functional parts.
5. Design for an easy processing.
6. Avoid screws.
7. Minimize the assembly directions.

8. Make the assembly easier.
9. Minimize the movements.

As seen before, DfA requires the project review to make it simpler and to reduce the components number, and to trigger ideas in line with these techniques, one can proceed by answering the following questions:

- During operation of the product, does the part move with respect of the other parts already assembled? (Do not consider elastic deformation).
- Is there any reason why a different material should be used with respect of the materials the other parts are made?
- Should the part to join be different from all other parts already assembled because otherwise necessary assembly/disassembly of other separate parts would be impossible?

These questions should be done for each components and, on the base of the answers, reduce the number of parts and make the project easier for assembly. But it must be kept in mind that integration of parts is not always the most economic solution and if a part *can* be eliminated/merged, it does not mean that the part *must* be eliminated; the assessment is up to the engineer. The analysis allows us to determine the minimum number of theoretically necessary parts.

The first action taken in the system assembly was to "reduce the total number of parts" starting from the smaller components and where possible they were blended with nearest

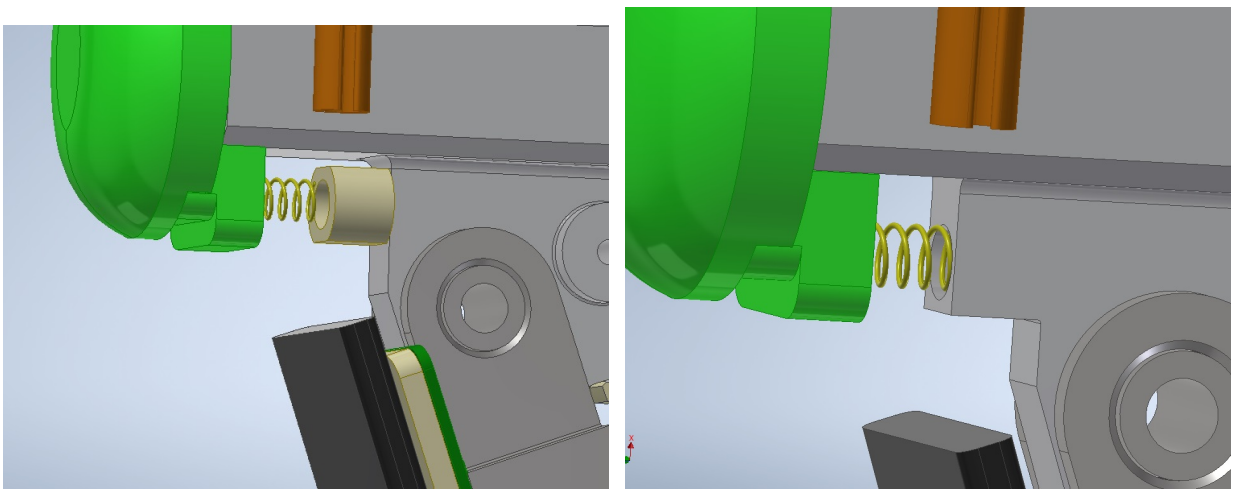

(a) Small spring's support (b) Housing body's spring support

Figure 3.4: Merging smaller parts with larger ones.

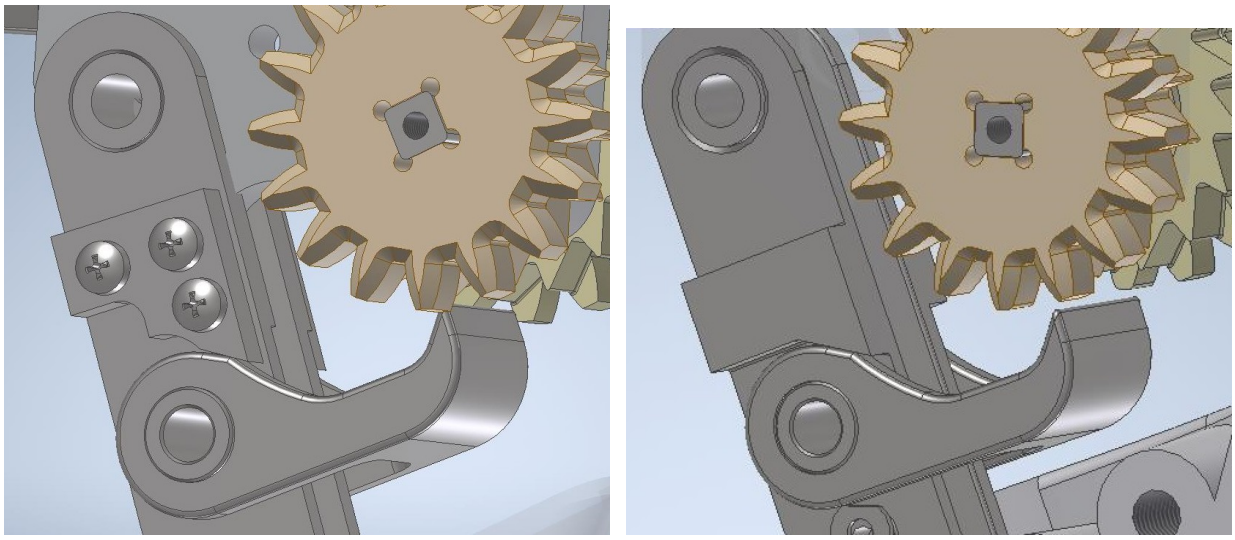

(a) Separated driving block. (b) Bar's extrusion for upper thrust hook constraint.

Figure 3.5: DfA application: reduce the number of parts and avoid screws.

larger components. As first integration, the back spring support could be blended to the housing body; in this way the total assembly was reduced by one element, see Figure 3.4. In the lever bar, during the first design attempt, the two lateral blocks designed to guide the thrust hook movements during loading were created separated from the lever and attached to it by means of three screws each. By merging these blocks into the bar creating an extrusion over it with the same block shape, six screws and two components could be saved reducing the assembly issues; this solution can be seen in Figure 3.5.

In the syringe sliding base there was the inner snap-fit joint composed by many components: inner snap-fit, sliding button and support connecting the snap-fit with sliding button. From DfA tables it can be seen that the parts thickness effect the handling time and consequently the assembly costs, also the component length has a similar effect. These last three components (snap-fit, metal support and sliding button) were merged together into a single plastic unit produced with 3D printing technology for the prototype and in injection moulding for future applications. For ensure enough strength polyether ether ketone (PEEK) was chosen as base material, as can be seen in Figure 3.6.

In Figure 3.7 the ring placed in front of injection system was conceived made of plastic, and it was the component coming in contact with the patient's body during the injection. The three springs placed after the three ring's supports were preloaded and ensured the right device pressure on patient's body. The three plungers placed inside the pressure ring were created with rubber tips on their extremities, this was the part coming in contact with the on-off switches, pressing them when the right pressure was achieved. In a first

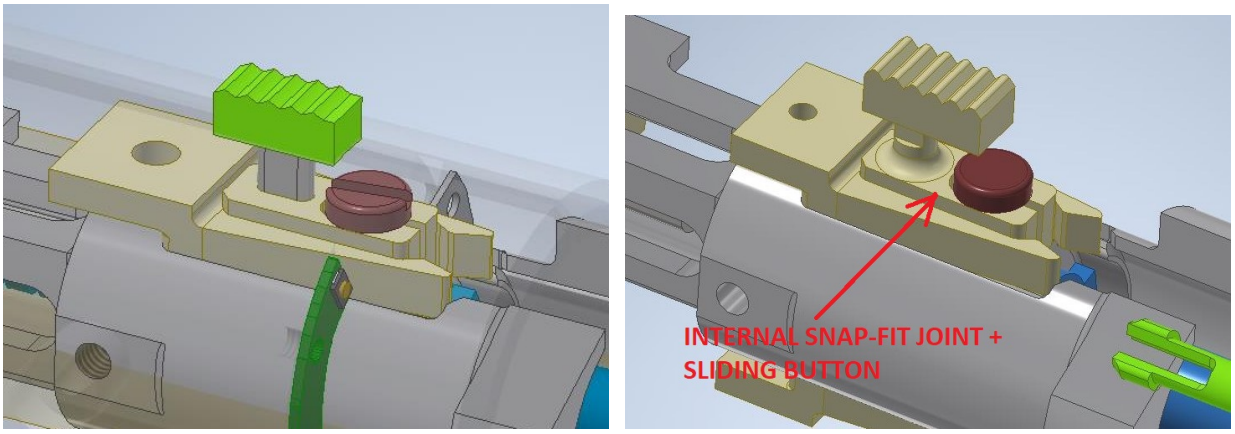

(a) Syringe sliding base. (b) Merging of snap-fit, support and sliding button.

Figure 3.6: DfA application: reduce parts and avoid small size components.

attempt without application of DfA techniques, these plungers were created using steel sticks. Applying DfA rules the question "Is there any reason why a different material should be used with respect of the materials the other parts are made?" was answered using plastic plungers made of the same ring's material, sufficiently rigid and strong, including their tips as well (Figure 3.7; the material selected was again 3D printed PEEK. Another improvement in reducing the elements total number regarded the extensible lever arm system, in particular to reduce the number of washers used for allow a smoother sliding between bars. This solution was an application of DfA since, true that washers could be taken from standard parts, but they were small and to keep all eight washers in place, in the same time, for placing and screwing the two bolts was difficult and time consuming for the assembler.

In DfA it is better to avoid the need of holding parts together to maintain their orientation during manipulation of the sub-assembly or during the placement of another part. If in place of two single washers, a double hole washer was placed, as can be seen in Figure 3.8, the assembly step would be much easier and fast. These washers were produced with 3D printing technology using nylon PA 12, for future application they could be manufactured with injection moulding.

For reduce the total number of bolts and screws used for joining the different elements, particular attention was payed to use the same type of screws and bolts were possible, meaning the same diameter and length. For example, as can be seen in Figure 3.9, the same bolt type was used for identical applications in four different positions. This was a DfA solution, in particular an application of the point "design multi-functional parts", because by using the same screw for multiple positions the assemblyman would not have to pay attention to find the right screw for each different position, saving time in assembly.

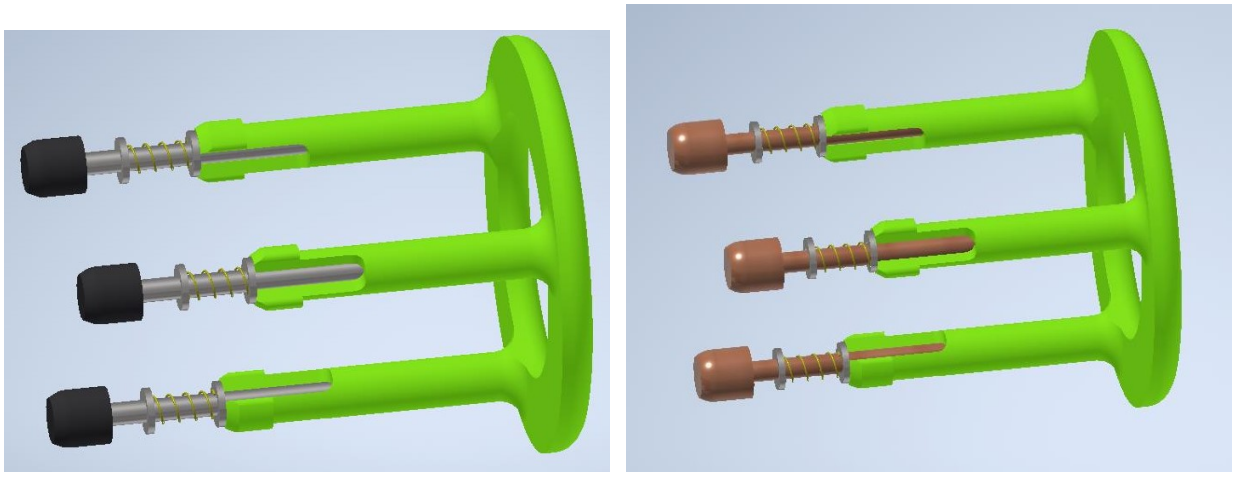

(a) Pressure ring and its components.

(b) Merging plungers and tips.

Figure 3.7: DfA application: reduce parts and use the same material.

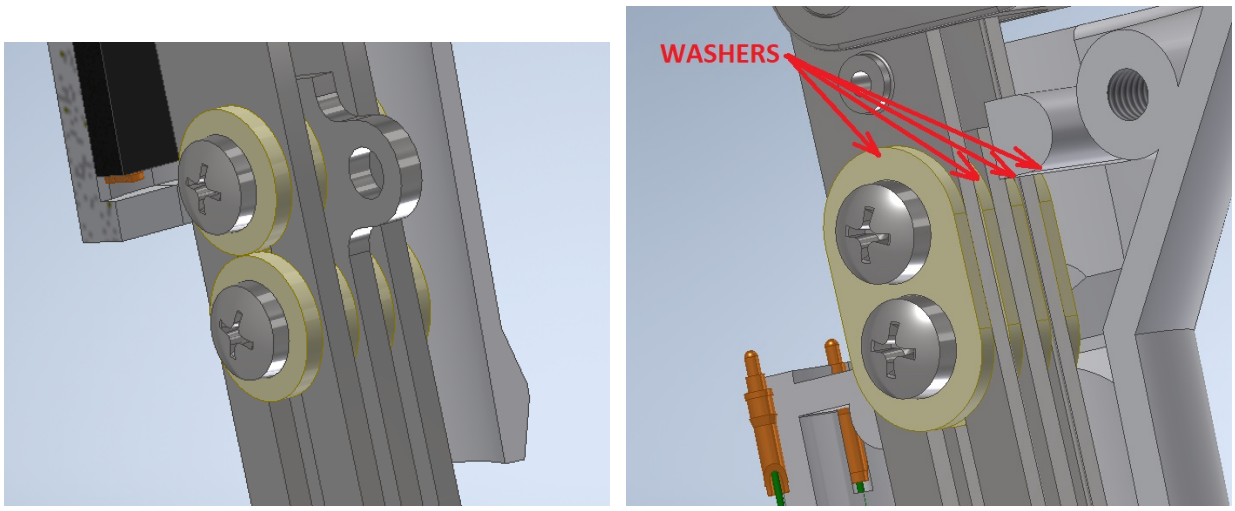

(a) Single washers.

(b) Double hole washers.

Figure 3.8: DfA application: simplify manipulation and parts' placement.

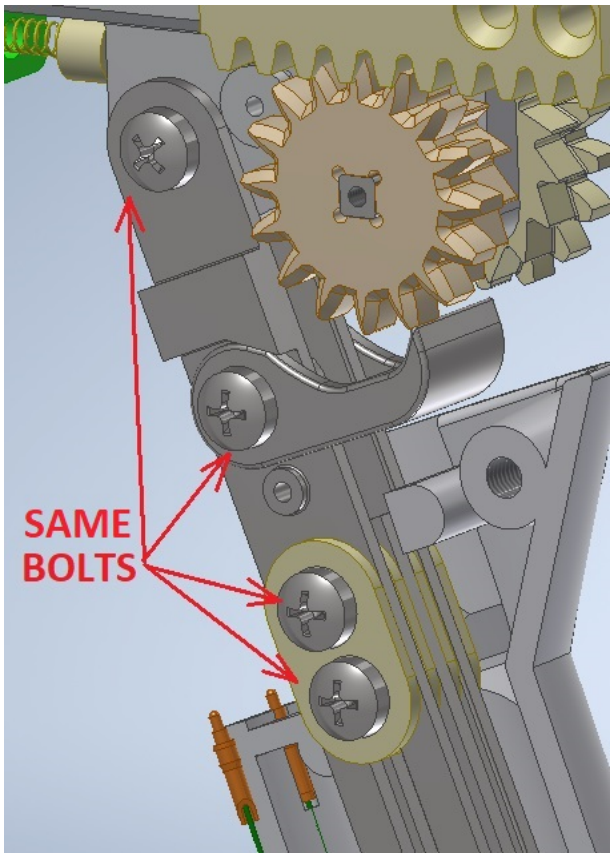

Figure 3.9: DfA application: use the same element where possible.

Another important aspect of DfA was the rule "Develop a modular project", this meant develop a sub-assembly of components that could be taken apart or assembled and mounted separately before to be added on the main assembly. This concept was applied to the assembly front part, in fact the ring with pressure plungers system was created with a dedicated plastic housing able to be assembled alone and added later on to the main assembly, fixing it to aluminium housing body by means of three screws; as shown in Figure 3.10.

As also seen before, to reduce the assembly time it was fundamental to "minimize the movements" and "make the assembly easier"; other parts where this principle could be applied were the external plastics by designing hexagonal cavities fitting with the external shape of hexagonal nuts used in the bolts to close the plastic handle. This solution would save time for the assembly step since the operator had less problem to fix and keep the nut down in place while screwing the bolt for connecting the plastics together, as we can see in Figure 3.11.

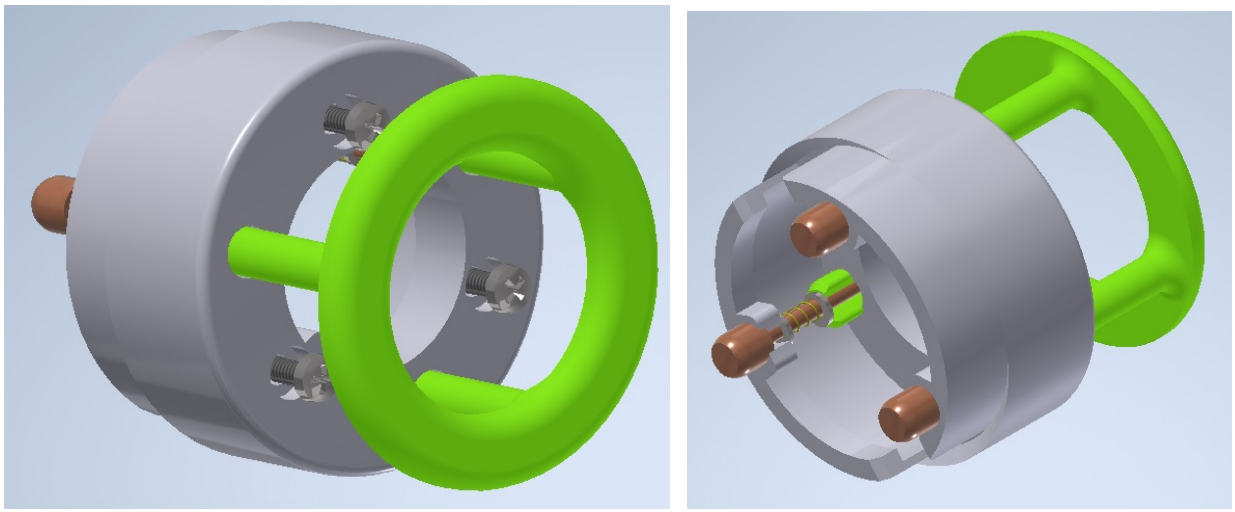

(a) Modular element front view. (b) Modular element back view.

Figure 3.10: DfA application: develop a modular project.

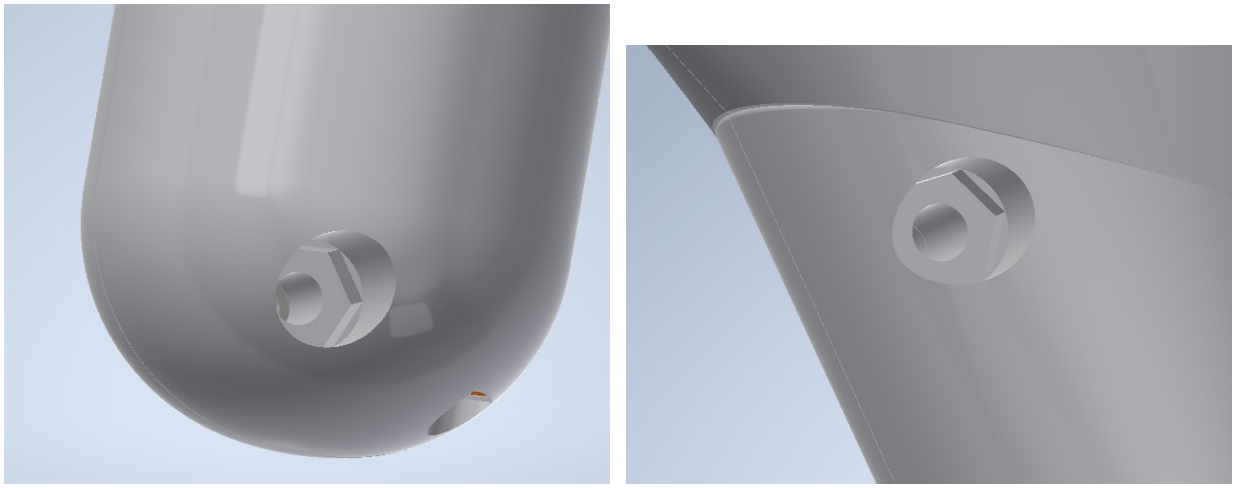

Figure 3.11: DfA application: add locations for keeping the elements in place.

3.1.3. Design for Environment

Design for the Environment (DfE) is a design approach to reduce the overall human health and environmental impact of a product, process or service, where impacts are considered across its life cycle, while still making products usable but minimizing resource use. The key focus of DfE is to minimize the environmental-economic cost to consumers, in fact practitioners of DfE have also found that effective DfE practice can maintain or improve product quality and cost while reducing environmental impacts [17]. Environmental impacts of a product may include energy consumption, natural resource depletion, liquid discharges, gaseous emissions, and solid waste generation. These impacts fall into two broad categories: energy and materials, and both represent critical environmental problems that need to be solved. For most products, addressing the energy problem means developing products that use less energy, but to address the material problem is not straightforward. During the early stages of the product development process, deliberate decisions about material use, energy efficiency, and waste avoidance can minimize or eliminate environmental impacts. However, once the design concept is established, improving environmental performance generally involves time-consuming design iterations. DfE therefore may involve activities throughout the whole product development process and requires an interdisciplinary approach. Industrial design, engineering, purchasing, and marketing all work together in the development of eco-friendly products. Even if the DfE can vary with the industrial sector they are applied, a series of guidelines has been defined and inspires the DfE actions in the different industrial sectors. The "Ten Golden Rules" [20] of DfE, developed at the Royal Institute of Technology in Stockholm (KTH), in Sweden, nowadays are used as reference in many industrial sectors (Bombardier, Volvo, Philips, etc). They were developed by Conrad Luttropp as the ten "lowest common denominators" of the most common issues that must be addressed in Eco-Design. These ten rules are a tool that should be used for the product design:

1. Rule 1 – *Do not use toxic substances and arrange closed loops for necessary but toxic ones.*
   Meaning to identify which toxic substances are currently used in the product which you are working with. Try to find a non-toxic substitute that fulfils functional and economic requirements of the product. Ascertain if closed loops are already established or can be developed and utilized for recycling materials including the toxic substances.

2. Rule 2 - *Minimise energy and resource consumption in production phase and transport through housekeeping.*

Re-use parts and components if they guarantee the same quality and performance. Optimize the provision and the distribution logistics (as fill the truck completely, use alternative and less-consuming energy systems). Optimize packaging. Reduce the use of consumables (as oil). Put the waste in dedicated containers.

3. Rule 3 – *Use structural features and high quality materials to minimise weight not interfering with necessary flexibility, impact strength or functional priorities.*
   Minimize the quantity of materials (de-materialize the product). Use light materials. If you are using aluminium, make sure it is recycled. Think about optimal solutions from a structural point of view (stiffness/weight, strength/weight, etc): this is important for products with many start and stop transients (as vehicles).

4. Rule 4 – *Minimize energy and resource consumption in the usage phase, especially for products with most significant aspects in the usage phase.*
   Choose renewable energy sources. Reduce the aerodynamic drag. Choose high-efficiency electronic components. Choose high-efficiency electronic components. Make easier the count of energy consumption. Use energy losses for other scopes.

5. Rule 5 – *Promote repair and upgrading, especially for system dependent products (cell phones, PC, CD players, TV, etc).*
   Try solutions able to make economically sustainable repairs and up-grading. Make sure that the parts to change or to up-grade are easily dis-mountable and/or accessible. Define modular products to make easier repairs. The instructions should have details on how making easier and simpler repairing.

6. Rule 6 – *Promote long life for products, especially for products with most significant environmental aspects out of usage phase.*
   Start from ”classical” solutions. Develop “robust-designed” products, able to satisfy the requests of the users even when the in-service conditions are different form the design ones. Optimize the maintenance intervals. Design for making easier updating. Design and/or use long-life components.

7. Rule 7 - *Use better materials, surface treatments or structural arrangements to protect products from dirt, corrosion and wear.*
   Reduce the wear-induced residuals (improve wear resistance). Identify coatings and treatments to avoid/reduce corrosion. Isolate hazardous or toxic substances and make not possible any leak. Prefer closed-loop water systems and avoid contamination of the used water. Prefer processes with reduced emissions.

8. Rule 8 - *Prearrange upgrading, repair and recycling trough access ability, labelling,*

modules, breaking points, manuals.
Make easier the removal of the parts to recycle by attaching labels, especially the ones that have toxic substances. Use the terms used by the ISO 11469 code to name polymers. Make sure that the instructions for recycling are in the product manual. Make easier assembly by means of markers.

9. Rule 9 - *Promote upgrading, repair and recycling by using few, simple, recycled, not blended materials and no alloys.*
Use as little materials as possible. Consider just homogeneous materials. Do not use paints or coatings if not needed. Leave the polymers clean, without any paint, glue, adhesive or metal inserts. Choose recyclable materials.

10. Rule 10 - *Use as few joining elements as possible and use screws, adhesives, welding, snap-fits, geometric locking, etc. according to the life cycle scenario.*
Use the minimum number of joints. Minimize the number of parts. Avoid glue. Use standardized joints. Do not use joints that must be destroyed to reuse the parts. Use snap-fits, screws, joints by shape, welding. This because disassembly plays an important role not only enabling parts and materials to be removed for recycling but also enabling reconditioning, refurbishment, re-manufacture, repair and service of the product and components extending their life. It is a design strategy that considers the cost and the need to disassemble a product for repair, refurbish or recycle.

The 10 Golden rules must be adapted to the different contexts where they are used, because some of them have contradictory aspects and it is not possible to define the "best solutions". There is the need to provide a guide for the definition of the best acceptable trade-off and justify and explain the proposed solutions.
In the needle-less syringe design *Rule 6* could be applied to plastics by adding ribs inside the central plastics and in the handle plastics. Ribs created a stiffer and more durable structure, and this was an important point for plastics subjected to hands grip pressure during loading. The ideal design for plastics, according to *Rule 3*, was having a limited overall plastic thickness, to save material, and where needed adding ribs and tilted side wall to reinforce the structure locally, as can be seen in Figure 3.3, described in Section 3.1.1. The material selected for these plastics was acrylonitrile butadiene styrene (ABS) suitable for medical application, also called ABS Medical with physical and mechanical properties shown in Figure 3.12:

Materiali	Tecnologia Fused Deposition Modeling (FDM)		
	ABS Medical classic	**ABS Medical** performance	**ABS Medical** top mechanical
Colore naturale del materiale	bianco		
Finiture disponibili	Bianco naturale		
Densità	1,20 g/cm³		
Formato massimo teorico	300x300x600mm (11.8x11.8x23.6 in)		
Applicazioni	L'ABS è usato ampiamente in svariati settori quali l'automotive e l'industria di beni di consumo grazie ad un interessante mix di proprietà meccaniche, duttilità e resistenza alle temperature. Questo materiale è stato sviluppato, testato e certificato dal nostro reparto R&D per garantire la compatibilità con la pelle e come dispositivo medico nelle più diverse applicazioni.		
Tolleranza minima	±0,50mm sotto 100mm ±0,6% oltre 100mm		
Carico di rottura [MPa]	47,8	50	52
Modulo elastico [MPa]	1375	1375	1375
Allungamento a rottura o allungamento [%]	5	5,5	6

Figure 3.12: Medical ABS properties.

With "top mechanical" set-up the 3D printing machine could be set to run at a speed 25% lower producing a higher quality print with less defects. Considering *Rule 8*, ABS plastic is a thermoplastic with high recyclability degree and chemically similar (compatible) with other plastics, meaning it can be disposed with other plastics and recycled. In Figure 3.13, it can be seen that ABS is very compatible with polycarbonate (PC), but it is not compatible with nylon (PA) and for this reason the double hole washers introduced in Section 3.1.2, instead of PA 12 nylon, it would be better to be manufactured with a PC or ABS plastic. Another application of the same golden rule regarded the same material use where possible, and this included using Aluminium 6082-T651 alloy where it was acceptable from a mechanical point of view. For example, for the housing body, sliding base, solenoid support and extensible arms Aluminium 6082-T651 was used. For other parts as the toothed bar, trigger, racks, cogwheels, hammer and thrust hook, the *Rule 6* was chosen in place of *Rule 9* and the reason for that was that in these components high localized stress could arise during motion causing wear due to an excessive low surface

hardness. For this reason for promoting longer life of these components Inox 304 steel alloy was selected for the first prototype.

		Additive											
Matrix Material	Important Plastics	PE	PVC	PS	PC	PP	PA	POM	SAN	ABS	PBTP	PETP	PMMA
	PE	1	4	4	4	1	4	4	4	4	4	4	4
	PVC	4	1	4	4	4	4	4	1	2	4	4	1
	PS	4	4	1	4	4	4	4	4	4	4	4	4
	PC	4	3	4	1	4	4	4	1	1	1	1	1
	PP	3	4	4	4	1	4	4	4	4	4	4	4
	PA	4	4	3	4	4	1	4	4	4	3	3	4
	POM	4	4	4	4	4	4	1	4	4	3	4	4
	SAN	4	1	4	1	4	4	4	1	1	4	4	1
	ABS	4	2	4	1	4	4	3	4	1	3	3	1
	PBTP	4	4	4	1	4	3	4	4	3	1	4	4
	PETP	4	4	3	1	4	3	4	4	3	4	1	4
	PMMA	4	1	3	1	4	4	3	1	1	4	4	1

Source: VDI 2243, Georgia Institute of Technology, USA

1 = Compatible
2 = Compatible with limitations
3 = Compatible only in small amounts
4 = Not compatible

Figure 3.13: Plastic compatibility grid.

Chemical surface treatments as painting were discarded for a future product industrialization given that not-coated materials are better recyclable. Mixing of components with different material were avoided, as such permanent metal inserts in plastics.

3.1.4. Design for Reliability

Reliability is a measurement of the probability that a component/system works correctly for the time expected and in well defined environmental conditions. In other words, reliability measures the likelihood that a system will operate in well known and defined service conditions [17]. The concept of reliability is quite different from endurance: a product can be designed to last long but could be not reliable at the same time, and a product designed to work in limited and short periods can be very reliable. Thus Design for Reliability (DfR) is aimed at assessing the probability that a system works correctly for a given mission time and, in many cases, is aimed at maximizing this probability. DfR assumes the experimental observation for determining statistical quantities needed

to perform a reliability analysis. The knowledge and the ability to manage the statistical tools offered by DfR and the consequent ability to determine the reliability level of the designed product is enough to determine the reliability of the system but can fail in improving it, at least if the determined reliability value does not consider the behaviour of operators while interacting with the product. To face this problem some techniques for a detailed analysis of system components potential failure modes have been developed. These tools make also possible the assessment of the impact of the possible failures modes on the characteristics and on the reliability of the system itself. These techniques require the definition of objective indices that, properly combined, allow us to define the priorities of the interventions before, during or after the production phase, needed to achieve the desired and fixed reliability levels. These techniques are based on the analysis of the mode, the effect and the cause of the possible failures. The Failure Modes and Effects Analysis (FMEA) is the simplest technique for risks analysis and it is based on approximate hazard rates determined for each component. FMEA provides a systematic process to:

1. Identify and evaluate potential failure modes and potential causes of failure modes.
2. Identify and quantify the impact of potential failure modes.
3. Identify and prioritize actions to reduce or eliminate the potential failure modes.
4. Implement action plan based on assigned responsibilities and completion dates.
5. Document the associated activities.

To perform an appropriate FMEA analysis, it is important to know which are the fundamental definitions of the practice:

- Failure Modes: A specific loss of a function. It is a concise description of how a part, system, or manufacturing process may potentially fail to perform its functions.
- Failure Mode "Effect": A description of the consequence or ramification of a system or part failure. A typical failure mode may have several effects depending on which customer you consider.
- Severity Rating: Seriousness of the effect. Severity is the numerical rating of the impact on customers.
- Failure Mode "Causes": A description of the design or process deficiency (global cause or root level cause) that results in the failure mode.
- Occurrence Rating: An estimated number of frequencies or cumulative number of failures (based on experience) that will occur in our design concept for a given cause

over the intended "life of the design".

- Failure Mode "Controls": The mechanisms, methods, tests, procedures, or controls that available on site to prevent the "cause" of the Failure Mode or detect it.
- Detection Rating: A numerical rating of the probability that a given set of controls will discover a specific "cause" of Failure Mode to prevent bad parts leaving the facility or getting to the ultimate customer.
- Action Planning: A thoroughly thought out and well developed FMEA With High Risk Patterns addressing the high priority problems and solving them with remedial actions.

FMEA analysis is performed in three phases: qualitative, quantitative and corrective. In qualitative analysis all the possible failure modes that can happen in the system are taken into account and listed. The aim of this step is to identify failure modes, their effects and possible causes. The analysis starts from dividing the system in its sub-systems and components: for each of them the potential failure modes, the effects/risks of that failure modes and the possible causes are listed in a table. More than one cause can be associated to each failure mode. The considered failures are not only accidental but can be also due to a wrong use of the system, unfavourable environmental conditions, overloads, etc. The quantitative analysis comprises the identification of causes and effects of failure modes and control. In this phase it is quantitatively assessed how dangerous is a failure in term of the three factors mode-cause-effect. The index of Risk Priority Number (RPN) is defined as the value of the product of the three characteristics of cause-mode-effect which are "occurrence" (O), "detection" (D) and "severity" (S).

$$RPN = O \cdot D \cdot S; \tag{3.1}$$

The O is the "occurrence": index of the probability that the cause of the failure take place; D is the "detection": measures the probability that the control procedures and tools are able to detect the possible failure mode; and S is the "severity": measures the gravity and how dangerous is the failure mode. The values of O, D, S are given by standards or by internal documents, as for Examples (SAE J 1739) [21], and these values range from 1 to 10. The steps to complete a FMEA analysis can be set in a standard table and filled for each critical component as shown in Figure 3.14:

Process Step / Input	Potential Failure Mode	Potential Failure Effects	SEVERITY	Potential Causes	OCCURRENCE	Current Controls	DETECTION	RPN
What is the process step and Input under investigation?	In what ways does the Key Input go wrong?	What is the impact on the Key Output Variables (Customer Requirements)?		What causes the Key Input to go wrong?		What are the existing controls and procedures (inspection and test) that prevent either the cause or the Failure Mode?		
								0
								0
								0

Figure 3.14: FMEA grid.

The occurrence ranking is based on the likelihood, or frequency, that the cause (or mechanism of failure) will occur. Once the cause is known, it is fundamental to capture data on the frequency of these causes. Sources of data may be scraps, rework reports, customer complaints and equipment maintenance records. A general tables of values is displayed in Figure 3.15; this reference can be used for an estimation of the real value to assign at a certain component or interaction.

Occurrence	Rank	Criteria
Extremely Unlikely	1	Less than 0.01 per thousand
Remote Likelihood	2	≈0.1 per thousand rate of occurrence
Very Low Likelihood	3	≈0.5 per thousand rate of occurrence
Low Likelihood	4	≈1 per thousand rate of occurrence
Moderately Low Likelihood	5	≈2 per thousand rate of occurrence
Medium Likelihood	6	≈5 per thousand rate of occurrence
Moderately High Likelihood	7	≈10 per thousand rate of occurrence
Very High Severity	8	≈20 per thousand rate of occurrence
Extreme Severity	9	≈50 per thousand rate of occurrence
Maximum Severity	10	≈100 per thousand rate of occurrence

Figure 3.15: Occurrence values table.

To assign detection rankings, it is fundamental to identify the specific process or product

type involved, and related controls available in place for each failure mode, then at each control a detection ranking is assigned; note that naked eye visual inspection is considered technically as a control. Detection rankings evaluate the current control process taken in place for a specific product or material. A control can be related to failure mode itself, the cause (or mechanism) of failure, or the effects of a failure mode. To make evaluating controls even more complex, controls can either prevent a failure mode or cause from occurring, or detect a failure mode, cause of failure or effect of failure after it has occurred. The table containing the values for the evaluation of detection rank is shown in Figure 3.16.

Detection	Rank	Criteria
Extremely Likely	1	Can be corrected prior to prototype/ Controls will almost certainly detect
Very High Likelihood	2	Can be corrected prior to design release/Very High probability of detection
High Likelihood	3	Likely to be corrected/High probability of detection
Moderately High Likelihood	4	Design controls are moderately effective
Medium Likelihood	5	Design controls have an even chance of working
Moderately Low Likelihood	6	Design controls may miss the problem
Low Likelihood	7	Design controls are likely to miss the problem
Very Low Likelihood	8	Design controls have a poor chance of detection
Remote Likelihood	9	Unproven, unreliable design/poor chance for detection
Extremely Unlikely	10	No design technique available/Controls will not detect

Figure 3.16: Detection values table.

The severity ranking is an estimation of how serious an effect would be if it occurs. To determine the severity, it must be consider the impact that effect would cause on the customer, on downstream operations or on the employees operating the process. Also severity ranking is based on a relative scale ranging from 1 to 10, with R = 10 meaning that effects have a dangerously high severity value leading to potential hazard without warning; the values 9 and 10 comprise hazardous effect which are, in most cases, unacceptable for a product. In some applications even if the "occurrence" (O) and "detection" (D) are low but the "severity" (S) value is high, corrective actions must be taken to reduce the severity even if the RPN value is relatively low. The table with severity values can be seen in Figure 3.17.

Effect	Rank	Criteria
None	1	No effect
Very Slight	2	Negligible effect on Performance. Some users may notice.
Slight	3	Slight effect on performance. Non vital faults will be noticed by many users
Minor	4	Minor effect on performance. User is slightly dissatisfied.
Moderate	5	Reduced performance with gradual performance degradation. User dissatisfied.
Severe	6	Degraded performance, but safe and usable. User dissatisfied.
High Severity	7	Very poor performance. Very dissatisfied user.
Very High Severity	8	Inoperable but safe.
Extreme Severity	9	Probable failure with hazardous effects. Compliance with regulation is unlikely.
Maximum Severity	10	Unpredictable failure with hazardous effects almost certain. Non-compliant with regulations.

Figure 3.17: Severity values table.

After the evaluation of the RPN index of each critical components with Equation 3.1, another column is added to the last one, with the corrective actions to reduce the RPN value, i.e. the criticality and danger of the failure mode. The solution can be suggested by the analysis of the RPN index (high values of O, D or S suggest the corrective actions), if one of the three constituent points is reduced individually or in combination with another the total RPN value can be monitored. In fact RPN gives a relative risk ranking and higher the RPN is, higher is the potential risk. Of course, as mentioned before, prioritize the risks by sorting the RPN from highest score to lowest score will help the team to determine most critical inputs and causes generating failures. The "Action Plan" outlines what steps are needed to implement the solution, who will do them and when they will be completed. At the end, after the corrective action plan has been taken the RPN is calculated again for each critical component to check if it dropped satisfactorily. In Table 3.1 the first FMEA analysis performed on our assembly components is shown, and then the elements with the highest RPN value or an unacceptable high value of "severity" were considered one by one and handled with proper corrective actions aimed to reduce the final RPN value. In Figure 3.18 the assembly with the critical elements considered for FMEA are shown.

ELEMENT	FAILURE MODE	EFFECT	CAUSES	O	D	S	RPN
CAP BUTTON (1)	Button sliding part wear out and have a high roughness	Higher force is required from the user's finger. Button can be blocked inside.	Wear during usage. Friction coefficient between the trigger and the cap button is too high.	4	7	7	196
TRIGGER (2)	Undesired loose of grip with the toothed bar	The spring cannot be kept charged, undesired shoot.	Wear and wrong angle of attach between trigger and toothed bar.	3	6	7	126
TOOTHED BAR (3)	Teeth breaks after many cycles.	The spring cannot be kept charged, undesired shoot.	Wear due to friction. Fatigue failure.	3	6	7	126
LOCK SNAP-FIT JOINT (4)	Snap-fit breaking.	The syringe base cannot be held in place.	Fatigue, wrong element dimensioning or defects inside the material.	5	3	6	90
ON-OFF SWITCH PCB (5)	They are not pushed in the same time even if the right pressure is reached.	The solenoid is not dis-activated. The system can not shoot.	Wrong geometric tolerances, the calibrated springs are too stiff.	3	4	7	84
RACK (6)	Racks teeth breaking.	The loading system does not work.	Defect inside the material. Fatigue failure.	3	5	7	105
COGWHEEL (7)	Cogwheel's internal teeth breaking or wearing out.	Decrease of performances or the system can not be loaded.	Wear between thrust hook and cogwheels internal teeth.	6	6	6	216
THRUST HOOK (8)	Slip on cogwheels teeth without transmitting the force. Loose of contact.	Spring cannot be loaded properly. Loss of efficiency.	Wrong tolerances or geometries.	6	5	6	180

THRUST HOOK (8)	Thrust hook goes in contact with cogwheels teeth during shooting.	The system is blocked and cannot shoot.	Wrong geometric tolerances or geometries.	4	5	7	140
HANDLE PLASTIC (9)	Plastics get cracked.	Aesthetic defects. Usability problems.	Wrong thickness and defects.	5	5	5	125
BACK SWITCH PCB (10)	The on-off switch is not pushed when the lever is in place.	The solenoid is not dis-activated and the system cannot shoot.	Wrong geometric tolerances or wrong on-off switches.	5	4	8	160

Table 3.1: Failure Mode and Effect Analysis.

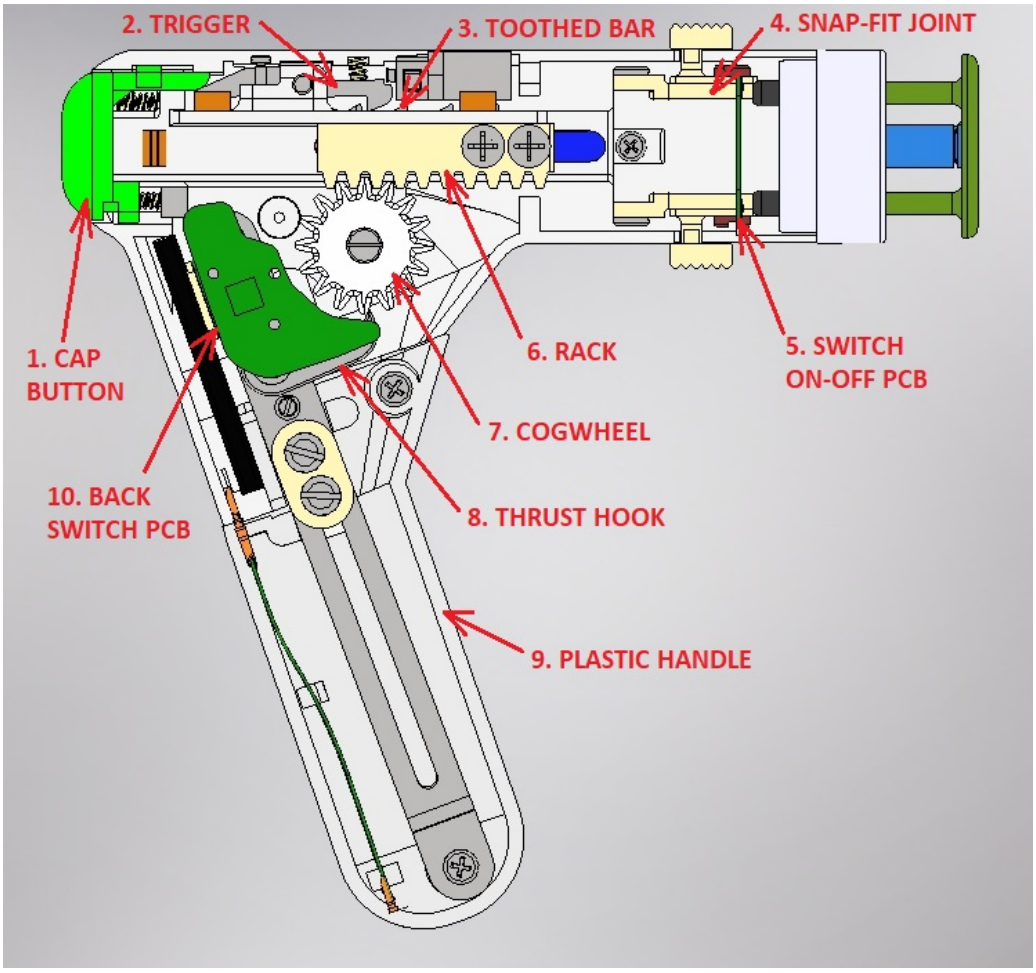

Figure 3.18: Assembly list for FMEA.

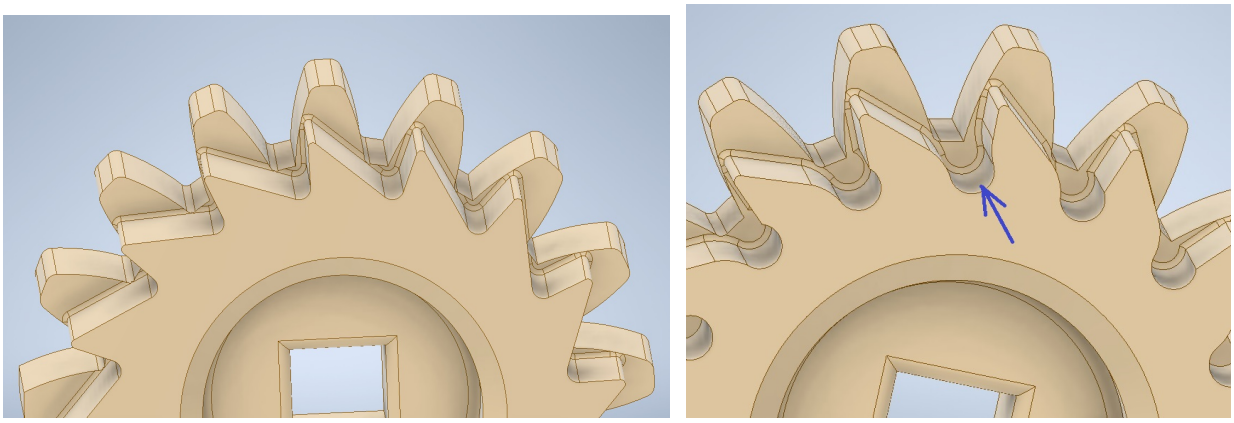

Figure 3.19: Contact surface increasing of cogwheels internal teeth.

From the FMEA analysis the element found with the highest RPN value was the cogwheels shark-tooth-shaped internal teeth. Due to continuous contact back-and-forth with the thrust hook during the loading action, they could wear out reducing the contact area and compromising the system efficiency. In order to prevent any premature wear, it was important to select a material with sufficient surface hardness or to treat the materials surface to increase the hardness. This point could be specifically improved by selecting a steel alloy as Inox 304, also in accordance with the point found in section 3.1.3, in Design for Environment. Another corrective action that could be taken into account for the same criticality was to increase the element's contact surface with the thrust hook: this solution would decrease the contact pressure between these two elements and consequently the local stress on the cogwheel tooth during contact. A hole at the cogwheels teeth base, as shown in Figure 3.19, would increase the available contact area between these elements.

After applying these considerations and modifications, this element was reassessed with FMEA reference tables an a new RPN value was obtained, as can be seen in Table 3.2.

ELEMENT	FAILURE MODE	EFFECT	CAUSES	O	D	S	RPN
COGWHEEL (7)	Cogwheel's internal teeth breaking or wearing out.	Decrease of performances or the system does not work.	Wear between thrust hook and cogwheels internal teeth.	3	6	6	108

Table 3.2: Cogwheels improvement and new RPN value.

The value of RPN was under control because with an accurate FEM analysis and proper

material selection the occurrence of unexpected failures or wear could be reduced. Moreover the surface on the contact area had to be smooth and hard, the smoothness was a parameter that could be controlled by means of a fine roughness in the technical drawing specification. The second element to be considered for increase the system reliability was the cap button. This element was made of plastic material and had a long sliding flap inside syringe body, moving over the trigger and activating it. For work properly the two surfaces had to be smooth and this could be controlled by selecting the proper plastic material and technology for the cap button and control the roughness on the trigger area in contact with button at 0.8 μm. If this control parameter was specified on technical drawing the occurrence of wrong surfaces could be avoided, Table 3.3.

ELEMENT	FAILURE MODE	EFFECT	CAUSES	O	D	S	RPN
THRUST HOOK (8)	Slip on cogwheels teeth without transmitting the force. Loose of contact.	Spring cannot be loaded properly. Loss of efficiency.	Wrong tolerances or geometries.	2	4	6	48

Table 3.3: Thrust hook improvement and new RPN value.

For avoid any thrust hook slip on cogwheel during force transfer it was important to design properly the extrusions on the lever bars, guiding the motion of the thrust hook, with the right dimensional tolerances. This included also the lower circular extrusion, generating the lower motion constraint. The dimensional and geometric tolerances considered in technical drawing for lever bars extrusions are shown in Figure 3.20. In addition to these tolerances, in the housing body technical drawing, another tolerance on the distance of lever's hinge hole and shaft's hole, dedicated to support the two cogwheels, had to be controlled with a positional control. These tolerances were important for the same reason explained in Section 2.2.1: ensure the right contact and positioning at the beginning and end strike between the thrust hook and cogwheel; Figure 3.21. The roughness in the contact area between shaft and housing body was 0.8 μm for the sliding coupling.

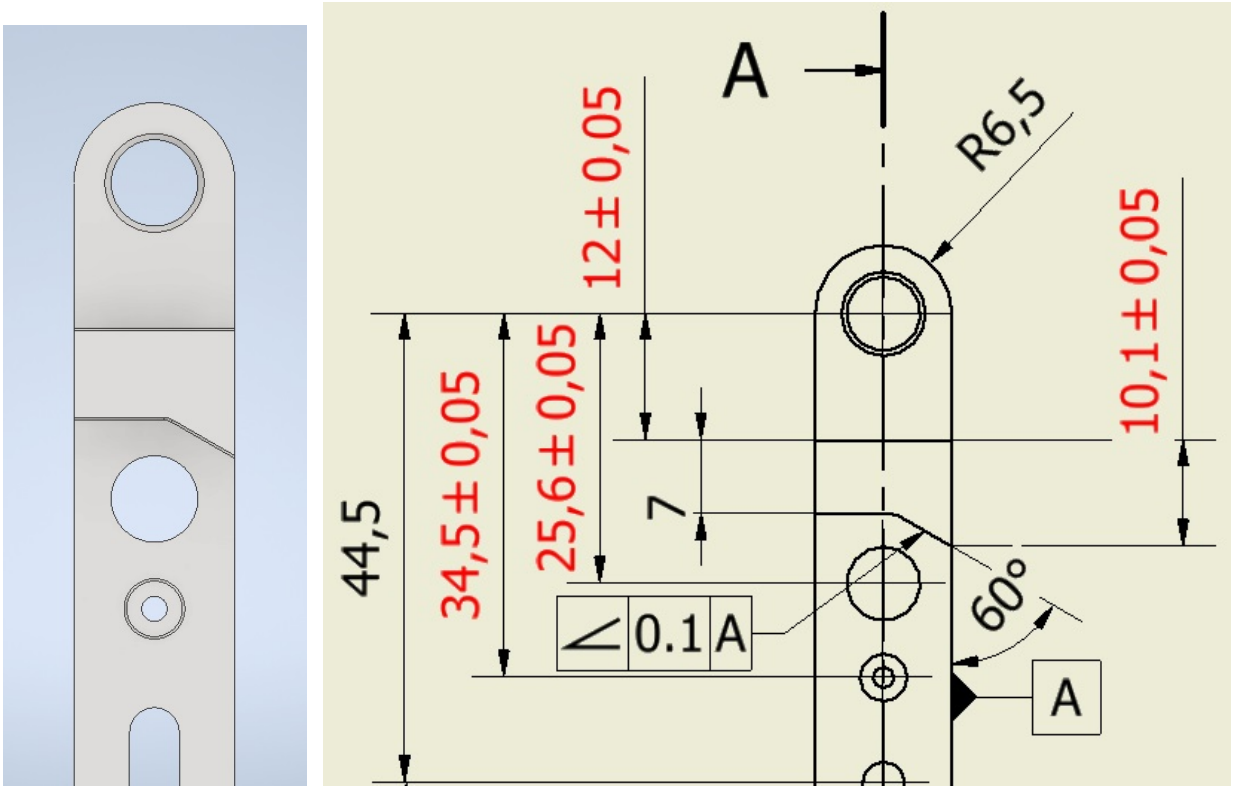

Figure 3.20: Dimensional and geometric tolerances after FMEA application.

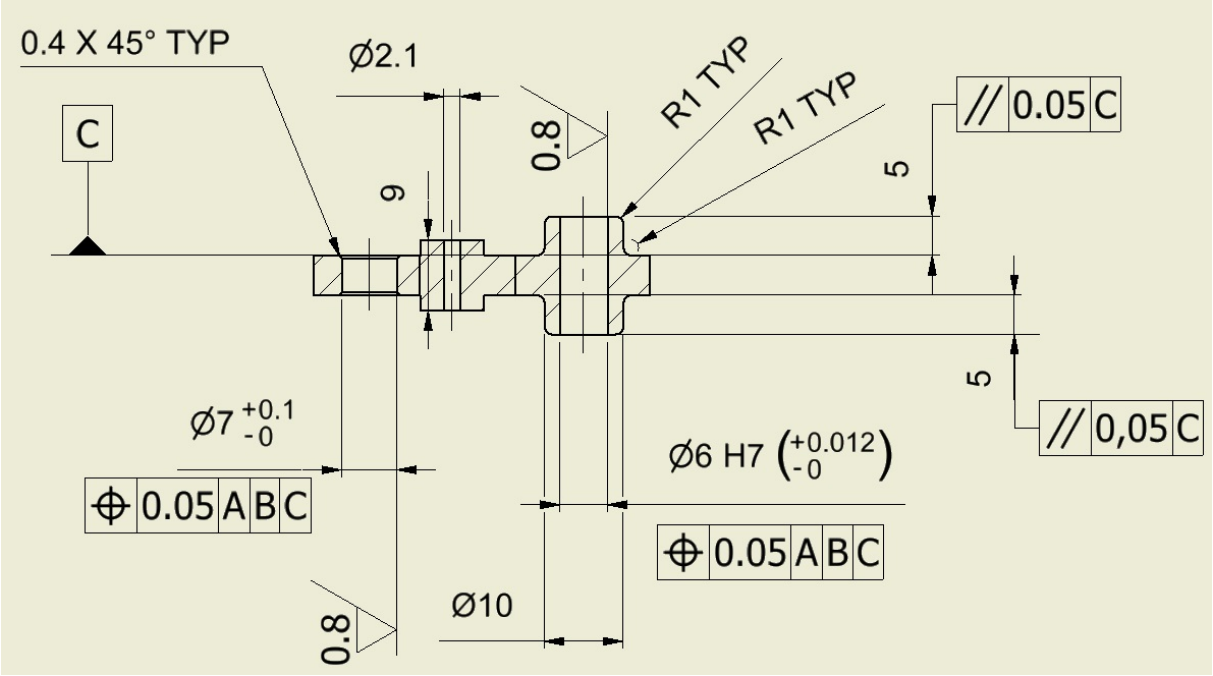

Figure 3.21: Dimensional and geometric tolerances on housing body's section.

Another element to take into account for increase the system reliability was the on-off switch behind the lever arm. This element was placed there to signal the solenoid to open or close when necessary. During the loading step, in fact, when the lever arm was detached from its usual position and moved forward to perform the loading action, the solenoid must be activated by the current making the solenoid plunger withdraw inside it. The solenoid had a spring inside its main body leaving the plunger out when no current flowed inside it, while when electrically exited, plunger was withdrawn inside. When it was not electrically exited the solenoid blocked with its plunger the trigger, while when it was exited it kept the plunger retracted and the trigger was left free to move, in this way the system could be mechanically loaded. The back switch had the task to let the solenoid be exited when the loading arm was moved from its starting position, but it had a high severity index because if the arm was, for any reason, not exactly in its original position pushing it, the system could not work properly: this would have meant an unlocked system able to shoot by accident. To decrease the severity index and the RPN while increasing the reliability, two back on-off switches working in parallel, instead of only one, were designed. This increased the system reliability since if just one of the two switches was pushed the signal of “arm placed in position” would be correctly achieved. The logical cycle handling the two switches was an "OR" cycle; it increased the system reliability despite the "AND" cycle, where two elements must work correctly at the same time to have the system working.

ELEMENT	FAILURE MODE	EFFECT	CAUSES	O	D	S	RPN
BACK SWITCH PCB (10)	The on-off switch is not pushed when the lever is in place.	The solenoid is always electrically activated and the system has the safety lock out of use.	Wrong geometric tolerances or wrong on-off switch (too stiff to be pushed).	3	4	6	72

Table 3.4: Switches set-up improvement and new RPN value.

In the overall system the choice to have double cogwheels, racks and double snap-fit joints has been made also considering the theoretical improvement of reliability having two elements working in parallel in place of one working in series with others.

4 | Components validation through Finite Element Method

Optimum design is defined by the Oxford Dictionary of Mechanical Engineering as "a design in which a particular feature is optimized, such as a structure designed to have minimum weight when satisfying all the specifications" [15]. After have reached an acceptable assembly quality in terms of manufacturability, assemblability, reliability and other main DfX requirements it is necessary to validate the mechanical stability and strength of elements subjected to the highest strains and stresses. In this section the process applied to reach a robust and optimum design for each critical component is performed with the use of Finite Element Method (FEM) using Abaqus CAE.

4.1. Analytical analyses

An analytical analysis or analytical method is a procedure or method for the analysis of a problem by means of a defined mathematical calculation. Before perform a FEM analysis, analytical analysis is useful to obtain a reference value to be compared with same result obtained with FEM analysis and evaluate the goodness of the numerical analysis just carried out. It is not always applicable, since some problems can be only modelled and worked out with computer software, for the reason that no analytical formulas are present for a specific component shape or type of analysis. However, when it is possible, one should always apply an analytical approach to estimate, even roughly, the value of stress, strain or displacement expected.

4.1.1. Lever extensible bar analytical analysis

The first element subjected to stress during loading step was the lever bar. The most critical condition for this element was when the user had the lever completely extended and pushed the bar forward loading the spring in its last loading strike, when the force was maximum. As calculated in subsection 2.1.1 with Formula 2.2, when the spring had

to be fully compressed the maximum force on it was 200 N and in the lever bar end the resultant applied force was 19.5 N. In this condition lever bar length was L = 200 mm, while the distance between the thrust hook's hinge hole and the other lever's hole, i.e. the length A-B shown in Figure 4.1 was l = 25 mm. For the analytical analysis a 1D beam element model was created in place of the bar element and the model was isostatic since the F force is applied vertically with respect to the beam axis, with no forces on horizontal direction. In calculating the resultant internal forces only the moment was taken into account since it gave the major contribution on stresses and strains, while the shear forces could be neglected. The structure was assumed working in linear elastic condition and, as can be seen in Figure 4.1, the maximum bending moment was at point B:

$$M = F \cdot (L - l) = 3412.5 \ N \cdot mm; \tag{4.1}$$

.

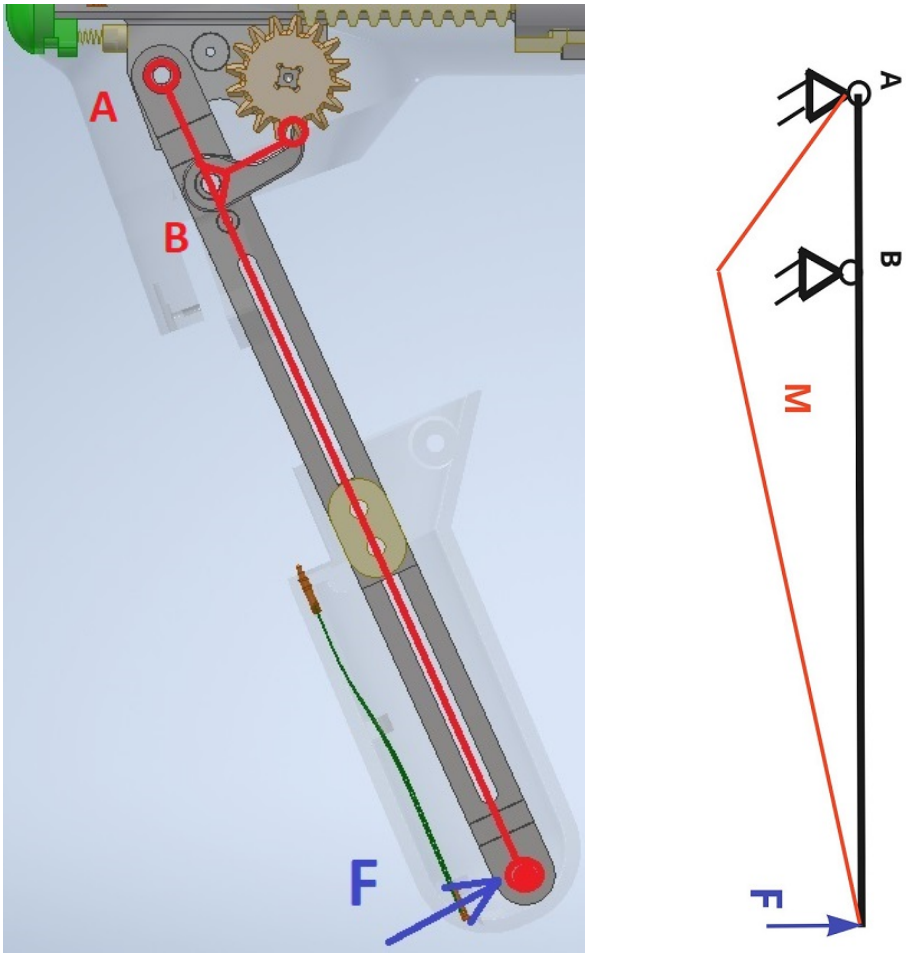

Figure 4.1: Lever bar analytical model

At point B, where the maximum bending moment was located, the bar section had a hole, the hole created for thrust hook's hinge and this had to be subtracted to the cross section area to calculate the section resistant modulus. The value of the maximum stress in point B was calculated as:

$$\sigma_{max} = \frac{M \ \cdot h}{2 \ \cdot I}; \tag{4.2}$$

where h is the section height equal to 13 mm, and I is the second moment of inertia which in case of a rectangular holed section is:

$$I = \frac{b \ \cdot h^3}{12} - \frac{b \ \cdot d^3}{12} = \frac{2 \ \cdot 13^3}{12} - \frac{2 \ \cdot 4^3}{12} = 355.5 \ mm^4; \tag{4.3}$$

where b is the rectangular section thickness which was assumed to be 2 mm and d is the hole's diameter assumed to 4 mm.

The value for the maximum stress at point B was then calculated as:

$$\sigma_{max} = \frac{M \ \cdot h}{2 \ \cdot I} = \frac{3412.5 \ \cdot 13}{2 \ \cdot 355.5} = 62.4 \ MPa; \tag{4.4}$$

.

This value will be compared with the one obtained using Finite Element Method, in Section 4.2.1.

4.1.2. Housing body analytical analysis

The second critical element in the assembly was the housing body containing the main spring: the core element in the assembly. When the spring was fully compressed, the bottom end of this part had to withstand a force of S = 200 N. With analytical formulas a balance of forces could be done to find the tensile stress acting on the ring of material in the housing body's section. The circular bottom area where the spring exerted its force, generated a pressure which had to be counteracted by the material section tensile strength and the main stress generated by this interaction was placed at the bottom edge notch radius. In Figure 4.2, the internal area "Ai" was the contact area between spring and housing body, where the hole diameter was d = 10.4 mm and the internal area was calculated as: $Ai = \pi \cdot (d/2)^2 = 84.9 \ mm^2$. The tensile stress calculated on the cross section of the hosing body was calculated as follows:

$$\sigma_{tensile} = \frac{S}{Ac} = \frac{200 \ N}{107.4 \ mm^2} = 1.9 \ MPa; \tag{4.5}$$

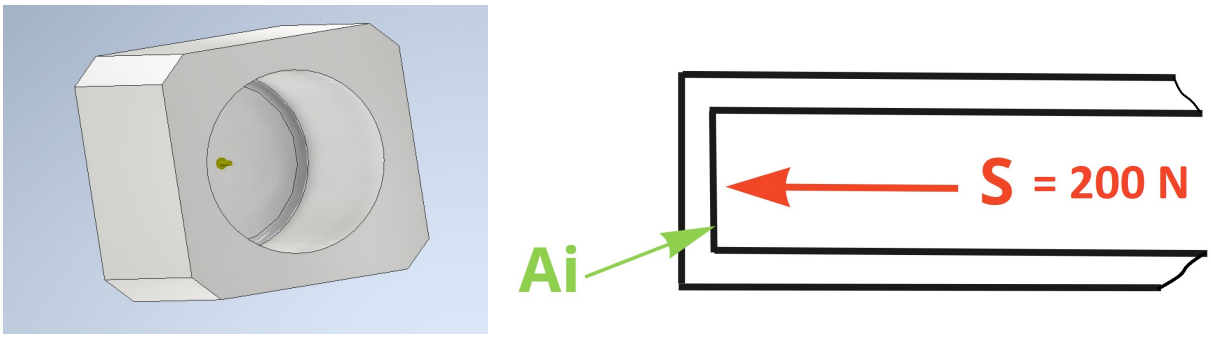

Figure 4.2: Housing body's analytical model.

where Ac was the cross section area calculated automatically in Autodesk Inventor environment as: $Ac = 107.4\ mm^2$.

Since in Ai area perimeter a notch radius of 0.2 radius was present due to machining tool's edge radius for the calculation of maximum stress a stress intensity factor (K_t) had to be taken into account. The value of it was estimated approximately from standard tables related to notched specimens subjected to tensile forces, as can be seen in Figure 4.3. The notch radius was r = 0.2 mm and the hole's diameter could be made to correspond to h = 10.4 mm, and the value of housing body's total height could be made to correspond to H = 14 mm.

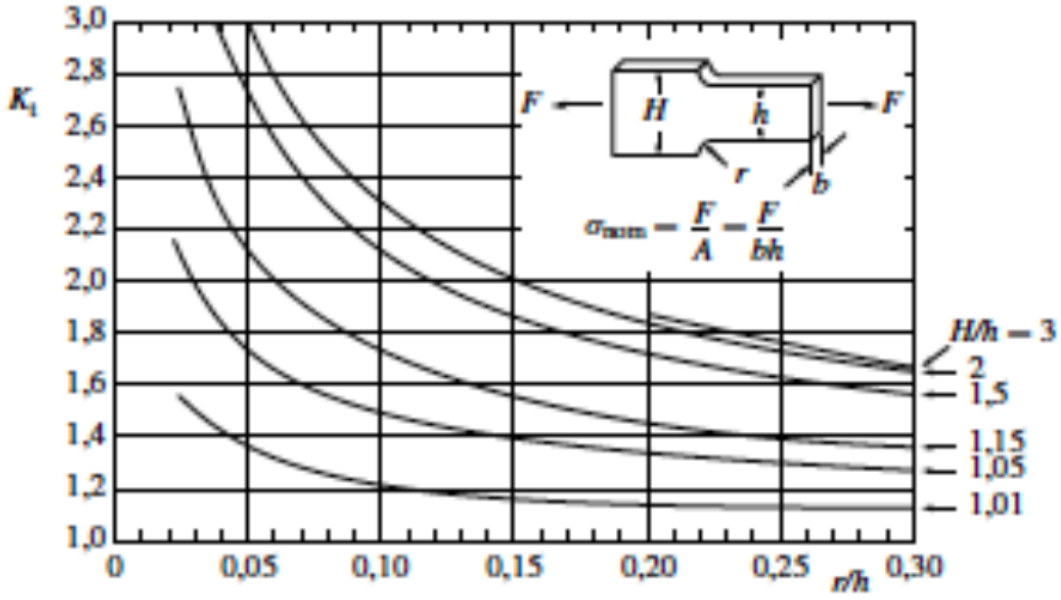

Figure 4.3: Stress intensity factor coefficient in tensile load condition.

With these inputs the stress intensity factor extrapolated was $K_t = 3$, leading to a maximum stress on the notched zone of $\sigma_{max} = \sigma_{nominal} \cdot K_t = 1.9\ MPa \cdot 3\ = 5.7\ MPa$.

4.1.3. Sliding base's snap-fit joint analytical analysis

The front snap-fit joints system was designed to have a outer snap-fit joint hosting within an internal snap-fit joint attached to the sliding base and hold it in place during the impact caused by injection. This brake system was explained in section 2.1.3 and can be observed in Figure3.6. This external snap-fit joint was composed by two arms acting as cantilever beams, which had to be properly designed to resist at maximum stress applied to open them and in such a way that they were not too hard to be open by the user while inserting or extracting the sliding base system for ampoule replacement. In fact they had to be designed appropriately for a limited mating force required by the user when he/she would use the system, and likewise to resist the snap motion during the injection. For cantilever snap-fit joints in Figure 4.4, analytical formulas for its dimensioning were found from Bayer MaterialScience in the paper "Snap-fit joints for plastics" [22]. A large proportion of snap joints are basically simple cantilever snaps, which may be of rectangular or of a geometrically more complex cross section; see Figure 4.5. It is suggested to design the snap-fit arm so that either its thickness (h) or width (b) tapers from the root to the hook; in this way the load-bearing cross section at any point bears a more appropriate ratio of local load. The maximum strain on the material can therefore be reduced and less material is needed.

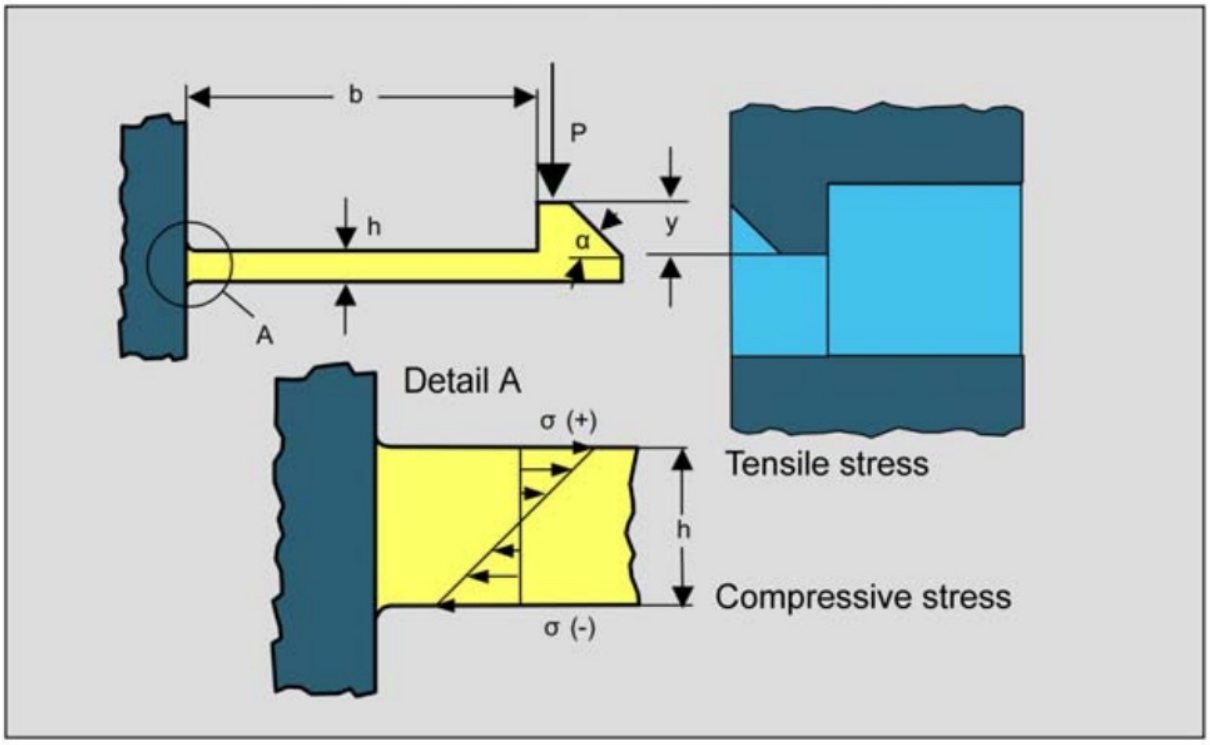

Figure 4.4: Simple rectangular cantilever snap-fit arm.

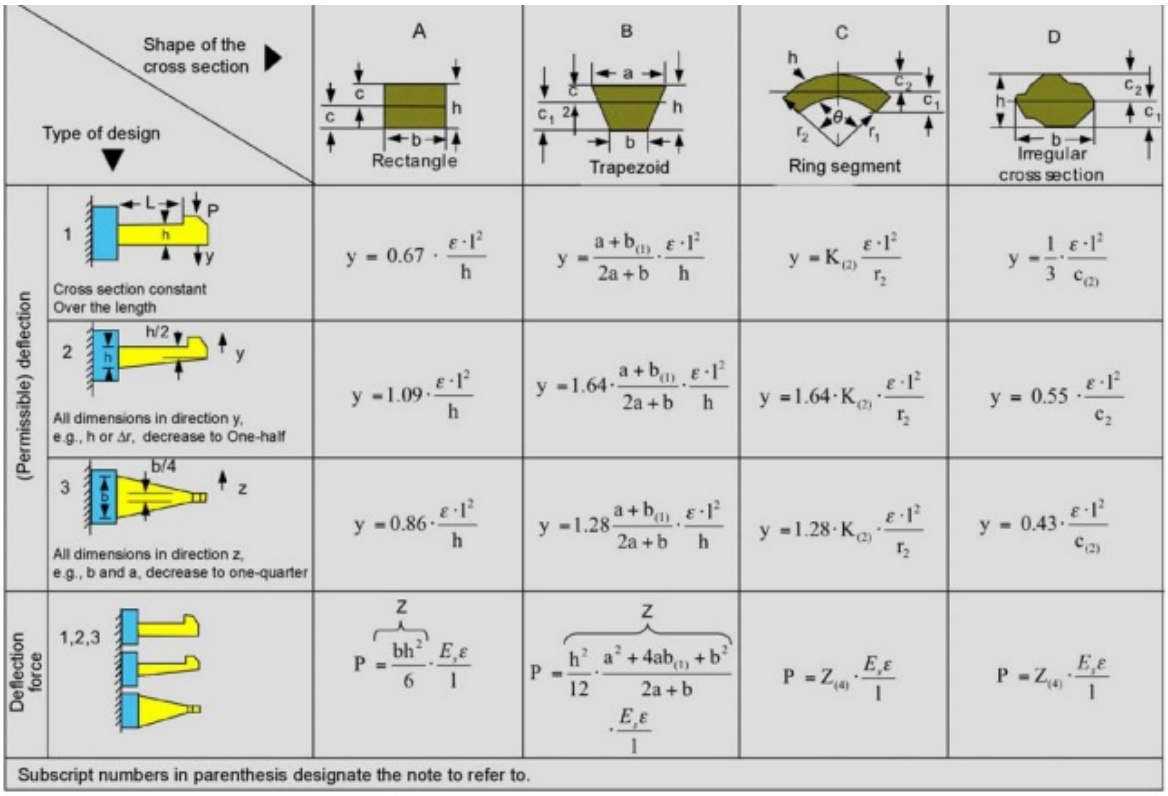

Table 1: Equations for dimensioning cantilevers

Symbols

y = (permissible) deflection (=undercut)
E = (permissible) strain in the outer fiber at the root; in formulae: E as absolute value = percentage/100 (see Table 2)
l = length of arm
h = thickness at root
b = width at root
c = distance between outer fiber and neutral fiber (center of gravity)
Z = section modulus Z = I c, where I = axial moment of inertia
Es = secant modulus (see Fig. 16)
P = (permissible) deflection force
K = geometric factor (see Fig. 10)

Notes

1) These formulae apply when the tensile stress is in the small surface area b. If it occurs in the larger surface area a, however, a and b must be interchanged.

2) If the tensile stress occurs in the convex surface, use K2, in Fig. 10; if it occurs in the concave surface, use K1, accordingly.

3) c is the distance between the outer fiber and the center of gravity (neutral axis) in the surface subject to tensile stress.

4) The section modulus should be determined for the surface subject to tensile stress. Section moduli for cross-section shape type C are given in Fig. 11. Section moduli for other basic geometrical shapes are to be found in mechanical

Permissible stresses are usually more affected by temperatures than the associated strains. One pref-erably determines the strain associated with the permissible stress at room temperature. As a first approximation, the compu-tation may be based on this value regardless of the tempera-ture. Although the equations in Table 1 may appear unfamiliar, they are simple manipula-tions of the conventional engineering equa-tions to put the analysis in terms of permissible strain levels.

Figure 4.5: Snap-fit joints shapes and formulas.

From this scientific study results have been obtained by reducing the thickness (h) of the cantilever linearly, so that its value at the hook end was equal to one-half the value at the root, alternatively the snap-fit arm width may be reduced to one-quarter of the base

value (see Table 1 in Figure 4.5, designs 2 and 3). With designs illustrated in this table, the vulnerable cross section was always at the root, as it is displayed in Figure 4.4, Detail A. Special attention must therefore be given to this area to avoid stress concentration higher than the allowable limit for used material. In Figure 4.6 is graphically represented the effect root radius had on stress concentration factor. At first glance, it seemed that an optimum reduction in stress concentration was obtained using the ratio R/h as 0.6, since only a marginal reduction occurs after this point. However, using R/h of 0.6 would result in a thick area at the intersection of the snap-fit arm and its base. Thick sections will usually result in sinks and/or voids, as seen in Section 3.1.1 with injection moulding rules, which are points of high residual stress. For this reason, the designer should reach a compromise between a large radius to reduce stress concentration and a small radius to reduce the potential for residual stresses due to the creation of a thick section adjacent to a thin section. In the mentioned research, internal testing showed that the radius should not be less than 0.015 inch (0.38 mm) in any instance.

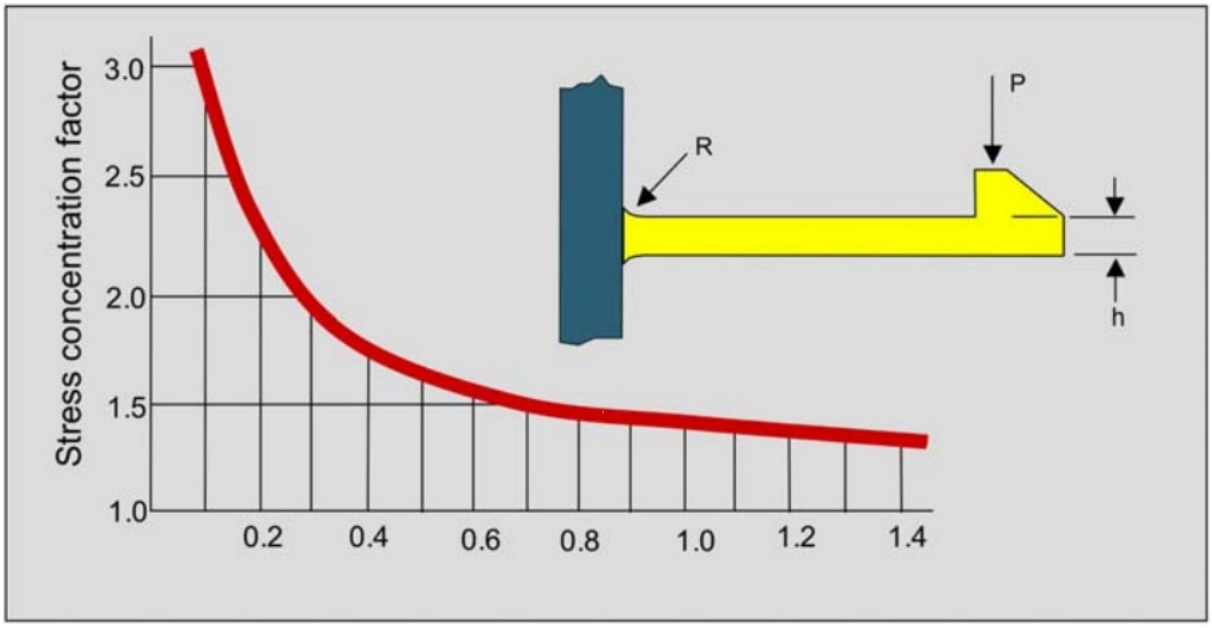

Figure 4.6: Effects of fillet radius on stress concentration.

The deflection y occurring during the joining operation, was the maximum permissible deflection of the snap-fit arm, i.e. the permissible undercut on the snap-fit head which depends not only on the shape but also on the permissible strain ϵ for the material used. In general, during a single brief snap-fitting operation, part of the crystalline materials may be stressed almost to the yield point, amorphous ones up to about 70% of the yield strain. Using the equations given in Figure 4.5, the permissible deflection y can be determined easily even for cross sections of complex shapes. A particularly favorable form of

snap-fitting arm was "design 2" in Table 1 of Figure 4.5 in which the thickness of the arm decrease linearly until half its initial value. This version increased the permissible deflection by more than 60% compared to a snap-fitting arm with constant cross section as in "design 1". In Figure 4.7 the definition of secant modulus (E_s) is shown. The secant modulus or strain dependent modulus of elasticity is one of several methods used to calculate modulus of elasticity, which is a measurement of a material elasticity. Calculating secant modulus involves using two points on a stress-strain curve to calculate the stress/strain slope. When using this method, the first point can be set to zero and the second is always a non-zero value. The formula for the calculation of it is:

$$E_s = \frac{\sigma_2 - \sigma_1}{\epsilon_2 - \epsilon_1}; \tag{4.6}$$

The values for σ_1 and ϵ_1 can be set to 0 if the origin is chosen as starting point.

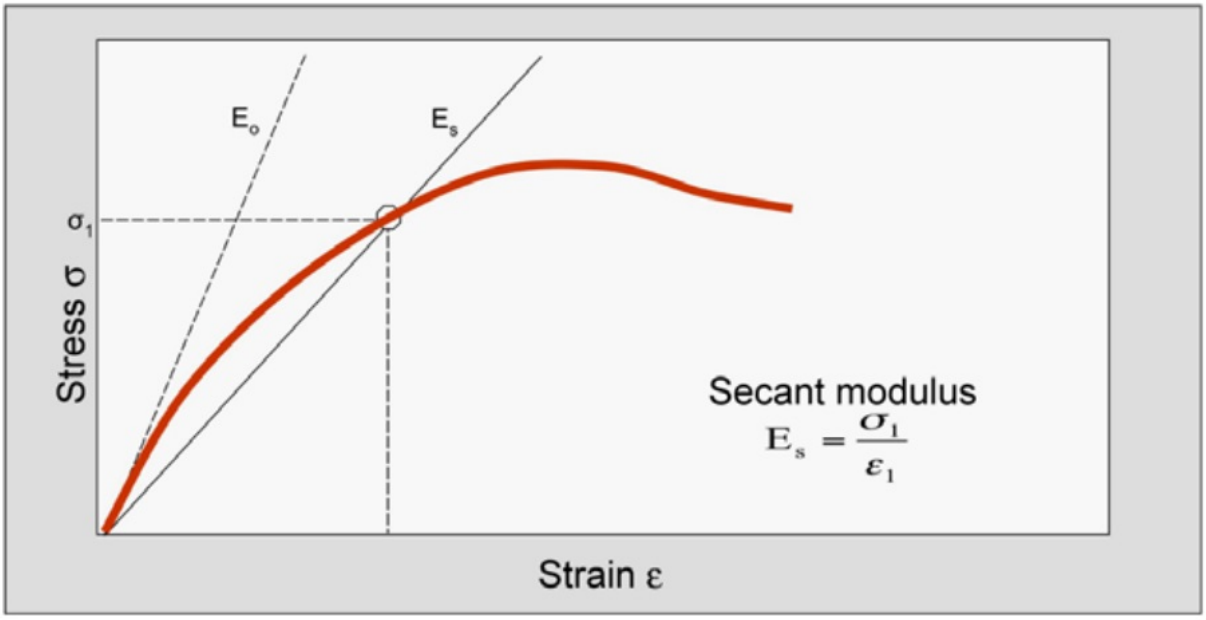

Figure 4.7: Graphical definition of Secant Modulus.

In our case the chosen material was polyether ether ketone (PEEK) which is a thermoplastic material with good mechanical properties, that with annealing heat treatment and formation of the semi-crystalline phase, reaches a ultimate tensile strength (UTS) up to 100 MPa. The E_s of PEEK can be extrapolated by its engineering stress-strain curve, as can be displayed in Figure 4.8. With a strain ranging from 0 to $\epsilon_2 = 2\%$ the material worked in linear elastic field. In this field the secant modulus was equal to $E_s = 35\ MPa$.

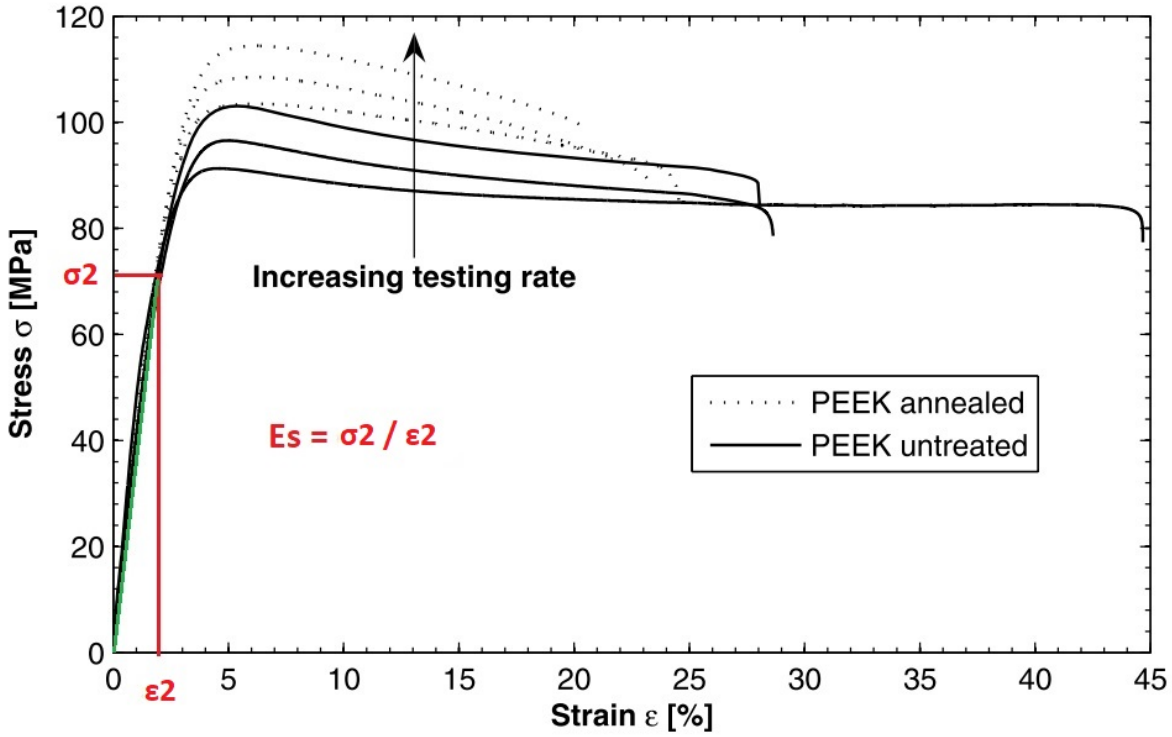

Figure 4.8: Secant Modulus extrapolation from PEEK's stress-strain curve.

During the fitting operation between the outer snap-fit and the inner one attached to the sliding base the deflection force P and friction force F had to be overcome, as can be seen graphically in Figure 4.9.

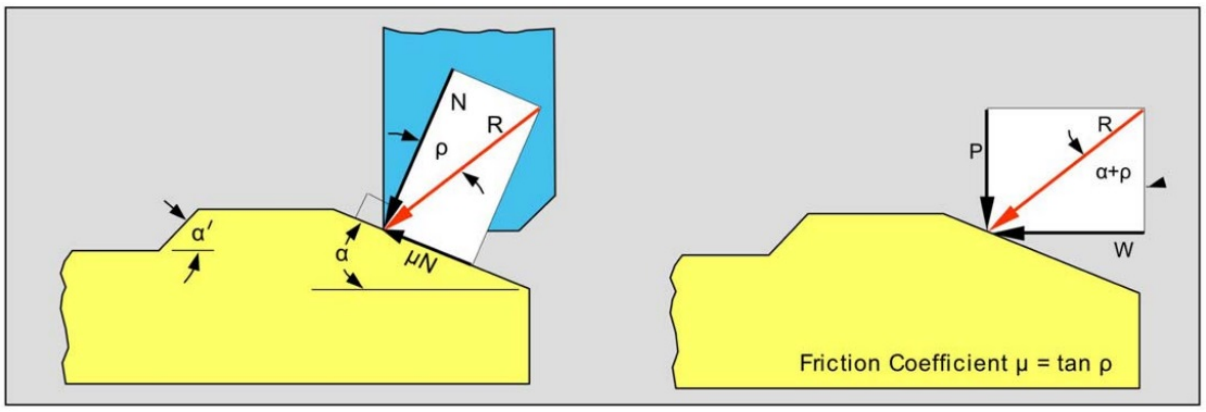

Figure 4.9: Snap-fit joint's mating force.

The mating force for the arm was given by:

$$W = P \cdot \tan(\alpha + p) = P \cdot \frac{\mu + \tan\alpha}{1 - \mu \tan\alpha}; \tag{4.7}$$

For this particular application PEEK seemed the best choice for its high strength combined with flexibility, with a low friction coefficient of 0.11 - 0.13; these values were taken from the work performed on PEEK in laboratories of Applied Materials Science of Department of Engineering Sciences, in Uppsala University [23]. In case of separable joints (non-permanent joints), as in this case, the separation force could be determined in the same way as the mating force by using the above equation. The angle of inclination to be used here was the angle α', as can be seen in Figure 4.9. The snap-fit arm was designed to have a rectangular cross section with a constant decrease in thickness from h at the root, to h/2 at the end, as shown in Figure 4.10). This design of decreasing section was used, as explain theoretically before, to permit a greater deformation, reducing the maximum stress and saving material at the same time. The snap-fit internal length was set to l = 18 mm. The permissible short term strain limits could be taken equal to the one of reinforced polymers of comparable strength [22] and equal to $\epsilon = 2.0$ %. The undercut was set equal to y = 2 mm.

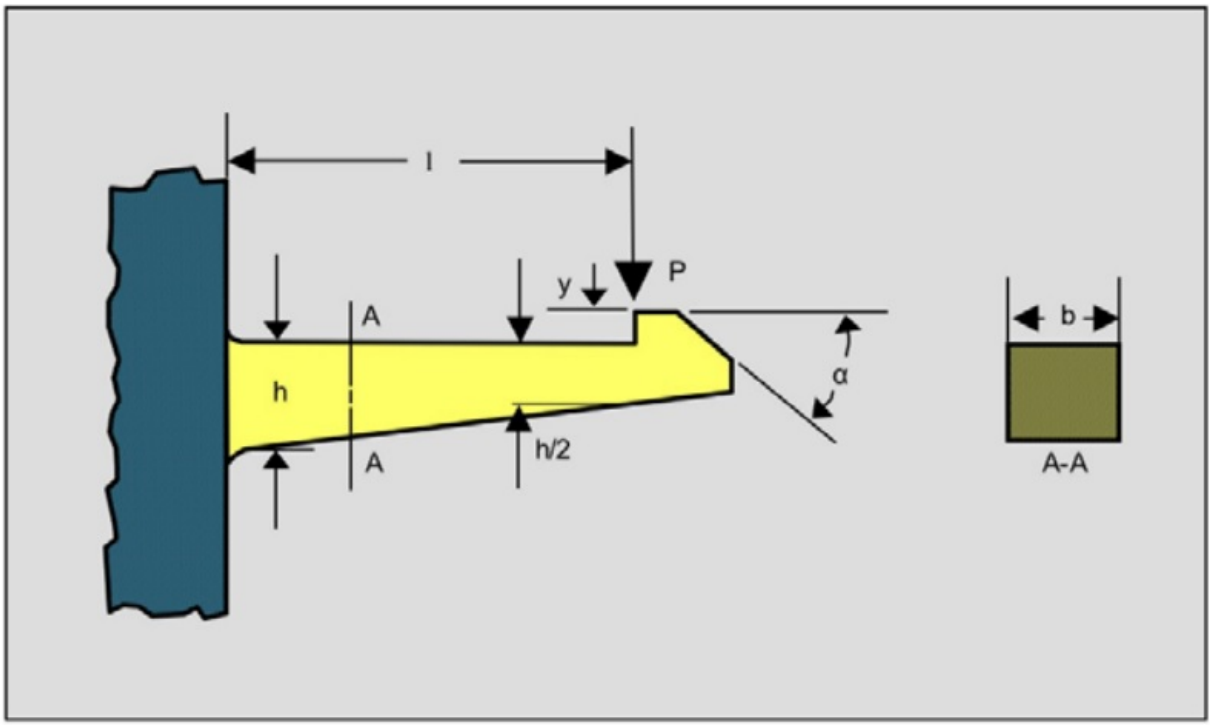

Figure 4.10: Rectangular cantilever snap-fit with decreasing section.

With these preliminary values the wall thickness "h" could be calculated using the formula of table in Figure 4.5:

$$h = \frac{1.09 \cdot \epsilon \cdot l^2}{y} = \frac{1.09 \cdot 0.02 \cdot 18^2}{2} = 3.5\ mm; \tag{4.8}$$

Then, the determination of deflection force P comprised the use of the following formula from the Table of Figure 4.5:

$$P = \frac{b \cdot h^2 \cdot E_c \cdot \epsilon}{6 \cdot l} = \frac{3 \cdot 3.5^2 \cdot 34 \cdot 0.02}{6 \cdot 18} = 231\ N; \tag{4.9}$$

Where b was the snap-fit arm thickness and was set equal to b = 3 mm. The friction coefficient was averaged at 0.12 and the angle of inclination for combine the snap-fit joints was $\alpha = 20°$. The mating force W was determined as follows:

$$W = P \cdot \frac{\mu + \tan(\alpha)}{1 - \mu \cdot \tan(\alpha)} = 231 \cdot \frac{0.12 + \tan(20°)}{1 - 0.12 \cdot \tan(20°)} = 116\ N; \tag{4.10}$$

For reduce the effort applied by the user to insert the two snap-fit joints one inside the other a tilted edge angle for the internal snap-fit was created, as can be seen in Figure 4.11; this solution was able to create a more gradual exchange of forces during the insertion.

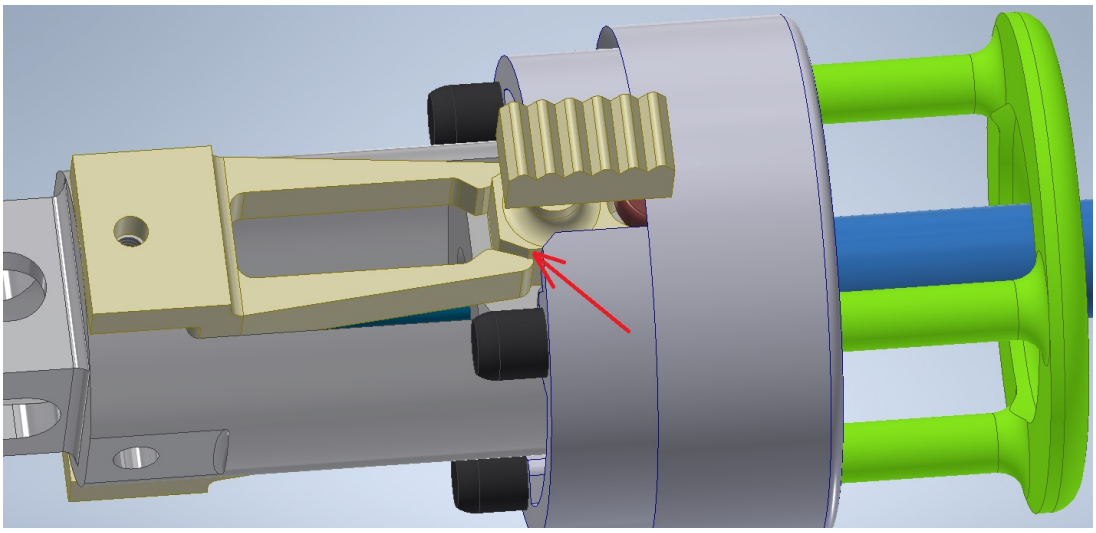

Figure 4.11: Inner and outer snap-fit joint in base's braking system.

4.1.4. Front ring's snap-fit joint analytical analysis

The second snap-fit joint used was in the front ring support end: in this case the three supports had permanent snap-fit joints on their ends which were inserted by pressure inside the cap-head holes, as can be seen in Figure 4.12. In this case the arm was not of rectangular section type as before but a ring segment type, as reported in table of Figure 4.5. For this element the material chosen was medical ABS as the external plastics for its good mechanical properties, compatibility with human skin and possibility to be sterilized; its properties can be seen in Figure 3.12. The snap-fit arm was designed to

have a length l = 6 mm.

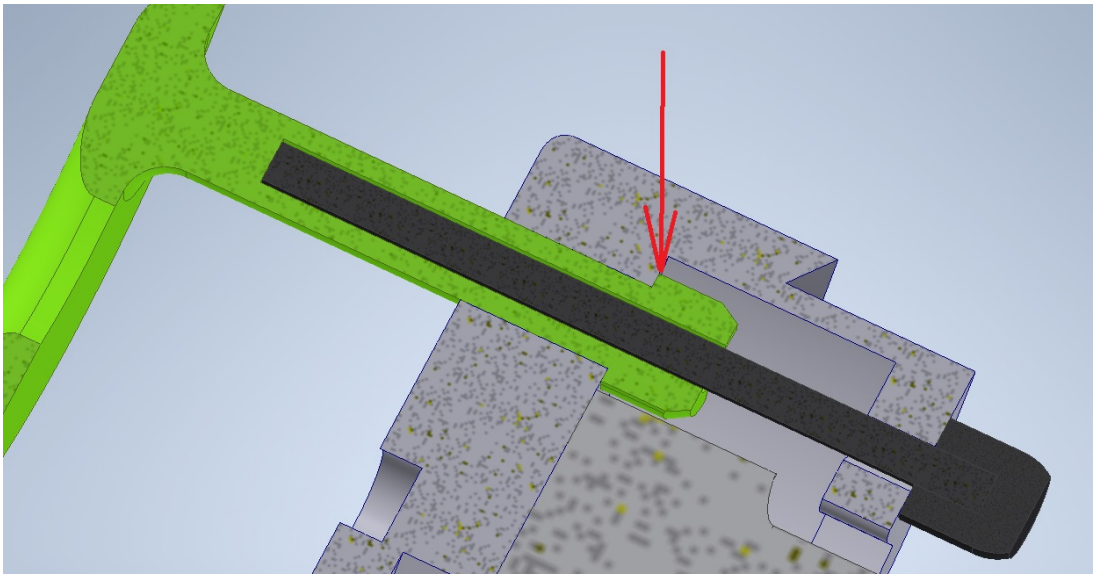

Figure 4.12: Front ring's permanent snap-fit joint.

The permissible short term strain limit was taken from tables of previously mentioned paper [22] and it was equal to $\epsilon = 2.5$ %, and its undercut was set equal to y = 1 mm. The value of geometric factor K_i was found in the right diagram of Figure 4.13 since the stress occurred in the convex surface and geometrical values were: $r_1 = 1.2\ mm$; $r_2 = 2.9\ mm$; with angle $\theta = 85°$; and the value of the geometric factor was $K_2 = 1.2$.

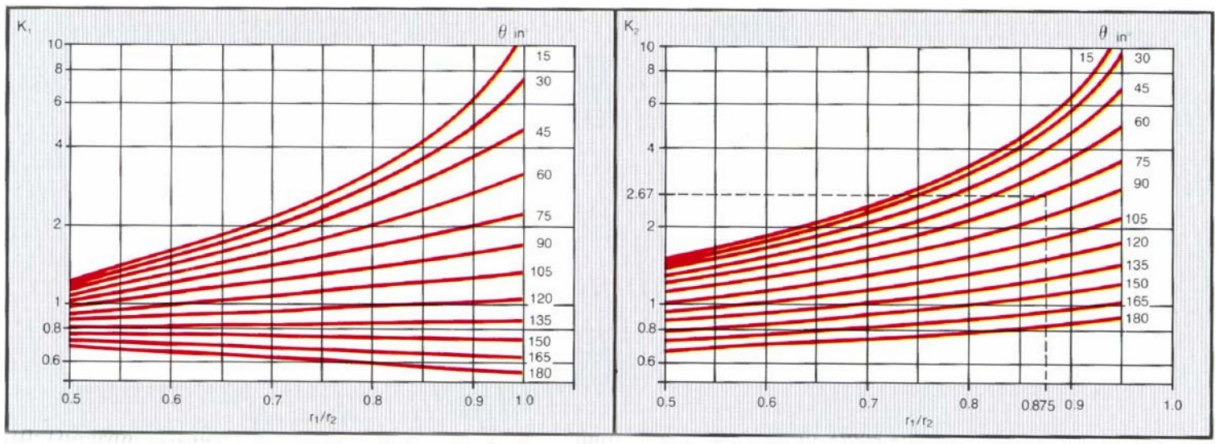

Figure 4.13: Ring segment snap-fits geometrical factor.

With these preliminary values the deflection "y" could be calculated using the formula of Table in Figure 4.5:

$$y = K_2 \cdot \frac{\epsilon \cdot l^2}{r_2} = 1.2 \cdot \frac{0.06 \cdot 6^2}{2.8} = 0.92\ mm; \tag{4.11}$$

This value was acceptable and was used to design the snap-fit head in contact with the outer plastic hole after the permanent fitting. The value of permissible strain was set at 0.06 (6%), because even if the material started yielding at this point it was acceptable since it was a permanent joint bent once per life-cycle. For this application the limit maximum strain was the one corresponding to the ultimate tensile strength (UTS) $\epsilon = 0.025$.

4.1.5. External plastics snap-fits joints analytical analysis

For keeping the extensible handle in place, attached to the main body when there was no loading need, two lateral snap-fits were created; as indicated in Figure 4.14. The material selected for the external plastics was ABS medical, with permissible short term strain limit equal to 0.025 (2.5 %) [22]. In this case the choice of having short term strain limit was necessary instead of ultimate strain limit because the joint was not permanent, but subjected to multiple opening and closing cycles, thus a long-period resistance was required.

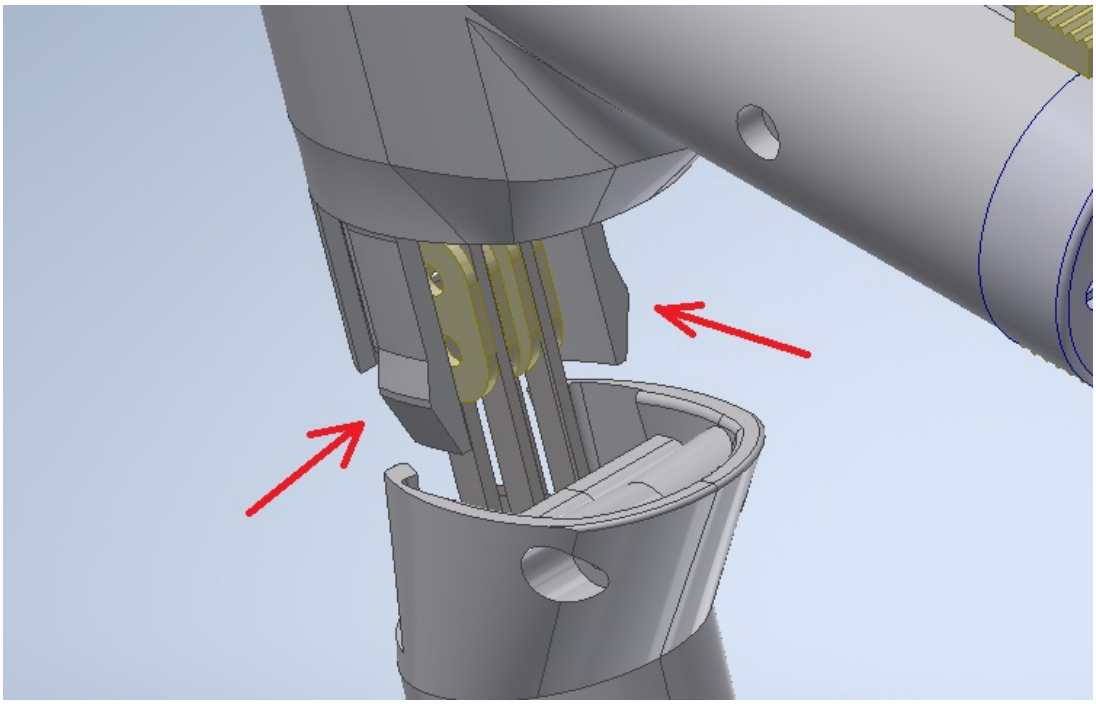

Figure 4.14: External plastics non-permanent snap-fit joints.

In this case it is another cantilever snap-fit with constant rectangular section through all the arm length. The equation for the maximum deflection was:

$$y = 0.67 \cdot \frac{\epsilon \cdot l^2}{h} = 0.67 \cdot \frac{0.025 \cdot 22^2}{3} = 2.7\ mm; \tag{4.12}$$

For the ABS the value of the secant modulus [22] for a 0.025 (2.5 %) strain was 1.5 MPa. And the deflection force P was:

$$P = \frac{b \cdot h^2 \cdot E_c \cdot \epsilon}{6 \cdot l} = \frac{10 \cdot 3^2 \cdot 1.5 \cdot 25}{6 \cdot 22} = 25\ N; \tag{4.13}$$

where the arm width b was set at 10 mm, the height h = 3 mm and length l = 22 mm as starting values. The value of friction coefficient for ABS was 0.55 and the angle of inclination $\alpha = 20$. The mating force was calculated as:

$$W = P \cdot \frac{\mu + \tan(\alpha)}{1 - \mu \cdot \tan(\alpha)} = 25 \cdot \frac{0.55 + \tan(20)}{1 - 0.55 \cdot \tan(20)} = 25 \cdot 1.14 = 28.5\ N; \tag{4.14}$$

Since two snap-fits of this kind were present, one for each side, the total force required was 57 N. This value was reduced by decreasing the deflection to 1.5 mm instead of 2.7 mm, changing the snap-fit design and the grooves design for hosting them in the handle. With this value of maximum strain became:

$$\epsilon = \frac{y \cdot h}{0.67\ l^2} = \frac{1.5 \cdot 3}{0.67\ 22^2} = 0.138; \tag{4.15}$$

And the deflection force became:

$$P = \frac{b \cdot h^2 \cdot E_c \cdot \epsilon}{6 \cdot l} = \frac{10 \cdot 3^2 \cdot 1.5 \cdot 13.8}{6 \cdot 22} = 14.1\ N; \tag{4.16}$$

The new mating force was then calculated as follows:

$$W = P \cdot \frac{\mu + \tan(\alpha)}{1 - \mu\ \tan(\alpha)} = 14.1 \cdot \frac{0.55 + \tan(20°)}{1 - 0.55\ \tan(20°)} = 14.1 \cdot 1.14 = 15.5N; \tag{4.17}$$

Leading to a total mating force of $15.5 \cdot 2 = 31\ N$.

4.2. Finite Element analysis of critical parts

The Finite Element Method (FEM) is a numerical method of solving differential equations and hence problems comprising stress, strain and deflection analysis in mechanical engineering. With this technique the component model is divided into regions (elements) with shapes and sizes appropriate to the problem, and the governing equations of every element are written down. Elements are then reconnected at nodes, resulting in a set of simultaneous algebraic equations, solutions of which solve the problem [15]. By the process of reconnecting nodes, the field quantity of interest (in stress analysis it is the displacement field) becomes interpolated over the whole body in a piece-wise fashion by as many polynomial expressions as there are elements. The best values of the nodal field quantities are those that minimize some function such as the total potential energy. The general approach used for the static analysis of critical parts in the assembly, using Abaqus CAE, was comprised in the following steps:

1. Create the solid 3D or shell 2D models in the Abaqus environment.
2. Insert the materials linear elastic properties in the models.
3. Assemble the system, assigning the surface interactions between components where needed.
4. Create boundary conditions and apply the loads with respect to the real problem.
5. Select the elements type suitable for the analysis (elements shape and order).
6. Select "full" or "reduced" integration for the number of Gauss points required to integrate the polynomial terms in an element's stiffness matrix, for a proper simulation without inducing a too stiff models behaviour.
7. Generate the mesh with mesh refinement and control in the zones of interest for the stress analysis.
8. For convergence analysis, iterate the process reducing the mesh elements size in the areas of interest. Check if the convergence analysis leads to an acceptable error, otherwise improve the mesh quality and iterate the process.
9. Post-process the results by switching off the averaging at nodes option when needed and probe the required value of stresses.

In some cases, in the display of stresses on the processed model it was necessary to exclude the maximum stresses pinpointed in the results because they were related to model's "computational errors" due to mesh and uncorrelated to real stress values occurring in

practise. In FEM analysis is always necessary to critically evaluate the results obtained and use a good sense of engineering to interpret the results and take decisions.

4.2.1. Lever arm validation with FEM analysis

For the lever arm assessment with FEM the condition of maximum lever extension and maximum applied load was considered. To simplify the analysis the model was created as a single planar shell 2D element, and since the two parallel bars attached to the housing worked simultaneously, just one bar was modelled and the external force applied by the user was divided by two in order to have coherent results. Two reference points were created within the model, one in the middle of each hole cut and two fixed couplings were assigned between the reference points and the inner hole perimeter. Then, two pin constraints were assigned to the reference points, to simulate the physical real constraints whereas only the rotation was allowed in these holes. The material selected for this element, as explained in the previous chapter was Aluminium 6082-T651 Anticorodal whose mechanical properties can be seen in Figure 4.18.

Materiali	Leghe di alluminio		Leghe di ferro		
	Alluminio 7075 T6 Ergal	**Alluminio 6082** Anticorodal	**Acciaio 18NiCrMo5**	**Acciaio inox 316L** (inox A4)	**Acciaio inox 304**
Colore naturale del materiale	grigio	grigio	grigio	grigio	grigio
Finiture disponibili	Anodizzazione, pallinatura Lancet®	Anodizzazione, pallinatura Lancet®	Pallinatura Lancet®	Pallinatura Lancet®	Pallinatura Lancet®
Densità	2.88 g/cm³	2.70 g/cm³	7.85 g/cm³	7.85 g/cm³	8.00 g/cm³
Formato massimo teorico	496x496x400 mm	496x496x400 mm	260x260x200 mm	110x110x300 mm	110x110x300 mm
Applicazioni	Lega aeronautica ad alta resistenza: ingranaggi, alberi, telai di bicicletta e moto, pignoni, applicazioni aerospaziali, motori marini, stampi.	Lega dalle buone caratteristiche meccaniche ed elevata resistenza alla corrosione: componenti per macchinari, elementi strutturali.	Per elevate caratteristiche meccaniche unite ad una elevata durezza superficiale quali ingranaggi, perni, boccole, stampi per materie plastiche con elevata durezza superficiale.	Resistenza a corrosione e chimica. Scambiatori calore, condutture, materiali per costruzioni esterne in zone costiere. Attrezzature per uso marittimo e industria alimentare	Applicazioni domestiche e industriali come apparecchiature per la manipolazione e lavorazione degli alimenti, viti, parti di macchine, strumenti e scarichi di automobili. Elementi architettonici esterni.
Tolleranza minima	±0,05	±0,05	±0,05	±0,05	±0,05
Limite di snervamento RM [MPa]	434-503	230-360	635-980	290-320	280-290
Carico di rottura [MPa]	510-572	310-385	900-1200	570-620	520-540
Modulo elastico [GPa]	72	69	190	200	190
Allungamento a rottura o allungamento [%]	5-11	10-11	13-16	50-55	65-70
Durezza Brinell	150	100	200-225	215-225	120-130

Figure 4.15: Aluminium 6082-T651 Anticorodal mechanical properties.

In the shell model a thickness of 2 mm was assigned with material properties of 69000 MPa as Young's modulus, and 0.35 as Poisson's ratio. A linear static step was created for the analysis and for the mesh a quadrilateral quadratic element type was chosen since it provides better results for bending problems as this one. Reduced-integration elements, which have fewer integration point in each direction than the fully integrated elements were used, even if they tend to be too flexible, because the mesh was strongly refined in the interested zone, avoiding any mistake in stiffness matrix calculation. The approximated global mesh size was set to 7 mm, while for the most stressed zone around the thrust hook hole, a mesh seed control equal to 2 mm was set and around the hole's perimeter a second seed control at 1 mm was used. In the stress results Von Mises stress was selected since aluminium is a ductile material; they are displayed in Figure 4.16. The maximum stress was not in the thrust hook's hinge hole as expected from analytical approach, but closer to the long loop cut. This result has been generated by the effect of the long loop cut along the lower bar side, decreasing the section resistant modulus and the mechanical stiffness, and leading to a local higher deformation and stress concentration. The result of Von Mises maximum stress, turning the averaging at nodes option off, was 67 MPa, only 7% higher that the analytical result. The safety factor with reference to the yield stress was calculated as:

$$\eta = \frac{\sigma_{yield}}{\sigma_{max}} = \frac{230\ MPa}{67\ MPa} = 3.4; \tag{4.18}$$

For this FEM simulation no convergence analysis was needed since the maximum stress value was far from the critical stress value represented by the yield point, and it could be considered reliable due to the refined mesh size selection and uniform stress distribution showed in the result.

4.2.2. Housing body validation with FEM analysis

To assess the housing body a 3D model representing only the bottom part of the element was created. The material used for the model was Aluminium 6082-T651, as the the previous analysis, working in linear elastic field. In this case a reference point rigidly connected to the inner hole's bottom surface was generated for the force application of 200 N. The element was constrained with a fixed boundary condition only to one side opposite to the hole's bottom, along a housing body's section. The elements used for the mesh were solid tetrahedral quadratic elements of 0.2 mm size, for better follow the strains concentrated at the inner hole's notch radius, which was the ring area where the highest concentrated stresses were expected. The results for maximum Von Mises stress, with averaging turned off, showed very few concentrated peaks of 39 MPa, but the common

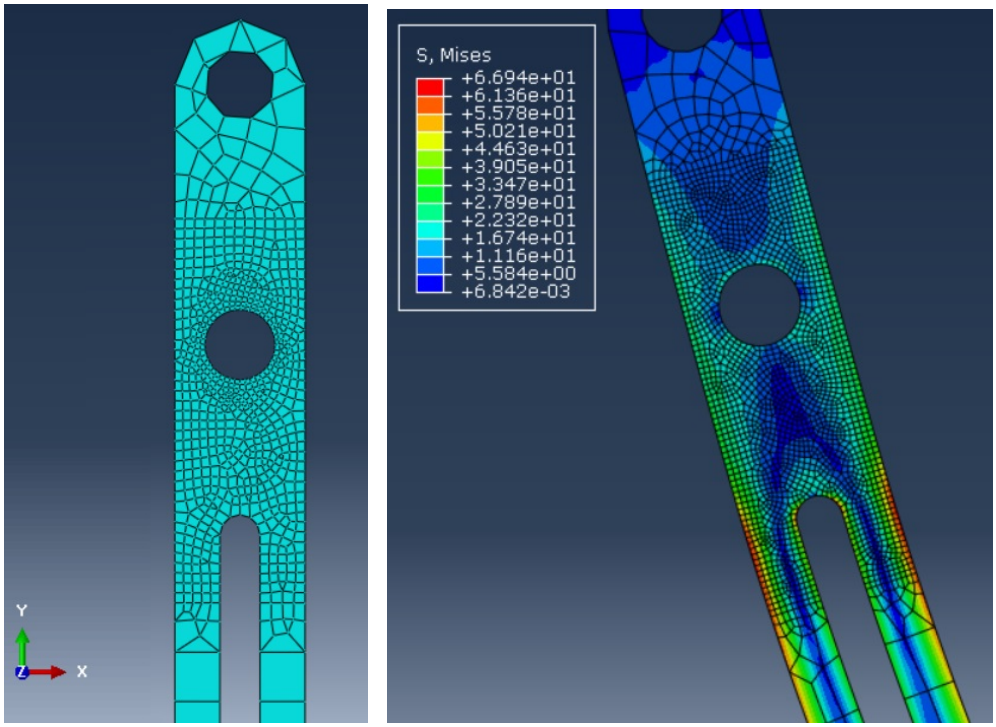

(a) Mesh seeding control. (b) Von Mises stress results.

Figure 4.16: Lever bar FEM analysis.

value of stress around the hole perimeter, at notch was 17 MPa. The random localized peaks were caused by the mesh, which was an idealization of the real component, and not related to the real model since there was no physical reason to have spots of high stress concentration in these points. The real value probed for the stress around the ring of interest was 17 MPa which is higher than 5.7 MPa found with analytical formulas. This result was acceptable since the 3D model was much closer to the real component than the analytical model containing strong geometrical approximations. Even in these case convergence techniques were unnecessary since the maximum stress was far from the yield stress and the mesh size was small enough. The safety factor was equal to:

$$\eta = \frac{\sigma_{yield}}{\sigma_{max}} = \frac{230\ MPa}{17\ MPa} = 13.5; \tag{4.19}$$

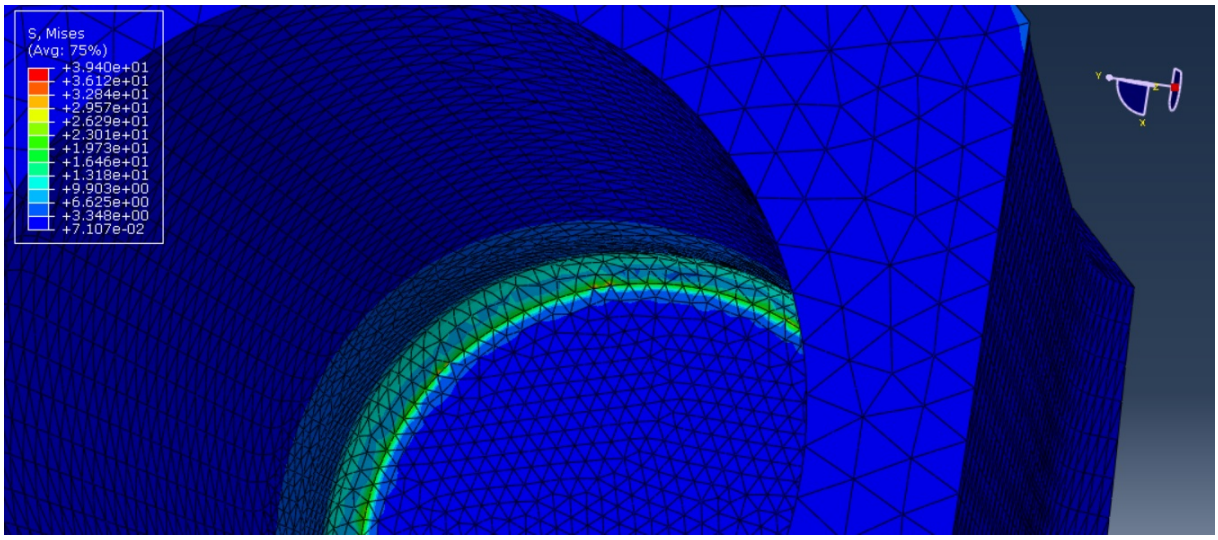

Figure 4.17: Housing body FEM analysis.

4.2.3. Snap-fit braking system with FEM analysis

The purpose of the front snap-fit braking system analysis was to assess the capability of the external snap-fit arms to withstand external force applications without breaking during the sliding base positioning and during the spring snap impact. While the sliding base was set in place the inner snap-fit entered to the outer snap-fit as explained in the previous chapters and doing so opened the outer snap-fit arms inducing stresses at its bases. For simulate this mechanical coupling the models of the two corresponding pieces were created with solid 3D models and assembled as they were placed in reality. The outer snap-fit was constrained at its bottom while the inner one was constrained in all direction but the one of sliding action, back and forth, and the constraint was placed only at the bottom side of it. The material for these elements was PEEK, with mechanical properties showed in the previous Sections. For simulate the interaction between the fits surfaces a master surface assignment was set for the inner snap-fit while for the outer one slave surface was assigned, remembering that the master surface can penetrate the slave surface. The contact enforcement method selected was “penalty method”, a general contact algorithm, and for the contact discretization method “node-to-surface method” was chosen. With traditional node-to-surface discretization method the contact conditions were established such that each “slave” node on one side of a contact interface effectively interacts with a point of projection on the “master” surface on the opposite side of the contact interface. Thus, each contact condition involves a single slave node and a group of nearby master nodes from which values are interpolated to the projection point. Traditional node-to-surface discretization has the characteristic that the slave nodes are

constrained not to penetrate into the master surface; however, the nodes of the master surface can, in principle, penetrate into the slave surface and the contact direction is based on the normal of the master surface [24]. The contact type between the two surfaces had a "friction-less" tangential behaviour and "hard" normal behaviour. The mesh was created with quadrilateral quadratic elements for both with a global seed size of 0.3 mm. Reduced integration method for the elements was selected. The process for the analysis was divided in ten different steps were the inner component, starting from a position outside the outer snap-fit, was displaced of a certain length (millimeter) toward the outer snap-fit, until they came in contact and developed the maximum stresses at fits arms base, closed to notch radius. With this computational method Abaqus calculated at each time step the elements stiffness matrix and related strains and stresses. In fragile materials as PEEK, Galileo-Rankine stress criterion should be used instead of Von Mises stress, but in this case the only applied stress during bending was the one along the horizontal direction, the principal stress, therefore Galileo-Rankine stress was very close to the stress evaluate with Von Mises stress, which are shown in Figure 4.18, and the maximum value probed was 31 MPa. Since the material was not consider anymore as a ductile material, the reference value for the safety factor was the ultimate tensile strength (UTS) = 100 MPa. The safety factor was thus:

$$\eta = \frac{UTS}{\sigma_{max}} = \frac{100\ MPa}{31\ MPa} = 3.2; \tag{4.20}$$

The second load condition was when the spring exert its force during injection, in this case the force was first directed to the needle-less ampoule attached to the sliding base which would tend to move forward, moving the pivot attached to it and pushing against the inner snap-fit arms as explained in Section 2.1.3. During this movement the inner snap-fit attached to the sliding base, while having its arms opened, would tend to open the outer snap-fit arms, creating interference with the aluminium housing body and braking the motion. The braking system depended on the opening of outer snap-fit arms and this element was the one subjected to the highest stress during this stage. One arm was modelled with 3D solid element and set in an assembly attached to a block representing the aluminium housing body side. The arm was constrained with fixed constraints at its base edge and a contact properties exactly as the previous application was applied between the snap-fit arm and the housing body's side; in this case snap-fit arm surface was the slave surface instead housing body surface was the master surface. The braking system to be simulated worked with the contact between the arm and the outer aluminium body, for this reason it was fundamental to have a side contact definition there. The force applied in this arm was 50 N in total, since in the real assembly two outer snap-fit joints

were present: one upward and the other in opposite position upside-down, and both of them had two arms, so the total force of 200 N could be divided by four resulting in 50 N loaded for each arm. This force was applied in two nodes at the snap-fit head; the high concentrated stress value there due to mesh and load application was not part of the real problem, i.e. completely negligible, but the stress value of interest was at notch in the arm base, as shown in Figure 4.19. The maximum Von Mimes stress close to the notch radius was 34 MPa.

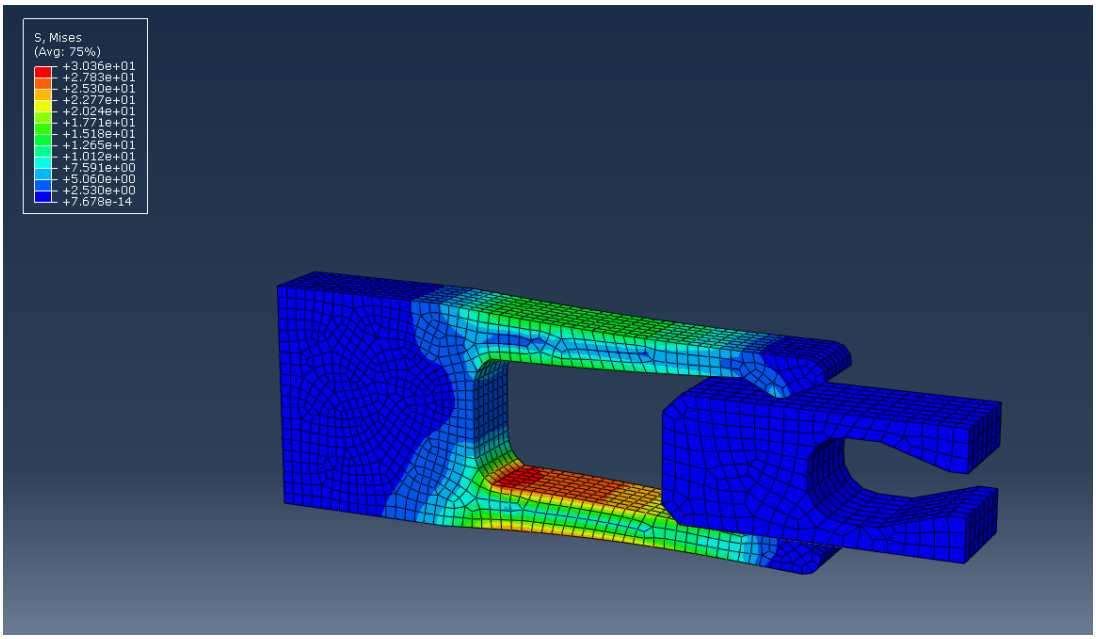

Figure 4.18: Braking system FEM analysis.

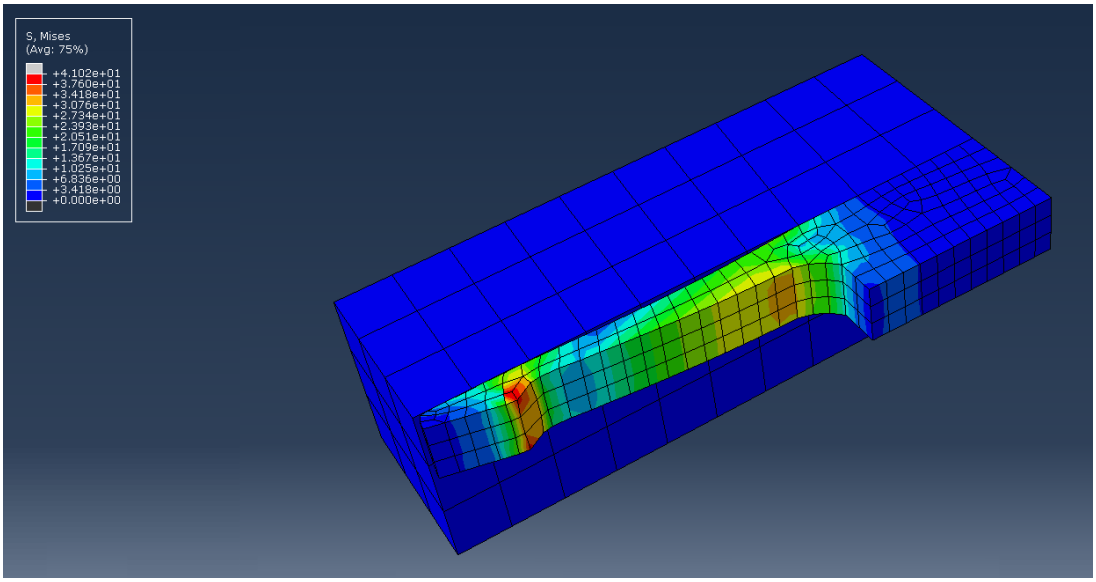

Figure 4.19: Outer snap-fit joint FEM analysis.

The stresses colored in red at the head were the ones generated by the local force application in two nodes and not related to the real behaviour of material. The safety factor was then evaluated and was similar to the one obtained with previous analysis:

$$\eta = \frac{UTS}{\sigma_{max}} = \frac{100\ MPa}{34\ MPa} = 2.9; \tag{4.21}$$

4.2.4. External plastics snap-fits validation with FEM analysis

The external plastics snap-fit joints had to be accurately validated with FEM analysis since they were frequently moved during a daily use, thus subjected to cyclic stresses. For the analysis a 3D solid model was created and fixed to its base side, and with an applied perpendicular force at head with magnitude equal to mating force found during the analytical analysis in Section 4.1.5. The material used was the one selected for external plastics, ABS medical, with Young's modulus equal to 1375 MPa, Poisson's ratio 0.35 and UTS = 52 MPa. The mesh was created with quadrilateral quadratic elements for both with a global seed size of 0.2 mm. Reduced integration method for the elements was selected also in this case since the mesh was selected fine enough to avoid problems due to reduced integration instead of full integration. In Figure 4.20 it can be seen that the maximum Von Mises stress probed at the notch was 15 MPa. The displacement of the snap-fit head, applied during the mechanical closing between plastics is equal to the undercut "y" and can be seen in Figure 4.20 equivalent to 1.48 mm. These values found with FEM analysis were complainant with the ones found with analytical analysis. The safety factor was then calculated as:

$$\eta = \frac{UTS}{\sigma_{max}} = \frac{52\ MPa}{15\ MPa} = 3.5; \tag{4.22}$$

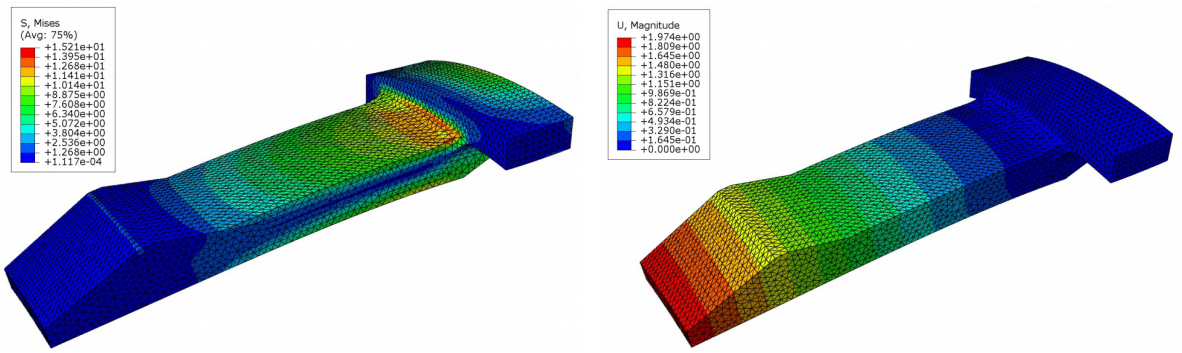

(a) Stress analysis. (b) Maximum displacement analysis.

Figure 4.20: External plastics snap-fit FEM analysis.

4.2.5. Trigger validation with FEM analysis

For the trigger no analytical model has been created since it was difficult to find the right formulation to evaluate correctly the geometry correlation and the right stress intensity factor at notch. The problem was tackled with a 2D shell model since the stress distribution along the model's thickness was uniform through all the thickness, due to plane stress condition. Only the front side of the trigger's profile was modelled, with an assigned thickness equal to 5.4 mm (shell property) and Aluminium 6082-T651 set as material, working in linear elastic condition. This model had a fixed constrain to one end, opposite to the hook, and a fixed coupling in the internal hook's side with a reference point linked rigidly to it and a force of 200 N applied. The step function was a linear static analysis created between time 0 and time 1. For a proper evaluation of stress around the notched area a local mesh control was set there with a seed size refined to 0.4 mm. The global mesh size was 1 mm, and since it was a bending problem a quadrilateral quadratic element type was assigned; in this case the total number of elements were 315. With these parameters the maximum local Von Mises stress was 141 MPa, obtained in correspondence to the notch. In this case it has been useful to perform a convergence analysis since a more accurate value of stress was needed for the fatigue assessment. The convergence analysis was performed creating two more mesh refinements in the notched area, one with local mesh control of 0.2 mm leading to a model with 617 elements, the other model with a mesh control set at 0.1 mm leading to a 1912 elements model. Perform a convergence analysis means to verify how small the mesh elements need to be to ensure that results of the FEM analysis are not affected by changing the mesh size. The type of mesh refinement used is related to the reduction of elements size and not related to increase of elements order. The results of Von Mises stress obtained with roughest

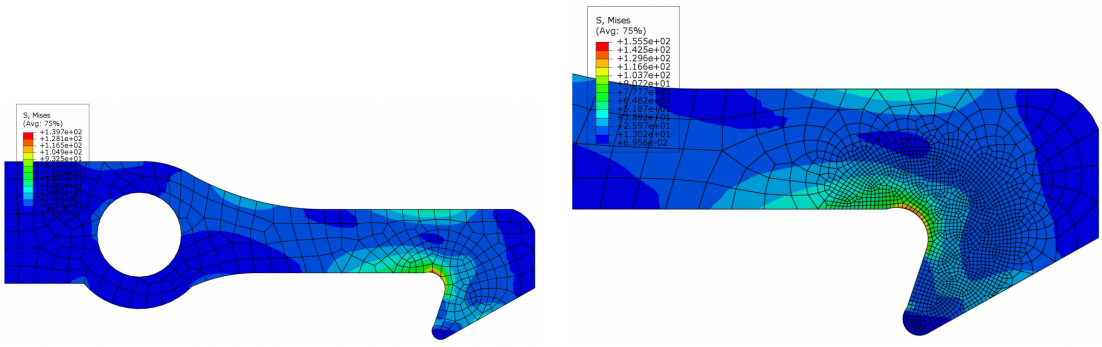

(a) Rough mesh size. (b) Fine mesh size.

Figure 4.21: Trigger FEM analysis.

mesh and finest mesh control at the notch can be seen in Figure 4.21 and the results for convergence analysis are displayed in Table 4.1; where h is an adimensional term for the calculation of convergence, depending on the number of elements in the structure. To find the final value of stress it was necessary create a Cartesian chart with in x-axis the values of h and in y-axis the corresponding values of stress. Interpolating these three points on the graph by linear interpolation the value of Von Mises stress for h tending to 0, i.e. the mesh size tending to be infinitesimally small, was 146 MPa. The error in this case had an acceptable value which was:

$$e = \frac{(\sigma_{max} - \sigma_{min}) \cdot 100\%}{\sigma_{max}} = \frac{(146\ MPa - 141\ MPa) \cdot 100\%}{146\ MPa} = 3.4\%; \tag{4.23}$$

LOCAL ELEMENTS SIZE	MAXIMUM STRESS (MPa)	ELEMENTS NUMBER (N)	h = 1/sqrt(N)
0.4	141	316	0.056
0.2	144	526	0.044
0.1	145	1230	0.029

Table 4.1: Table for convergence analysis.

Finally the safety factor was calculated considering the yield stress for Aluminium 6082-T651 equal to $\sigma_{yield} = 230\ MPa$:

$$\eta = \frac{\sigma_{yield}}{\sigma_{max}} = \frac{230MPa}{146MPa} = 1.58; \tag{4.24}$$

Fatigue assessment had to be performed for this element since the safety factor was not very high as in others components and aluminium is a ductile material subjected to possible fatigue issues. The fatigue limit or endurance limit is the stress level below which an infinite number of loading cycles can be applied to a material without causing fatigue failure. Some metals such as ferrous alloys have a distinct limit, whereas others such as aluminium do not, however a fatigue limit can be calculated at $5 \cdot 10^6$ cycles using standard coefficients depending on component's dimension, surface roughness, notch effect and type of applied loads. In this case the load applied was a bending moment generating a stress on the notch, shown in the previous figures, and the fatigue limit was evaluated with the following standard formula [25]:

$$\sigma_e^{'} = \frac{0.4 \cdot UTS \cdot m_s \cdot m_d}{1 + q \cdot (K_t - 1)}; \tag{4.25}$$

where m_d is the dimensional coefficient which in this case is equal to 1 since the element had a small thickness/diameter (thickness below 10 mm), m_s is the surface finish coefficient which is equal to 0.95 as can be extrapolated from the graph of Figure 4.22, for roughness 3.2 μm and UTS (Rm) = 310 MPa.

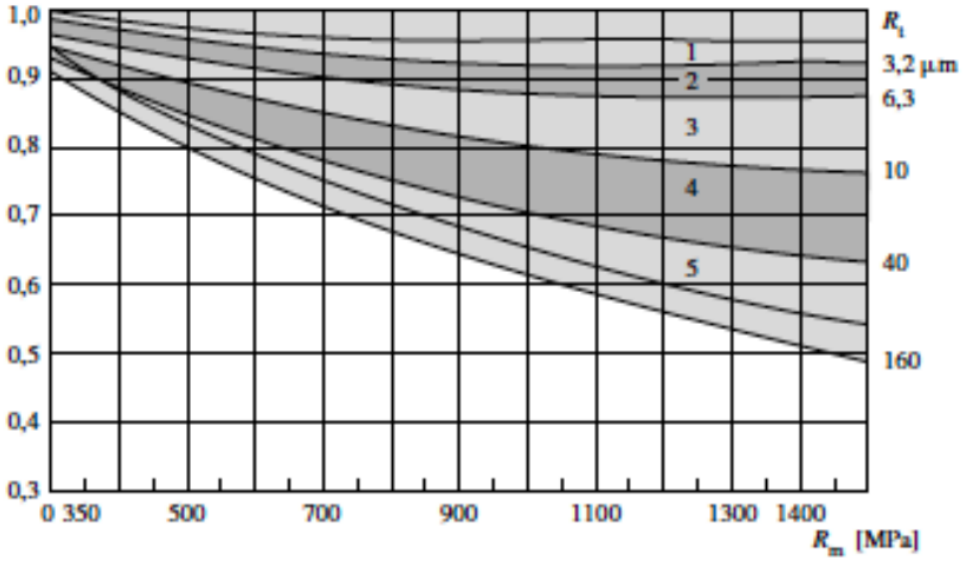

Figure 4.22: Surface finish coefficient.

The parameter "q" is the notch sensitivity factor and it is determined by the type of material and notch radius, as can be seen in Figure 4.23, where "a" is a empirical material constant, as well as ρ used in Neuber rule; in this case q = 0.6. The value K_t was estimated with standards tables on notch intensity factor for bending problems, as done in Section 4.1.2, and evaluated to be around 1.5. The coefficient to use at the beginning

of fatigue limit formula is evaluated to be, from texts in literature, at 0.4 - 0.5 for bending problems and 0.35 for axial fatigue loads; in our case the value of 0.4 was selected for being conservative. The fatigue limit was thus calculated as:

$$\sigma_e^{'} = \frac{0.4 \ \cdot 310 \ \cdot 0.95 \ \cdot 1}{1 + 0.6 \ \cdot (1.5 - 1)} = \frac{147 \ MPa}{1.3} = 90.6 \ MPa; \tag{4.26}$$

Peterson rule	Neuber rule
$q = \frac{1}{1 + \frac{a}{r}}$	$q = \frac{1}{1 + \sqrt{\frac{\rho}{r}}}$

a = 0.0634 mm (tempered and quenched steel)
a = 0.254 mm(annealed steel)
a = 0.634 mm (aluminum alloys)

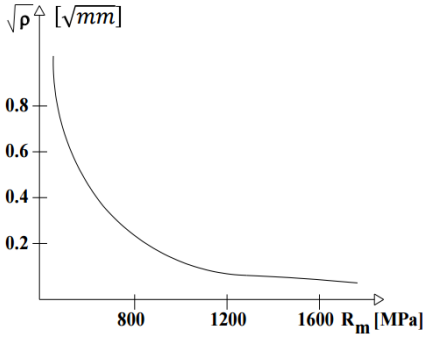

Figure 4.23: Notch sensitivity factor.

The Wöhler's diagram was generated considering a fatigue limit equal to 0.9 $\cdot UTS$ at $N_1 = 10^3$ cycles and the fatigue limit value of $\sigma_e^{'} = 90.6 \ MPa$ at $N_2 = 5 \ \cdot 10^6$ cycles, and the resultant plot of Wöhler's diagram related to our component can be seen in Figure 4.24. The dashed line represent the fatigue limit curve without the corrective factors meaning the same condition of load applied to an Aluminium 6082-T651 specimen without notches and with a polished surface roughness. In the trigger's notch a stress value of 146 MPa was previously calculated by convergence analysis: since the trigger tooth was subjected to pure bending moment in that point, the probed stress value could be considered as principal stress acting along the circumferential notch shape. The load was a pulsating load generated by interaction with the toothed bar; for the assessment only the interaction with the last tooth (at the fourth loading strike) was considered for simplicity. The cycling loading stress ratio was R = 0, different from the stress ration used for the Wöhler curve which is always R = -1 due to completely reversed stress application. To transform the pulsating stress into an equivalent completely reversed stress to be used in the Wöhler curve, the Haigh diagram was used, since it show the fatigue limit curve, defined by the equivalence between different loading scenarios comprising different alternate stress

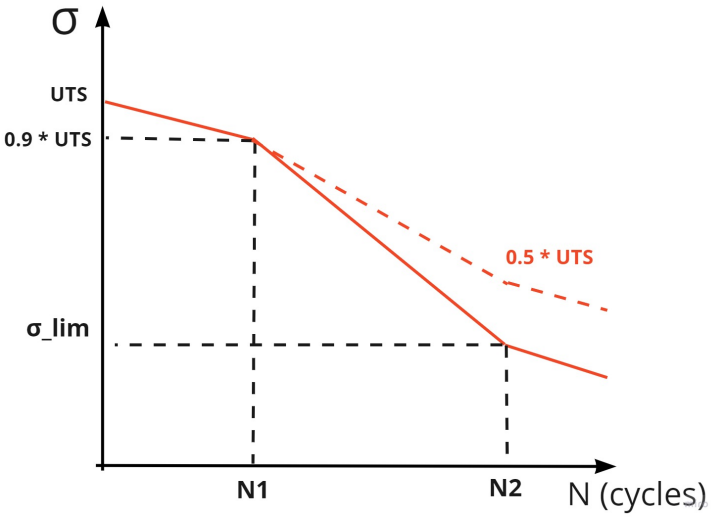

Figure 4.24: Wöhler diagram.

amplitude as a function of the mean stress. Using this graph, any combination of mean stress σ_m and amplitude σ_a was thus expected to produce the same life as the stress amplitude σ_{ar} applied at zero mean stress. Hence σ_{ar} may be thought of as a completely reversed stress that is equivalent, with respect to the fatigue life produced, to any σ_m and σ_a combination that satisfies the equation:

$$\sigma_{ar} = \frac{\overline{\sigma_a}}{1 - \frac{\overline{\sigma_m}}{\sigma_u}} = \frac{73\ MPa}{1 - \frac{73\ MPa}{310\ MPa}} = 95MPa; \tag{4.27}$$

where σ_u is the material UTS. This value overtook the fatigue lower limit value, thus the total number of cycles fell between N_1 and N_2 in the Wöhler's diagram. The equation governing the fatigue limit line between N_1 and N_2 is:

$$\sigma_A = A\ \cdot N^B; \tag{4.28}$$

where the value B was calculated considering that x-axis (cycles axis) of Wöhler's diagram is in logarithmic scale:

$$B = \frac{log(\frac{\sigma_e^{'}}{0.9\ \cdot UTS})}{log(\frac{5 \cdot 10^6}{10^3})} = \frac{log(\frac{90.6\ MPa}{0.9\ \cdot 310 MPa})}{log(\frac{5 \cdot 10^6}{10^3})} = -0.132; \tag{4.29}$$

and the value A was calculated as:

$$A = \frac{0.9 \ \cdot UTS}{(10^3)^B} = \frac{0.9 \ \cdot 310}{(10^3)^{-0.132}} = 694; \tag{4.30}$$

And the limit number of cycles expected before failure were:

$$N_{fail} = (\frac{\sigma_{ar}}{A})^{(\frac{1}{B})} = (\frac{95}{694})^{(\frac{1}{-0.132})} = 3\ 488\ 959\ cycles; \tag{4.31}$$

For the syringe device 150 injections (cycles) per day were expected, then the expected trigger's life calculated as total number of years before failure (Y_f) was calculated as:

$$Y_f = \frac{3488959\ cycles}{150\ cycles/day \cdot 365\ days/year} = 64\ years; \tag{4.32}$$

The trigger element could be definitively manufactured using Aluminium 6082-T651 alloy.

4.2.6. Toothed bar validation with FEM analysis

The toothed bar attached to the hammer and in grip with the trigger element during loading was modelled as a planar 2D shell model. Also in this case the condition was of plain stress, thereby using a shell model was an acceptable approximation. This simulation was very similar to the trigger one: the element had a 200 N force applied to a reference point rigidly connected to its tooth. Just one tooth was modelled because only the maximum stress condition has been taken into account. This element was constrained at its base by roller contact, simulating the coupling over the hammer and it was fixed at its ends. The step analysis was linear static performed between two time instants 0 and 1 as in the previous analysis. A fine mesh control of 0.1 mm was used in the tooth area were the highest stresses were expected and the global mesh size was of 1 mm with quadrilateral quadratic elements type. Also in this case reduced integration was used. The stress results were similar to the ones found in trigger analysis and the maximum Von Mises stress was 147 MPa, as can be seen in Figure 4.28. The tooth's tip maximum displacement was of the order of few micrometers, not affecting the grip performance with trigger. The safety factor was:

$$\eta = \frac{\sigma_{yield}}{\sigma_{max}} = \frac{230MPa}{147MPa} = 1.56; \tag{4.33}$$

.

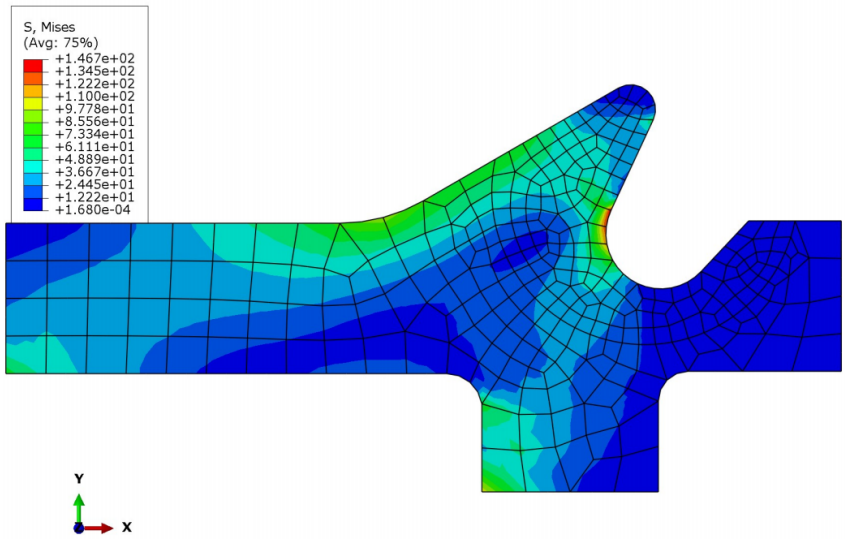

Figure 4.25: Thrust hook FEM analysis.

4.2.7. Rack validation with FEM analysis

In this analysis the most stressed rack's tooth, made in PEEK material, were modelled using a planar 2D shell element model in contact with another shell 2D model tooth of Aluminium 6082-T651. The interaction between these two elements was created using surface-to-surface contact with friction-less tangential behaviour and "hard contact" normal behaviour. The aluminium tooth was placed below and fixed at its lower end, while the rack's tooth was set above it and constrained with a roller contact, left free to move in its horizontal direction. A force of 100 N, obtained from the half of the spring's force (since two racks in parallel were present in the system) was applied at PEEK tooth base in horizontal direction. A fine mesh control of 0.1 mm was applied just on the PEEK tooth right side in contact since only in this area there was the interest to study the material behaviour. The aluminium tooth was left with rough mesh, even because the master surface in a contact definition has always a rougher mesh size. The mesh elements type was quadrilateral and of quadratic order, also in this case reduced integration was used. The step for the analysis was linear static. In fragile materials as PEEK, Galileo-Rankine stress criterion should be used instead of Von Mises stress, but in this case the only applied stress during bending was the one along the tooth profile, corresponding to its tensile principal stress. Therefore Galileo-Rankine stress was very close to the stress evaluate with Von Mises stress and the results of stresses for this analysis can be seen in Figure 4.28, with averaging element output at nodes turned off. The maximum Von Mises stress was 59 MPa.

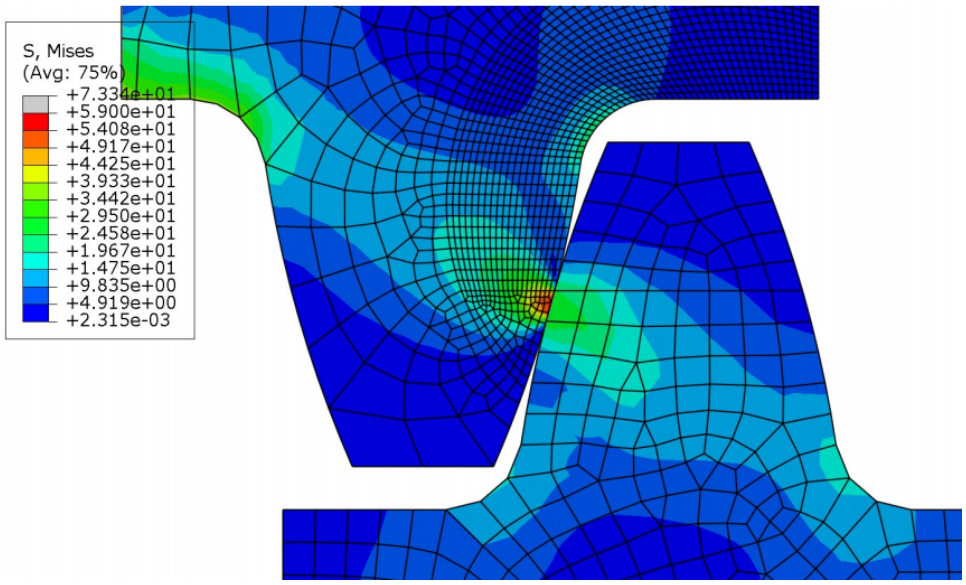

Figure 4.26: Rack and cogwheel contact FEM simulation.

The safety factor, in this case, was calculated using UTS instead of σ_{yield} as used for plastics:

$$\eta = \frac{UTS}{\sigma_{max}} = \frac{100\ MPa}{59\ MPa} = 1.69; \tag{4.34}$$

4.2.8. Cogwheel validation with FEM analysis

For the cogwheel simulation with Abaqus a solid 3D model was created for only a small portion of the entire element body, the one subjected to the worst stress condition. This approach is called sub-modeling technique, it consists in bring into depth analysis only a portion of the structure subjected to loads and displacements evaluated through a global model. The mesh can, in this way, be refined for small portion modelled, saving time and obtaining reliable results. The material selected for the model was Aluminium 6082-T651 with Young's modulus of 69000 MPa and Poisson's ratio of 0.35. A fixed constraint was applied to its base, in opposite direction with respect to the teeth, and at its sides roller constraints were applied, letting it expand radially. A reference point was created at a certain distance from the shark-tooth-shaped internal tooth, which was the most stressed part of the model in contact with the thrust hook element, and a fixed coupling between reference point and it was created; at the end a force of 100 N was applied to the reference point since each cogwheel is subjected to a force obtained by $200/2 = 100$ N. For the mesh a global size of 0.1 mm was used with tetrahedral quadratic elements, because quadratic elements usually perform better in a bending problem, and with reduced integration. The step was a linear static analysis as in the previous analyses. The maximum Von Mises

stress was present just above the contact area, in the notched tooth's base, with a stress value of 95 MPa, as can be seen in Figure 4.27. It was interesting to see that the most stressed areas were two in this case, one above the contact area and the other aside of it. The safety factor was thus calculated as:

$$\eta = \frac{\sigma_{yield}}{\sigma_{max}} = \frac{230\ MPa}{95\ MPa} = 2.4; \tag{4.35}$$

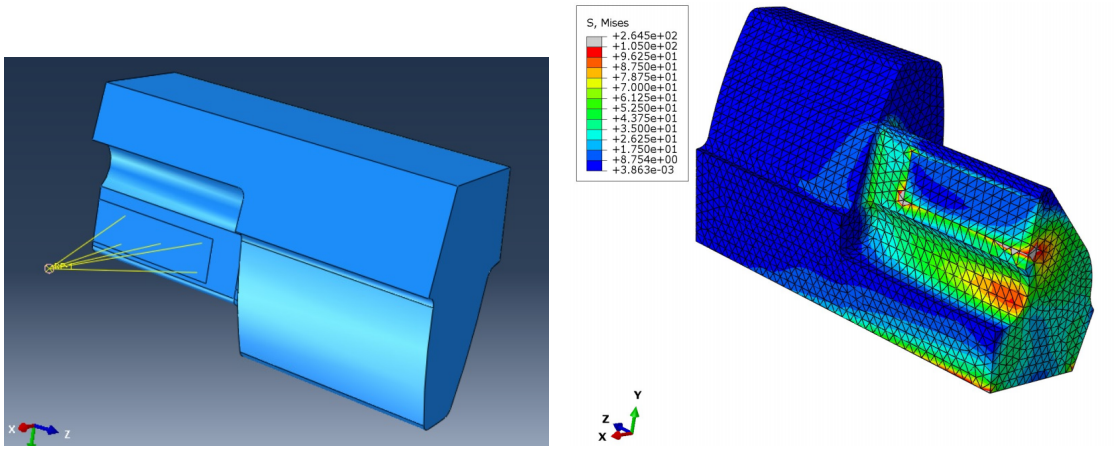

(a) Cogwheel model with applied force. (b) Cogwheel FEM analysis.

Figure 4.27: Cogwheel FEM simulation.

4.2.9. Thrust hook validation with FEM analysis

For thrust hook simulation with Abaqus a solid 3D model of the entire body was created. The material selected for this element was again Aluminium 6082-T651 working in linear elastic field, with the same mechanical properties of the previous simulation. The step created for the analysis was linear static between time instant 0 and 1, the load was applied as a step function. Roller constraints were used for the hole's inner surfaces and another constraint was set on the upper part of the element, where in reality it came in contact with the lever's upper constraint. A force of 200 N was applied to external side of hook's tip, simulating the real exchange of forces with the system throughout the use of a reference point rigidly coupled with this surface. For the mesh a global size of 0.4 mm was used with tetrahedral linear elements; reduced integration was selected. In this case linear elements were selected instead of quadratic elements since the whole body was modelled and meshed, and the computational costs could be reduced with linear elements, moreover the overall mesh size was small so reliable results could be expected even with linear elements. The maximum Von Mises stress, as can be seen in 4.27 was present at

the notch after the hook's tip and the stress value was 104 MPa. The safety factor was thus calculated as:

$$\eta = \frac{\sigma_{yield}}{\sigma_{max}} = \frac{230\ MPa}{104\ MPa} = 2.2; \tag{4.36}$$

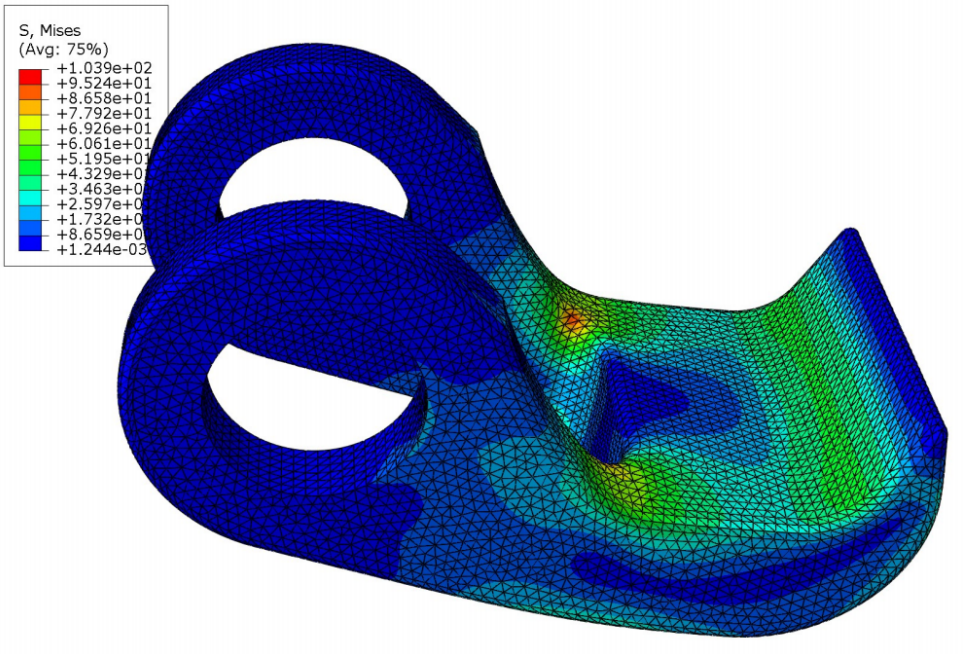

Figure 4.28: Thrust hook FEM simulation.

5 | First prototype production

After improving the product design and selecting the suitable materials for the first prototype, the technical drawings were produced to communicate the exact dimensions, specifications and tolerances for each piece in the assembly. The 3D printed components were produced starting from their ".step " file format, with a general tolerance of $\pm 0.6\ mm$. Most of parts and 3D printed parts were produced by Weerg, a CNC and 3D printing company specialized in the production of components for prototypes. Few others pieces were produced by ProtoLabs and Xometry, which are companies specialized in rapid prototyping; this choice was driven by best price/delivery time solution. The Aluminium 6082-T651 housing body was produced using both CNC machining and electrical discharge machining (EDM), to perform the deep hole for hosting the main central spring. The start button had to be produced having low roughness to increase the smooth sliding contact with the trigger, with good mechanical properties and made with transparent material for let the LED light pass through it. The material selected for this application was a translucent ABS-like material called WaterShed XC 11122, made with 3D stereolithography. Stereolithography technology is a 3D Printing process which uses a computer-controlled moving laser beam, pre-programmed using CAM/CAD software, used to create concept models, rapid prototypes, and complex parts even with intricate geometries. With this technology a tolerance of $\pm 0.05\ mm$ could be reached. Once arrived, mechanical components were assembled in the laboratory of Dondi Ingegneria S.r.l. and later the electrical components were implemented with the help of an electrical designer. Finally the medical device for needle-less injections was tested.

5.1. Detailed drawings for the workshop

In this section some technical drawings of produced components are shown, with the tolerances and selected materials. An assembly drawing with components names is added after the single components drawings and finally some exploded view assembly drawings used also for the patent document are displayed.

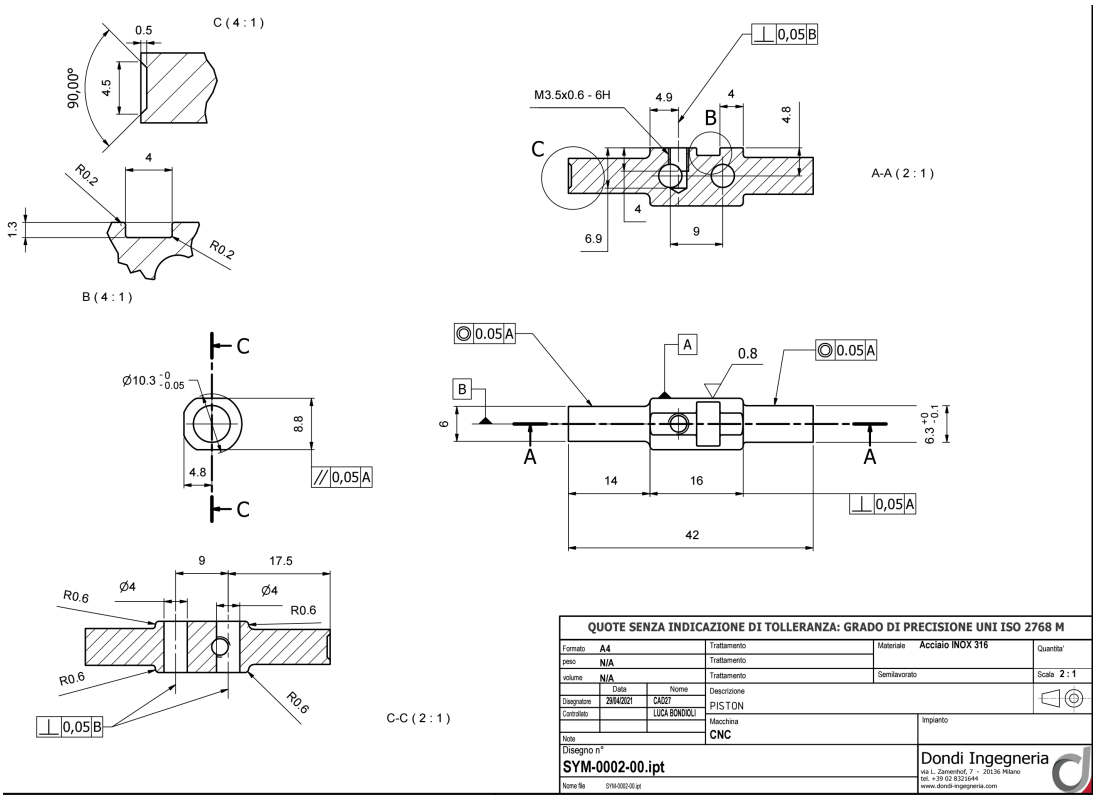

Figure 5.1: Hammer technical drawing.

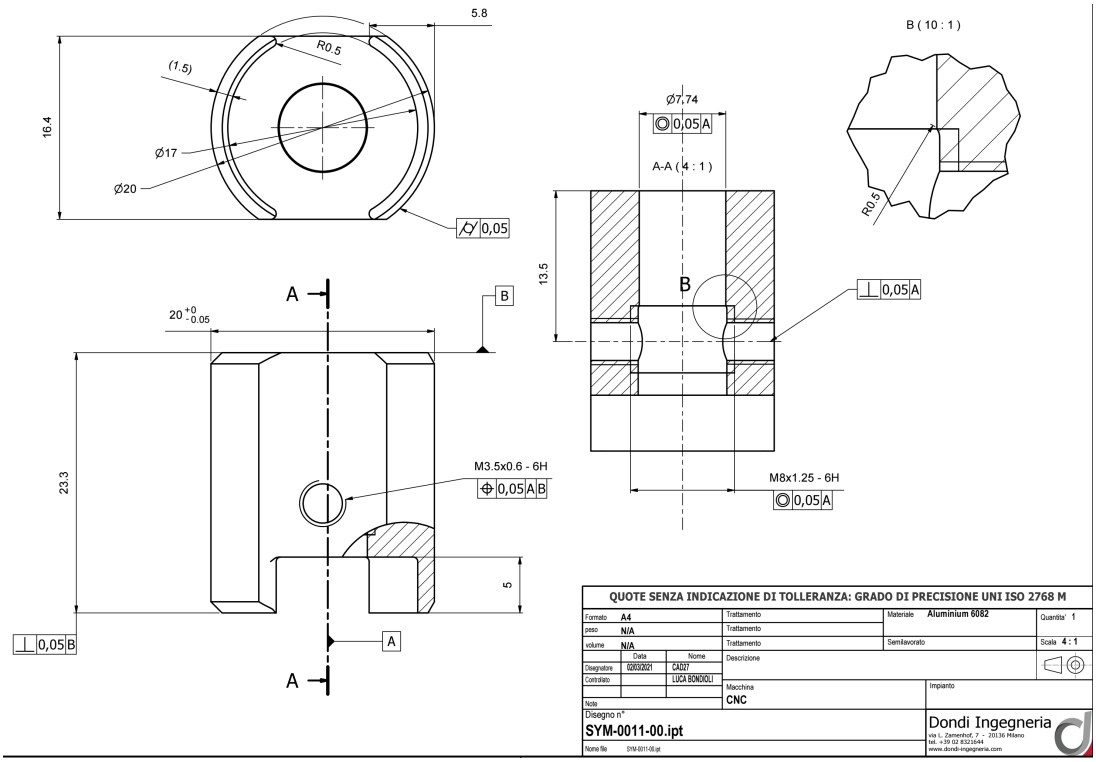

Figure 5.2: Sliding base technical drawing.

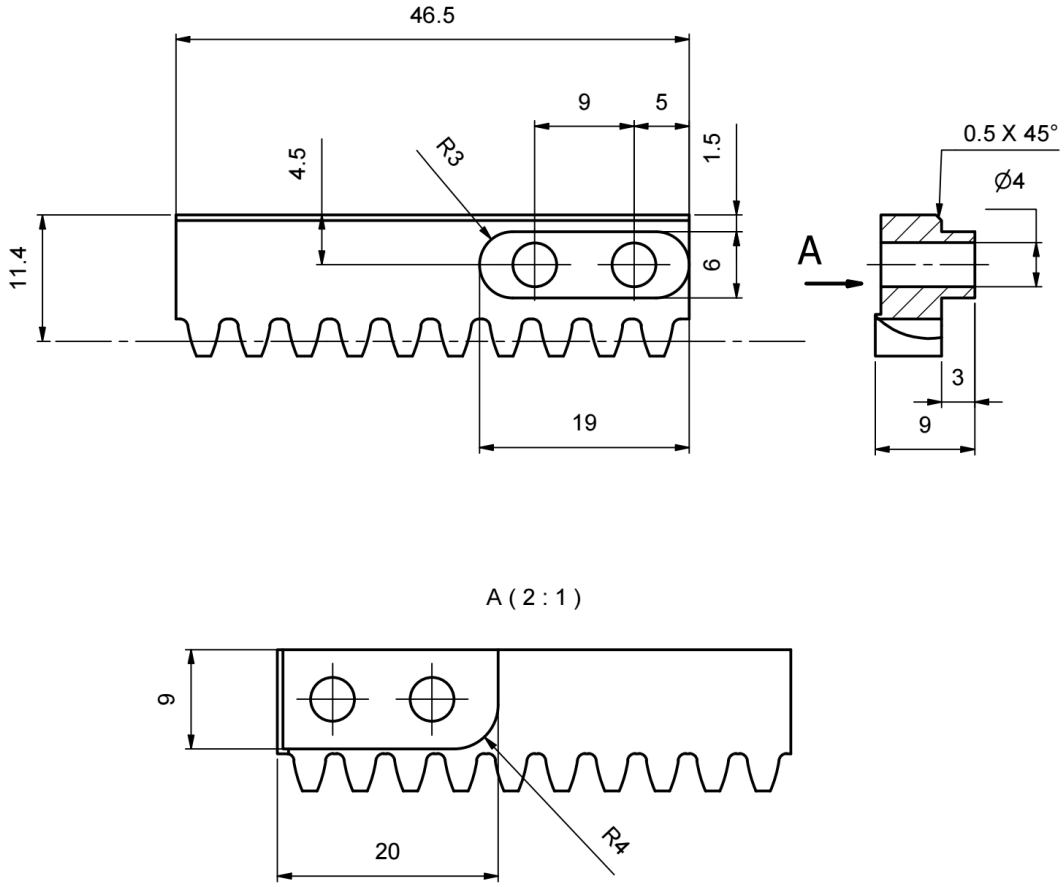

Figure 5.3: Rack base technical drawing.

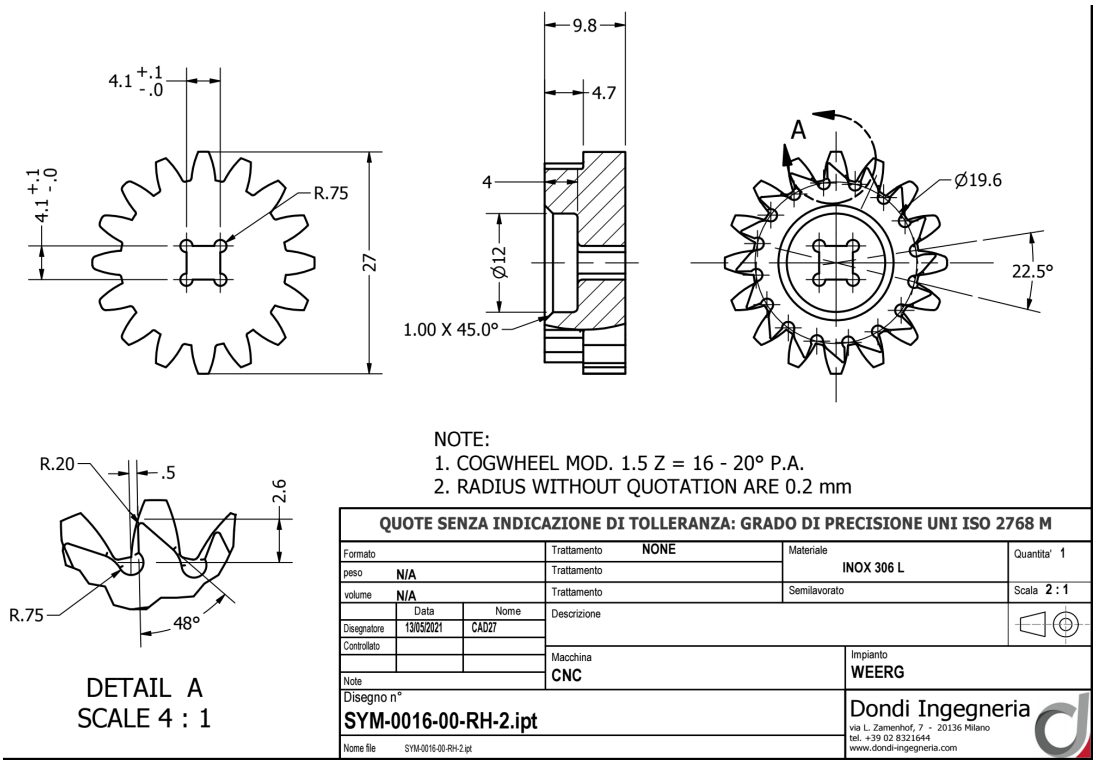

Figure 5.4: Cogwheel technical drawing.

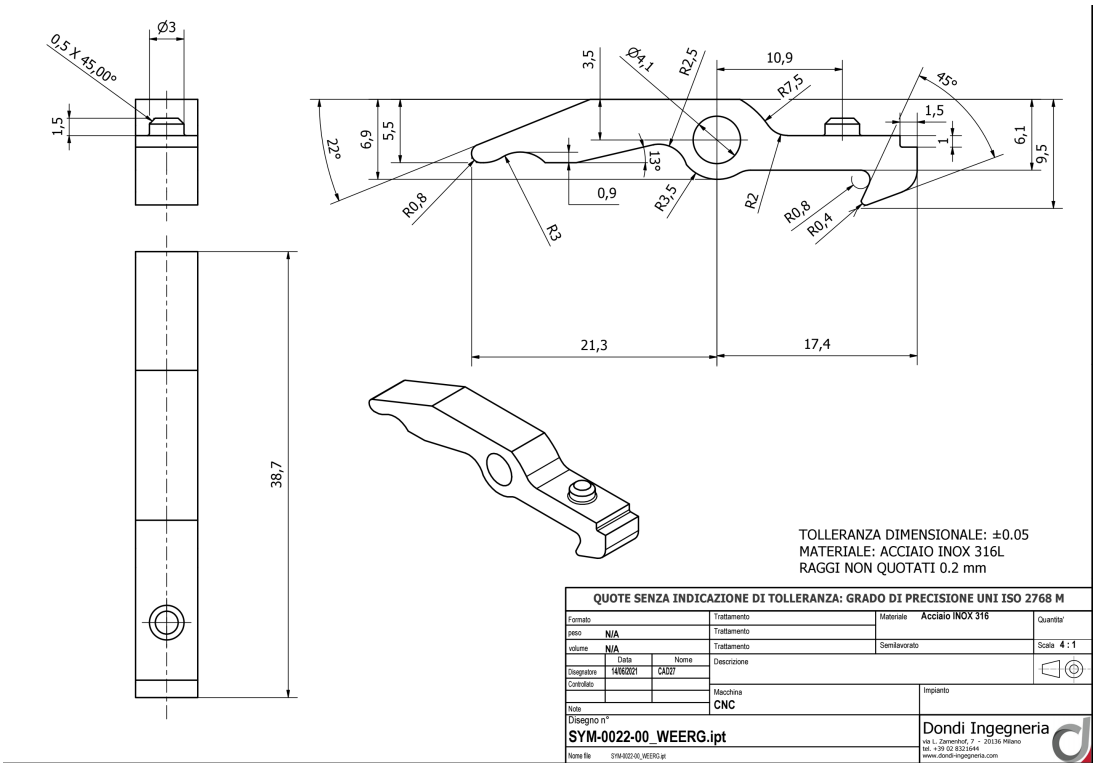

Figure 5.5: Trigger technical drawing.

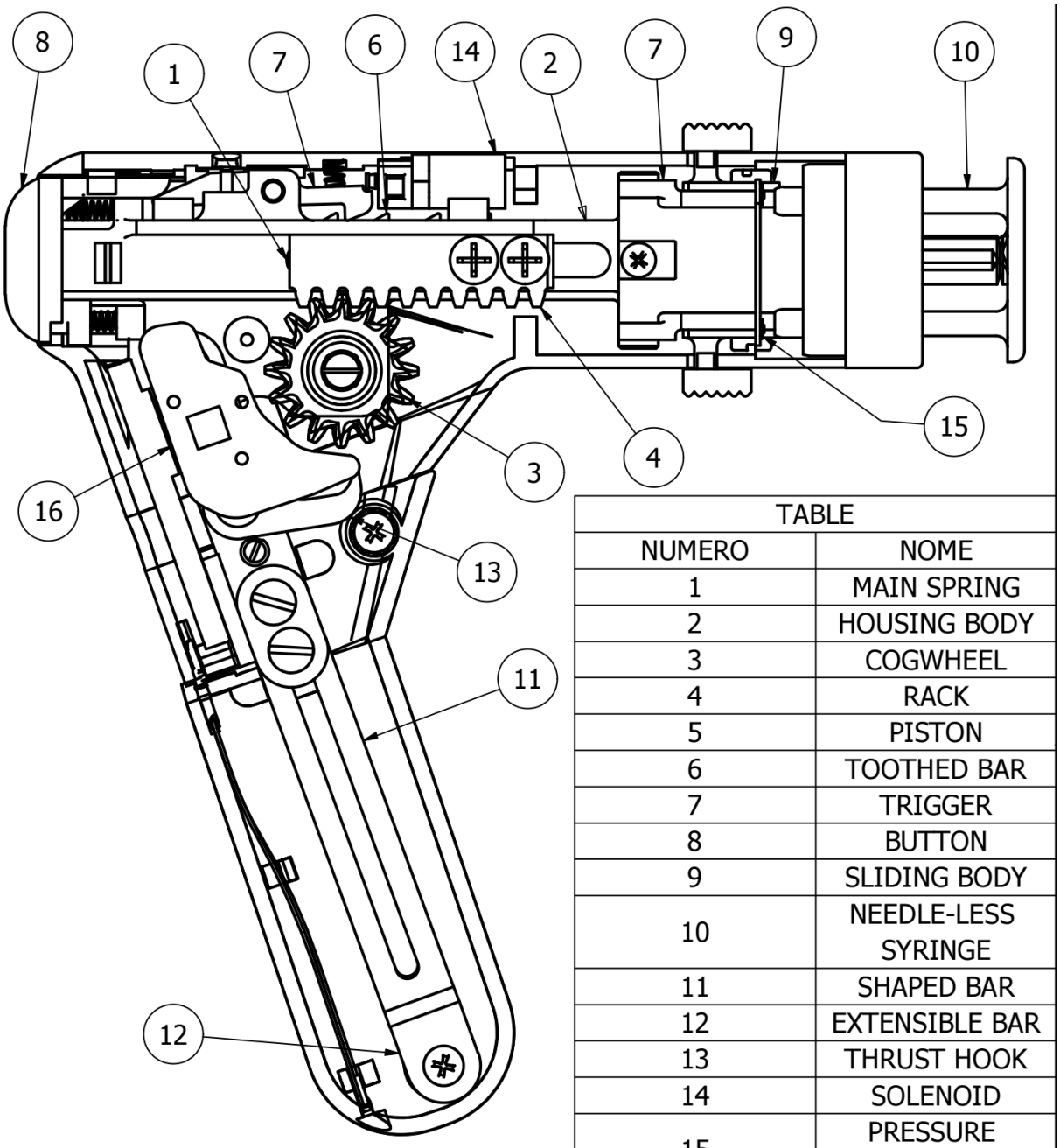

TABLE	
NUMERO	NOME
1	MAIN SPRING
2	HOUSING BODY
3	COGWHEEL
4	RACK
5	PISTON
6	TOOTHED BAR
7	TRIGGER
8	BUTTON
9	SLIDING BODY
10	NEEDLE-LESS SYRINGE
11	SHAPED BAR
12	EXTENSIBLE BAR
13	THRUST HOOK
14	SOLENOID
15	PRESSURE SENSOR
16	CENTRAL PCB

Figure 5.6: Assembly with components names.

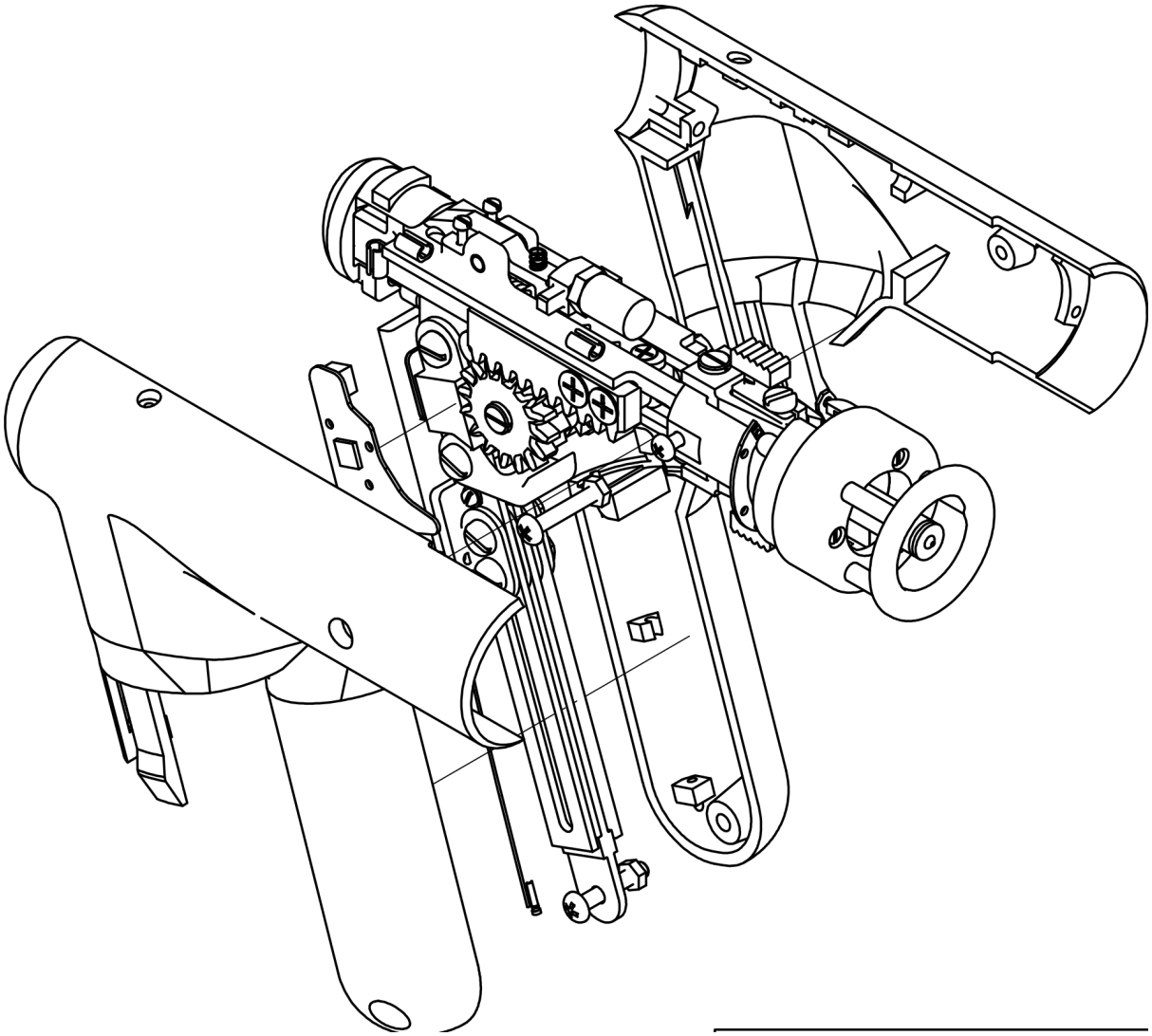

Figure 5.7: Assembly overall view.

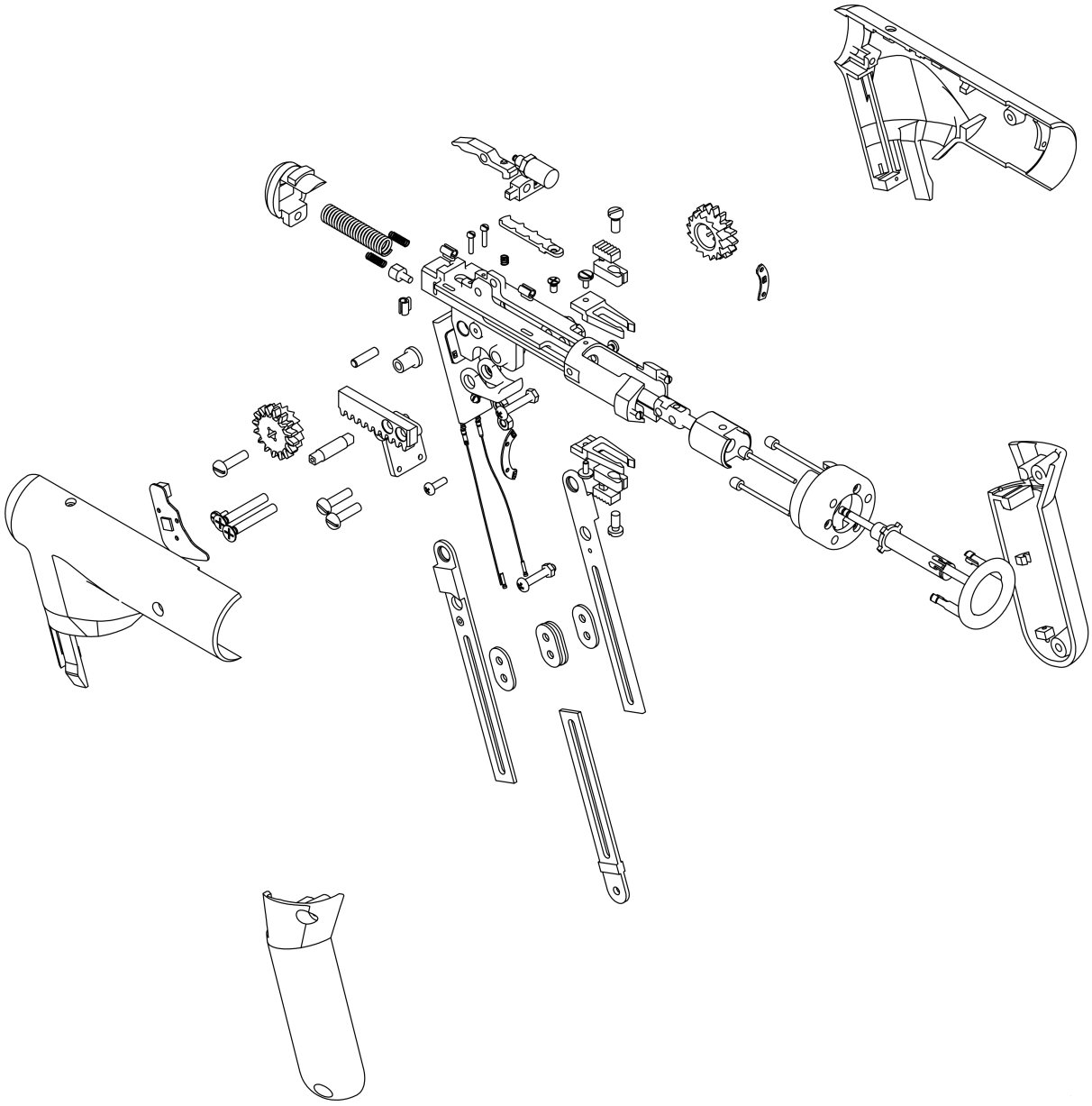

Figure 5.8: Assembly exploded view.

5.2. Prototype assembly

The assembly of mechanical components performed in the laboratory of Dondi Ingegneria S.r.l. are shown in the following steps, described through pictures taken during each main step:

1. Main spring placement inside the housing body.

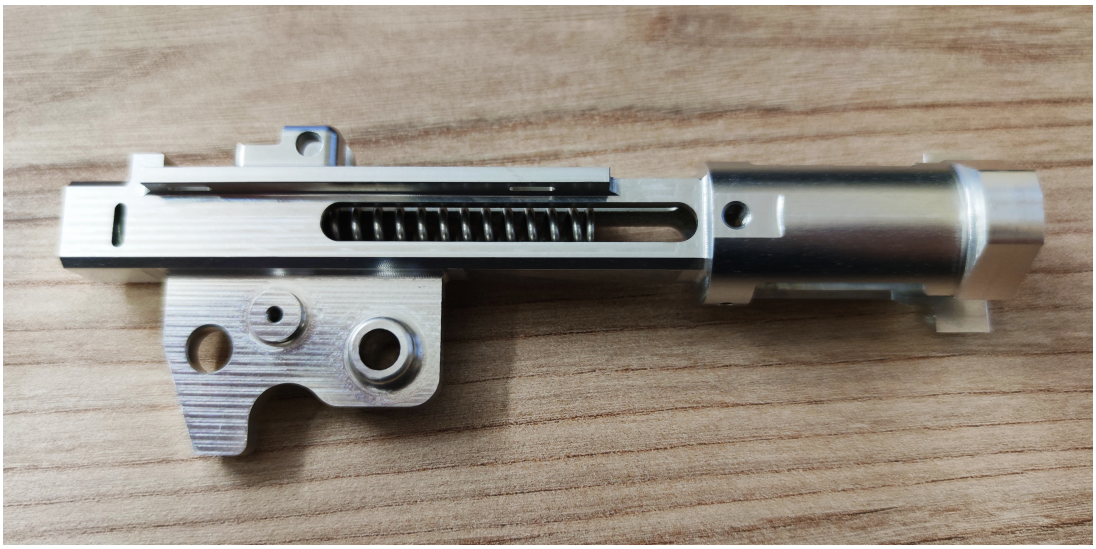

Figure 5.9: Housing body and main spring.

2. Racks, hammer, cogwheels and shaft positioning and screw fixing.

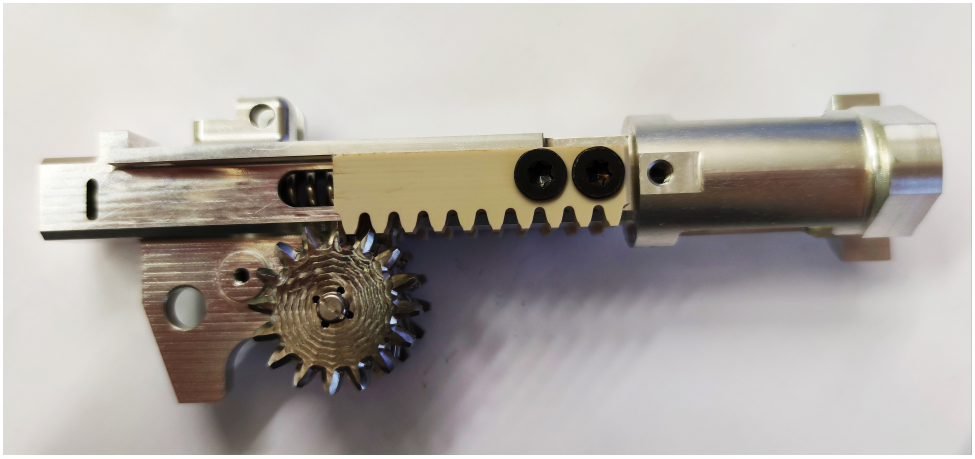

Figure 5.10: Spring loading mechanism.

3. Lever arm bars, thrust hook, trigger, toothed bar positioning and crewing.
4. Outer snap-fit joint positioning and crewing.

5. Insertion of plastic guides for electrical wires (in Figure 5.11, grey 3D printed components).

Figure 5.11: Internal mechanical components assembly.

6. Button, internal snap-fits, front ring, sliding base and plastics assembling.

Figure 5.12: Internal mechanical components assembly completion.

After the assembly was completed the device was placed on its base to check if plastics geometries fitted thoroughly and a stable coupling was present between them.

Figure 5.13: Needle-less injection device with charging base.

5.3. Electric part implementation

The main electrical part function was to control the syringe pressure system before the injection, in particular when the syringe pressure on patient's skin would reach a threshold value for a safe injection. The system comprised a front ring, with three supports moved back and forth by three preloaded springs, with three plungers moved by the front ring and going in contact with three on-off switches. Only when the three on-off switches were pushed the system was able to inject, otherwise the shooting was blocked by a solenoid holding the trigger in place. The three on-off switches signals and the solenoid were controlled by an electrical system implemented inside the syringe. The core hardware component of the electrical part was the central motherboard PCB which was installed at the right side inside the external plastics. The central PCB was powered by a Renata 3.7 V 420 mAh battery, placed in the main syringe body in the back of it, the central PCB was connected by means of 0.6 mm wires to two dependent PCB supporting the on-off switches. One more PCB was fixed inside the main body external plastics, in the back side, and it had two switches working in parallel as described in Section 3.1.4. Attached to this last PCB two on-off switches placed in parallel were set, they were created to be pushed or released by the lever arm during the loading action or still position: when the lever was in its starting position these PCB were pushed to signal the system was still and not loading, otherwise when the lever was moved from its starting position they had to signal the start of loading action, i.e. activating the solenoid. When the solenoid plunge was retracted (current flowing in it) the system could be loaded since the trigger was left free lo lift and let the sliding toothed bar moving in. Otherwise the solenoid with extended plunger (no current flowing in it) blocked the trigger for safety. A picture taken during the electrical part implementation is shown in Figure 5.14.

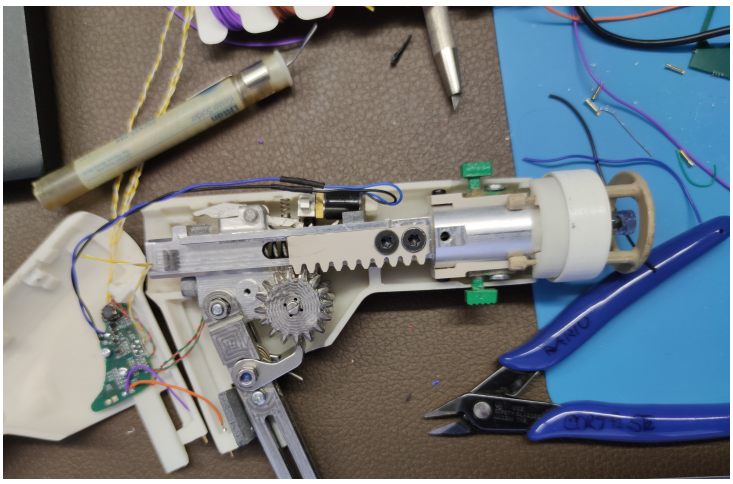

Figure 5.14: Electrical part implementation.

Three LED were set just behind the transparent start button, and connected to the central PCB, the function of these LED were to signal when the system was able to inject, i.e. when the right pressure was reached on the patient's body (condition of three switches completely pushed). The battery was selected to last one day of use, meaning a maximum of 150 injections per day, and after this time it had to be recharged placing the device on a base connected to the current supply. The battery inside the main body plastics was connected to two pogo pins, which were designed to come in contact respectively with two other pins placed inside the handle. Inside the plastic handle there were two electrical wire with two pogo pins each, and it was designed to be leaned on its charging base, a picture of it can be seen in Figure 5.15. In fact this system has been created to have a connection between the syringe's battery and its charging base by means of the handle, wired inside, that was able to close the circuit while retracted in place and leaned in its charging base. A pogo pin or spring-loaded pin is a type of electrical connector mechanism that is used in many modern electronic applications, they are used for their improved durability over other electrical contacts, and the resilience of their electrical connection to mechanical shock and vibration, suitable for this application.

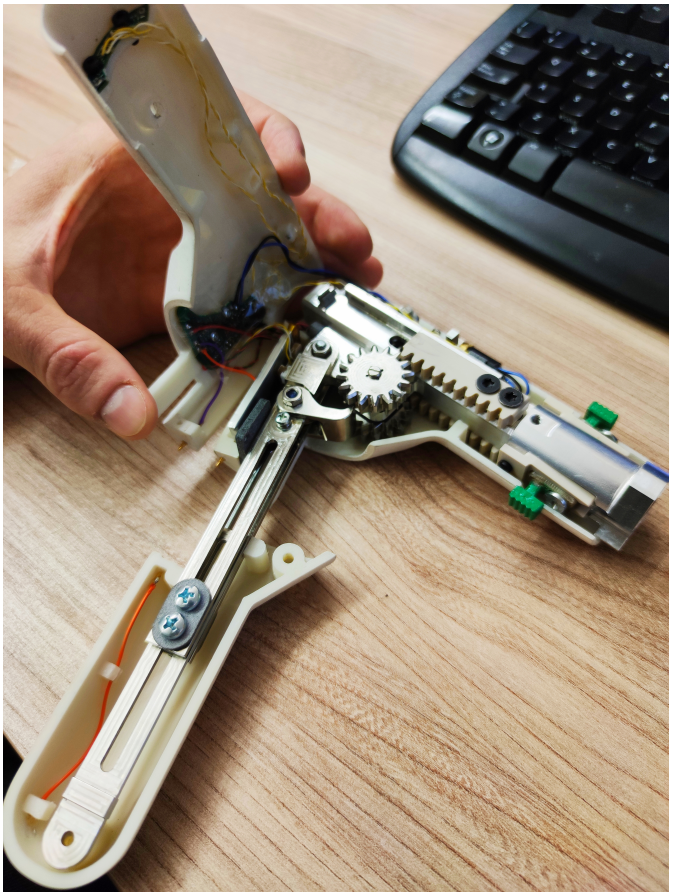

Figure 5.15: Electrical components.

5.4. Testing and first improvements

The first prototype tests were conducted in the laboratory of Dondi Ingegneria S.r.l. using water as medical fluid inside the needle-less ampoule. A sheet of soft rubber as substitute of patient's skin was used for the first tests and was observed that the system was able to produce a tiny hole, visible to naked eye, over the rubber created by the fluidic needle during its passage, and the fluid could be injected inside the rubber thick sheet. The force to perform the strikes and load the system was very limited, thanks to the ratchet loading system the effort required was not excessive at all even for a woman hand. However the first prototype showed flaws as for example in the brake system composed by two snap-fit joints designed to block the sliding base during the impact. The problem was that during the injection, the snap impact force exerted by the spring to ampoule was too quick and moved forward the sliding base attached to it bypassing the brake snap-fit system, in fact it had no time to open and block this sliding motion. The reason for that was the too high and quick impact, excessively high force in a too limited unit of time, and in this way the brake system had no time to activate the absorption of mechanical energy. If the ampoule was pressed over a body it could inject anyway but it would be an unacceptable discomfort for the patient due to the ampule impact over the skin, with possible small entity bruise over it. This problem was solved by removing the brake system based on snap-fit joints and replacing it with a fixed system for the sliding base: having a single block screwed to the housing body firmly could withstand the impact during the snap injection action and it seemed to be the right solution, even if the sliding base was no more able to slide forward to help the user to screw the needle-less ampoule over it. The tests showed anyway that the user was able to attach the ampoule on its base; the available space for doing so was reduced but it could be done. Another defect detected during testing was that after pushing the start button for activate the system it had problems to return back in place despite the two springs: this could be caused to the rough tolerances of the 3D printed external plastics. In fact this technology produced a $\pm$ 0.6 tolerance witch was rough and could create interference between parts as in this case. The main error in this case was that the long plastic flap, during the sliding action, was pushed upward by the contact with the trigger, and this interaction put the flap in interference with the external plastics blocking the start button in place. From a geometrical study it was concluded that the start button shape had to be re-designed, aiming to a more compact design and avoiding long flaps or extremities in interference. Another note of improvement was for the plastic handle; since it was not properly propped against the extensible lever it had unwanted lateral swinging, not compromising the use of the device but definitely a point to be improved. For the electrical components the CPU board was

placed close to the cogwheel and at the end this solution was considered dangerous for an industrialized product because the cogwheels could come in interference with the CPU board destroying it, moreover thin cables running close to cogwheel position could be tore off, compromising the electrical connection between parts. For the next prototype it was necessary to find a suitable, controlled, passage for wires inside the plastics. The last consideration for mechanical parts of the first prototype was related to the housing body, since it was the most important part, supporting the main spring and it had to have proper tolerances, but as shown in FEM analysis the maximum stress in this component during the spring compression was very limited and the Aluminium 6082-T651 choice resulted an expensive solution. For this element another cheaper material can be used for the next prototypes and the geometry can be improved too, avoiding expensive processing as electrical discharge machining.

6 | Conclusions and future developments

6.1. Project's conclusions

The goal of the internship at Dondi Ingegneria S.r.l. and this thesis work was to design and produce a workable innovative system for needle-free injections. As the TRIZ theory can teach, produce an inventive step for solving a technical problem is not a random process, but can be tackled with a systematic method for produce feasible solutions using available materials and principles from the physical universe. The design of a mechanical system is ruled by fundamentals laws guiding the designer toward a more efficient and ideal system. The most important guidelines to be taken into account before the creation of final design and technical drawings are give by the DfX rules as Design for Manufacturing (DfM), Design for Assembly (DfA), Design for Environment (DfE) and Design for Reliability (DfR). When the final design is achieved with respect of the rules of standard mechanical engineering and advanced mechanical design practice, an accurate analysis using Finite Element Method can provide reliable results on the device strength and level of optimization. With these information the right material can be selected and modifications on the elements geometry can be performed before production of the first prototype. During the production of pieces it is important to select the right dimensional and geometrical tolerances in order to have working couplings and at the end a working system. If for a certain reason the required tolerances cannot be ensured, it is important to take into account of it during the design phase and include in the 3D models technical solutions overcoming as much as possible the difficulties that could arise for the lack of tolerances; this considerations is done only for prototypes. In the field of medical injections, statistically, 10% of people worldwide are affected by belonephobia (fear of needles) [26] and in hospitals, especially in the Third-World, the risk of transmit diseases by the tip of a syringe needle is present, for this reason an efficient needle-free device can be a useful technology for improve life of other people world-wide. In future a cheaper device version can be created without electrical part but just a mechanical lock-unlock system able to

close-open the injection system when the right pressure on the patient's arm is reached. Use needle-free syringes in place of needle syringes is also an eco-sustainable choice because the first technology uses a 100 % disposable plastic ampoule, while the second has the steel needle inserted in the plastic, difficult to be disposed after usage. The inventive step created with this new device is that the spring loading system is integrated inside the main "boomerang-shaped" body and no need of external tool is needed. Moreover the force needed for load the spring is very limited, suitable even for a little nurse, thanks to the ratchet mechanism making use of two special cogwheels activated at will by the lever system. In addition to that the electrical system allows the user to have a signal when the right pressure for injection is achieved and it blocks the system when it is not reached or the system is in stand by, avoiding unwanted injections. This device has a European patent in pending, filled out with the consulting of Luppi Intellectual Property.

6.2. Prototype 2

The main idea for the next prototype, besides solving the technical issues of the first prototype, as described in section 5.4, is to reduce the overall costs. To achieve this goal it has been thought to review the project and see where it is possible to replace metal parts with polymers and composites. With the advent of high-performance polymers and composites, that enable new applications due to their mechanical properties, metals components can be replaced having a cheaper and lighter assembly. Among the major characteristics of plastics are: ease of processing, cost-effectiveness, thermal and electrical insulation, sound and vibration, and chemical and corrosion resistance; which are all very interesting characteristics for this device application. High performance polymers are thermoplastic polymers with high mechanical, thermal and chemical performance with countless uses, in fact in some applications they can replace metals such as stainless steel and aluminum alloys. The best suitable material of this kind seemed to be TECAPEEK GF30 30% glass fiber reinforced, whose mechanical properties are shown in Table of Figure 6.1. For this material the Young's Modulus is 9700 MPa, the ultimate tensile strength is 157 MPa and the coefficient of friction is around 0.2. In addition to select high performance material, the geometry of critical components can be reviewed to reduce the maximum stress in the critical areas.

Properties	ASTM Test Method	Units	TECAPEEK™	TECAPEEK™ GF30 30% Glass Reinforced	TECAPEEK™ CF30 30% Carbon Reinforced	TECAPEEK™ PVX
Physical						
Density	D792	lbs/in^3	0.0477	0.0538	0.0520	-
Specific Gravity	D792	g/cc	-	-	-	1.48
Water Absorption, @ 24 hours @Equilibrium	D570 D570	% %	0.5 0.5	0.11 -	0.06 -	- -
Mechanical						
Tensile Strength @ Yield, 73°F	D638	psi	14,000	22,800	30,200	17,300
Tensile Modulus	D639	psi	522,100	1,406,800	1,885,400	-
Elongation @ Break, 73°F	D638	%	4.9	-	-	-
Elongation, Ultimate, 73°F	D638	%	50.0	2.2	1.3	2.5
Flexural Strength, 73°F	D790	psi	27,700	33,800	46,100	30,000
Flexural Modulus, 73°F	D790	psi	530,000	1,495,200	1,885,400	1,400,000
Compressive Strength, 73°F	D695	psi	17,100	31,200	34,800	22,000
Shear Strength, Ultimate, 73°F	D3846	psi	7,600	14,100	14,100	-
Izod Impact Strength, 73°F	D256	ft-lbs/in	1.55	1.8	1.6	3.25
Rockwell Hardness, 73°F	D785	-	M99	M103	M107	-
Limiting PV @ 68°F 1200 in/min	-	(psi) (ft/min)	170,000	-	385,000	-
Wear Factor Against Steel, 40 psi, 50 fpm	D3702	in^3 /hr*1/PV	-	-	-	
Coefficient of Friction, @ 68°F 1200 in/min, 155 lbs Load	D1894-95	μ	0.18	-	0.22	.19-.21

Figure 6.1: TECAPEEK GF30.

For example in toothed bar design of the first prototype, the last tooth going in grip which the trigger's hook when the system is fully loaded has a considerable stress value. The stress generated in this area can be reduced improving the component geometry as increasing the vertical thickness of this last tooth, as can be seen in Figure 6.2. With this solution, the maximum stress is kept low even using TECAPEEK GF30 instead of a metallic material as Aluminium 6068-T6. As a matter of fact creating a model with the mechanical properties of this polymer, in elastic field, the maximum stress at notch resulted to 118 MPa, with a safety factor of:

$$\eta = \frac{UTS}{\sigma_{max}} = \frac{157\ MPa}{118\ MPa} = 1.33; \tag{6.1}$$

It is important to note here that, differently from metallic materials, the fatigue behaviour of high strength polymers shows a much flatter curve in the Wöhler's diagram fatigue limit. An interesting result taken from fatigue resistance tests of peek reinforced with short fibers is shown in the work done at Mechanical and Industrial Engineering Department in University of Brescia [27], where a peek short carbon fiber composite (CF10-PVX) subjected to cyclic loading at stress level up to 90% of its static strength showed a rather flat shape of fatigue S-N curve with a run out at 10^6 cycles. In the case of a PEEK composite with higher value of reinforcing fibers (30%) the static and fatigue resistance even improved. From these data it is possible to design high performance polymers with a safety factor reduced up to $\eta = 1.2$, to be appropriately validated with accurate FEM

simulations. Another element where polymeric material can be used is the trigger: in this part there is no space for increase the tooth thickness in vertical direction as in the case of the toothed bar, but the overall trigger's width can be increased, improving the structure stiffness and reducing the stress concentration on the tooth with applied load. As can be seen from the FEM simulation of Figure 6.3, the maximum stress is 93 MPa leading to a safety factor of:

$$\eta = \frac{UTS}{\sigma_{max}} = \frac{157\ MPa}{93\ MPa} = 1.7; \tag{6.2}$$

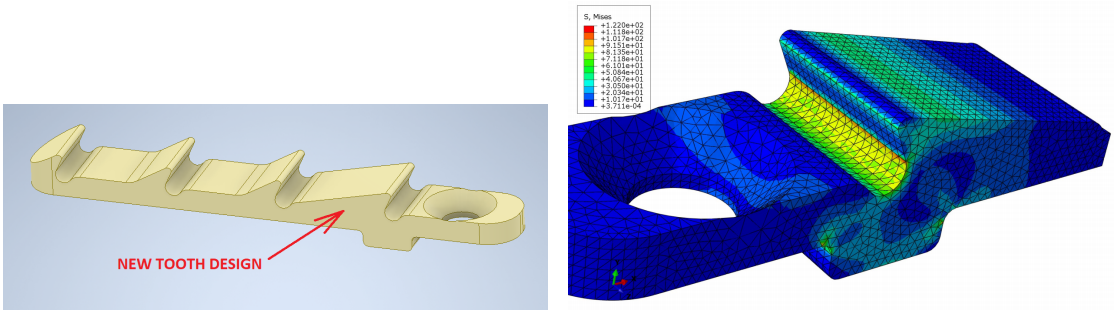

(a) New toothed bar in TECAPEEK GF30. (b) New toothed bar FEM analysis.

Figure 6.2: New toothed bar design in TECAPEEK GF30.

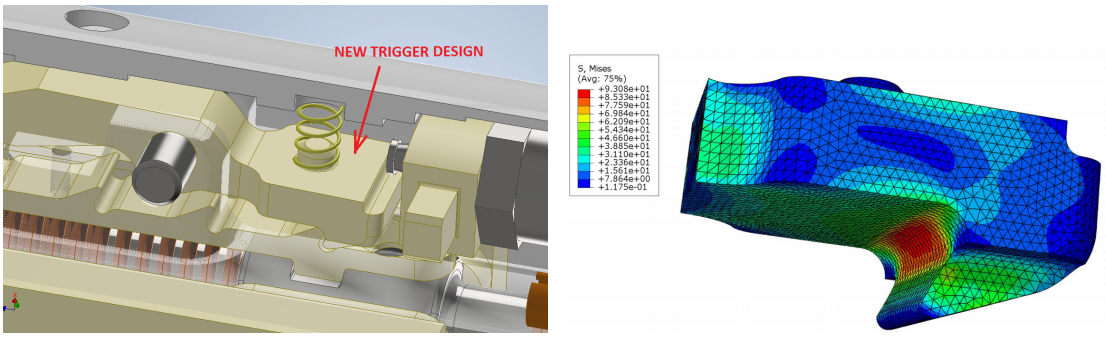

(a) New trigger in TECAPEEK GF30. (b) New trigger FEM analysis.

Figure 6.3: New toothed bar design in TECAPEEK GF30.

Bibliography

[1] Cécile Raynal. Médicaments irradiés, sources de santé. *Revue d'Histoire de la Pharmacie*, 98(369):53–70, 2011.

[2] Samir Mitragotri. Current status and future prospects of needle-free liquid jet injectors. *Nature reviews Drug discovery*, 5(7):543–548, 2006.

[3] Lisa A Grohskopf, Leslie Z Sokolow, Sonja J Olsen, Joseph S Bresee, Karen R Broder, and Ruth A Karron. Prevention and control of influenza with vaccines: recommendations of the advisory committee on immunization practices, united states, 2015–16 influenza season. *MMWR. Morbidity and mortality weekly report*, 64(30):818, 2015.

[4] S Wagner, G Dues, D Sawitzky, P Frey, and B Christ. Assessment of the biological performance of the needle-free injector injex using the isolated porcine forelimb. *British Journal of Dermatology*, 150(3):455–461, 2004.

[5] Daniel Eisinger, George Tsatsaronis, Markus Bundschus, Ulrich Wieneke, and Michael Schroeder. Automated patent categorization and guided patent search using ipc as inspired by mesh and pubmed. In *Journal of biomedical semantics*, volume 4, pages 1–23. Springer, 2013.

[6] Chris Cappello and John W Bingham. Needle-free syringe, September 24 2013. US Patent App. 29/439,506.

[7] Chris Cappello, Matt Wixey, and John W Bingham. Intradermal injection device without needle, 2015.

[8] Douglas Ivan Jennings and Charles Michael Dean. Injection device, March 3 2015. US Patent 8,968,236.

[9] Shyh-Jen Wang. Designing around patents: a guideline. *Nature biotechnology*, 26(5):519–522, 2008.

[10] Genrikh Saulovich Altshuller. *The innovation algorithm: TRIZ, systematic innovation and technical creativity*. Technical innovation center, Inc., 1999.

[11] Zinovy Royzen. Solving contradictions in development of new generation products using triz. *The TRIZ Journal*, 1997.

[12] Gordon Nayler. *Dictionary of mechanical engineering*. SAE, 1996.

[13] Francesco Pellicano. *Meccanica applicata alle macchine*. Universita degli Studi, 2007.

[14] Karlheinz Schaub, Gabriele Caragnano, Bernd Britzke, and Ralph Bruder. The european assembly worksheet. *Theoretical Issues in Ergonomics Science*, 14(6):616–639, 2013.

[15] Anthony G Atkins, Tony Atkins, and Marcel Escudier. *A dictionary of mechanical engineering*. Oxford University Press, 2013.

[16] Tsai-C Kuo, Samuel H Huang, and Hong-C Zhang. Design for manufacture and design for 'x': concepts, applications, and perspectives. *Computers & industrial engineering*, 41(3):241–260, 2001.

[17] Karl T Ulrich. *Product design and development*. Tata McGraw-Hill Education, 2003.

[18] SJ Park and TH Kwon. Optimal cooling system design for the injection molding process. *Polymer Engineering & Science*, 38(9):1450–1462, 1998.

[19] Geoffrey Boothroyd. Design for assembly—the key to design for manufacture. *The International Journal of Advanced Manufacturing Technology*, 2(3):3–11, 1987.

[20] Conrad Luttropp and Jessica Lagerstedt. Ecodesign and the ten golden rules: generic advice for merging environmental aspects into product development. *Journal of Cleaner Production*, 14(15-16):1396–1408, 2006.

[21] Dirk M Barends, Margryt Teatske Oldenhof, Marjo J Vredenbregt, and Maarten J Nauta. Risk analysis of analytical validations by probabilistic modification of fmea. *Journal of pharmaceutical and biomedical analysis*, 64:82–86, 2012.

[22] Bayer Material Science LLC. Snap-fit joints for plastics - a design guide. *Pittsburg*, 2000.

[23] Jonna Lind. *Tribology of polymer composites for elevated temperature applications*. PhD thesis, Uppsala University, 2017.

[24] Xiaomin Shu, Jianming Zhang, Lei Han, and Yunqiao Dong. A surface-to-surface scheme for 3d contact problems by boundary face method. *Engineering Analysis with Boundary Elements*, 70:23–30, 2016.

[25] Joseph Edward Shigley. *Shigley's mechanical engineering design*. Tata McGraw-Hill Education, 2011.

[26] Louisa Yim. Belonephobia: a fear of needles. *Australian family physician*, 35(8), 2006.

[27] A Avanzini, G Donzella, D Gallina, S Pandini, and C Petrogalli. Fatigue behavior and cyclic damage of peek short fiber reinforced composites. *Composites Part B: Engineering*, 45(1):397–406, 2013.